2017

STRIDE | Southeastern Transportation Research, Innovation, Development and Education Center

Final Report

On-Board-Diagnostics (OBD) Data Integration into Traffic Microsimulation for Vehicle-Specific Fuel Use & Emissions Modeling & In-Vehicle App Testing

(Project # 2013-034)

Authors: Dr. Scott S. Washburn, Ph.D., PE, University of Florida
Dr. H. Christopher Frey, Ph.D., North Carolina State University
Dr. Nagui Rouphail, Ph.D., North Carolina State University

May 2017

DISCLAIMER

TABLE OF CONTENTS

LIST OF TABLES

LIST OF FIGURES

LIST OF AUTHORS

University of Florida, Department of Civil and Coastal Engineering

Scott Washburn, Associate Professor

Seckin Ozkul, Graduate Research Assistant

North Carolina State University, Department of Civil, Construction, and Environmental Engineering

H. Christopher Frey, Professor

Nagui Rouphail, Professor

Jiangchuan Hu, Graduate Research Assistant

Acknowledgments

The authors thank Brandon Graver, Gurdas Sandhu, Behdad Yazdani, Bin Liu, Maryam Delavarrafiee, and Xiaohui Zheng for conducting field measurements and VSP-based model analysis of the selected vehicles.

ABSTRACT

The work reported here is for a study that aimed to: (1) evaluate the concordance between internally observable variable (IOV) based and externally observable variable (EOV) based predictors of engine power demand; (2) develop predictive models for vehicle energy use and emissions (EU&E) based on IOVs; (3) evaluate models for vehicle EU&E based on IOVs by comparing to models based on EOVs; and (4) implement the new predictive models for emissions and fuel use based on IOV's into SwashSim, a traffic microsimulation software program Based on this research, predictive models for vehicle EU&E are evaluated and recommendations are offered regarding choices among these models. The implementation of the IOV-based models into SwashSim demonstrates how this capability can be added to any microscopic traffic simulation tool.

Part I: Introduction

Background

Transportation accounts for 28% of all U.S. energy use (U.S. EIA, 2015). Highway transportation accounts for 32% of national annual emissions of nitrogen oxides (NO_x), 50% of carbon monoxide (CO), and 22% of volatile organic compounds (VOC) (U.S. EPA, 2015). This increasing concern regarding air quality has motivated the need for accurate estimates of micro-scale vehicle EU&E. This is especially important because of the increasing need to assess the environmental effectiveness of traffic management and operation strategies such as ramp metering, managed lanes, speed harmonization, and even connected vehicle systems on EU&E (Washburn *et al*., 2013).

Vehicle fuel use and emission rates are related to vehicle specific power (VSP) (Frey *et al*., 2008). VSP accounts for changes in vehicle kinetic and potential energy, rolling resistance, and aerodynamic drag (Jimenez-Palacios, 1999). For a given vehicle, VSP is a function of vehicle speed, acceleration, and grade.

Frey *et al*. (2010) conducted a detailed evaluation of the explanatory power and goodness-of-fit of 14 alternative modeling approaches for predicting vehicle EU&E based on use of EOVs compared with IOVs. An EOV can be observed from outside of a vehicle. Examples include vehicle speed, vehicle acceleration, and road grade. An IOV can be observed from inside a vehicle. Examples include manifold absolute pressure (MAP), engine speed in revolutions per minute (RPM), and others. Many IOVs are reported by a vehicle electronic control unit (ECU) via an on-board diagnostic (OBD) interface. Such IOVs can be recorded in real time using an OBD "scantool." Tailpipe emission rates were measured using a portable emission measurement system (PEMS). Models of fuel use and emission rates based on engine data, such as MAP and RPM, are more predictive than those based only on VSP (Frey *et al*., 2010).

Although VSP-based models are now widely used and offer significant explanatory power for fuel use and emission rates, models based directly on OBD data have the potential for better goodness-of-fit. For example, a VSP-based model for fuel use rate for a 2005 Chevrolet Cavalier had a coefficient of determination (R^2) of 0.87. However, an IOV model based on $P_{M\times R}$, which is the product of MAP and RPM, had a higher R^2 of 0.99 (Frey *et al*., 2010). Such improvement was expected, since the MAP and RPM are significant factors affecting fuel injection control and thus, are indicators of engine power demand (Heywood, 1998). Therefore, the direct use of IOVs based on OBD data may lead to improved estimates of vehicle fuel use and emission rates. However, tailpipe emission rates are also significantly influenced by the operational efficiency of the catalytic converter, for which the effect was not quantified (Frey *et al*., 2010). Models for emission rates of specific pollutants based on IOVs may have an R^2 not as good as for fuel use. The latter is not significantly influenced by the catalytic converter.

There is increasing interest in developing applications that use OBD data. In-vehicle data collection for proof-of-concept and feasibility assessment can be costly. There is growing demand for a traffic simulation platform that enables developers to test and evaluate products and for an improved method for quantifying EU&E to support transportation planning. A traffic simulation tool that is capable of using EU&E models based on IOVs would be of significant benefit to the transportation and environmental engineering communities. Historically, such tools determine vehicle acceleration rates through relatively simple methods that do not involve knowing the status of the vehicle power/drivetrain (McTrans, 2012). Concurrently, Washburn is developing a new traffic microsimulation program that explicitly models the power/drivetrain components of vehicles and thus can utilize IOV-based EU&E models. Furthermore, emission rate models based on IOVs could, in the future, be incorporated into vehicle electronic control units (ECU) to enable provision of feedback to drivers regarding how vehicle operation affects emissions. The integration of OBD data into vehicle fuel use and emission models provides more capabilities for predicting EU&E based on vehicle activity.

This report describes the development of models for estimating vehicle fuel use and emission rates based on IOVs that can be obtained from OBD data, and to demonstrate that IOV parameters can provide estimates of engine power demand consistent with the VSP approach based on EOVs. In addition, this work is intended to evaluate the performance of models for estimating vehicle fuel use and emission rates based on IOVs, such as $P_{M\times R}$, compared to models based on EOVs, such as VSP. Additionally, this report describes the implementation of this IOV-based approach for estimating EU&E into a traffic microsimulation program. This implementation approach can be used as a model for other traffic microsimulation programs.

Objectives

The specific research objectives are to: (1) evaluate the concordance between IOV- and EOV-based predictors of engine power demand; (2) develop predictive models for vehicle EU&E based on IOVs; (3) evaluate models for vehicle EU&E based on IOVs by comparing to models based on EOVs; and (4) implement the new predictive models for emissions and fuel use based on IOV's into SwashSim, a traffic microsimulation software program.

Scope

The scope of work completed includes the following:

- Measurements were made for fuel use, CO_2, CO, HC, and NO_x.
- Measurements were made on ten selected light-duty gasoline vehicles, including six passenger cars (PCs) and four passenger trucks (PTs).
- IOV- and EOV-based predictive models were developed for fuel use and emissions of CO, HC, and NO_x for each of the ten selected vehicles.

- Typically less than five percent of total data collected were excluded after quality assurance screening.
- Incorporation of test vehicles into a traffic microsimulation program, SwashSim. This includes characteristics such as dimensions, drive/powertrain details, and EU&E IOV-based models.

The work here focused on specific light-duty gasoline vehicles, and thus did not include a variety of other types of vehicles in the United States.

Part II: Development of Vehicle-Specific Fuel Use and Emissions Models Based on Internally Observable Activity Data

Method

Measurements and modeling were made on ten light-duty gasoline vehicles. The methodology includes study design, instruments, data collection, quality assurance and quality check, and data analysis.

Study Design

Field measurements of 10 light-duty gasoline vehicles have been conducted, including 6 passenger cars (PCs) and 4 passenger trucks (PTs). The selected vehicles vary by age, mileage, and engine displacement. Specifications of the selected vehicles are shown in Table 2-1. On average, the 4 PTs have 80% higher engine displacement, 70% higher curb weight, and 30% lower rated combined fuel economy compared to the 6 PCs.

For each vehicle, data were collected based on 110 miles of driving on four routes in the Raleigh, NC and Research Triangle Park, NC area, which is shown in Figure 2-1. These routes were designed in a prior study and that are used as a consistent basis for measuring vehicle activity, energy use, and emissions (Frey *et al.*, 2008). Routes A and C are alternative paths between North Carolina State University (NCSU) and North Raleigh (NR), and Routes 1 and 3 are alternative paths between NR and RTP. Routes A and 3 are comprised of major and minor arterials. Routes C and 1 additionally include freeway segments. These routes include local, minor arterial, major arterial, and freeway roads, with speed limits ranging from 25 mph to 70 mph. The selected routes have road grades ranging between plus and minus 10 percent. Thus, vehicle data collection includes a wide range of road types, traffic conditions, speed, acceleration, and grade.

Table 0-1 Specifications of Ten Selected Measured Vehicles

Year	Make	Model	Type[a]	Number of Cylinders	Engine Displace-ment (liters)	Curb Weight (lb)	Combined Rated Fuel Economy (mpg)
2005	Mazda	6	PC	4	2.3	3200	23
2008	Chevrolet	Impala	PC	6	3.5	3600	22
2004	Pontiac	Grand Am GT	PC	6	3.4	3100	21
2001	Volvo	S40	PC	4	1.8	2800	23
2009	Honda	Civic	PC	4	1.8	2800	29
1998	Buick	Century	PC	6	3.1	3300	21
2002	Chevrolet	Silverado	PT	8	4.8	4900	16
2011	Ford	F150	PT	8	4.6	5000	17
1998	Chevrolet	S10	PT	6	4.3	4600	16
2004	Chevrolet	Tahoe	PT	8	5.3	6800	16

[a] *Vehicle type: PC = Passenger Car, including sedans; PT = Passenger Truck, including SUVs and pickup trucks.*

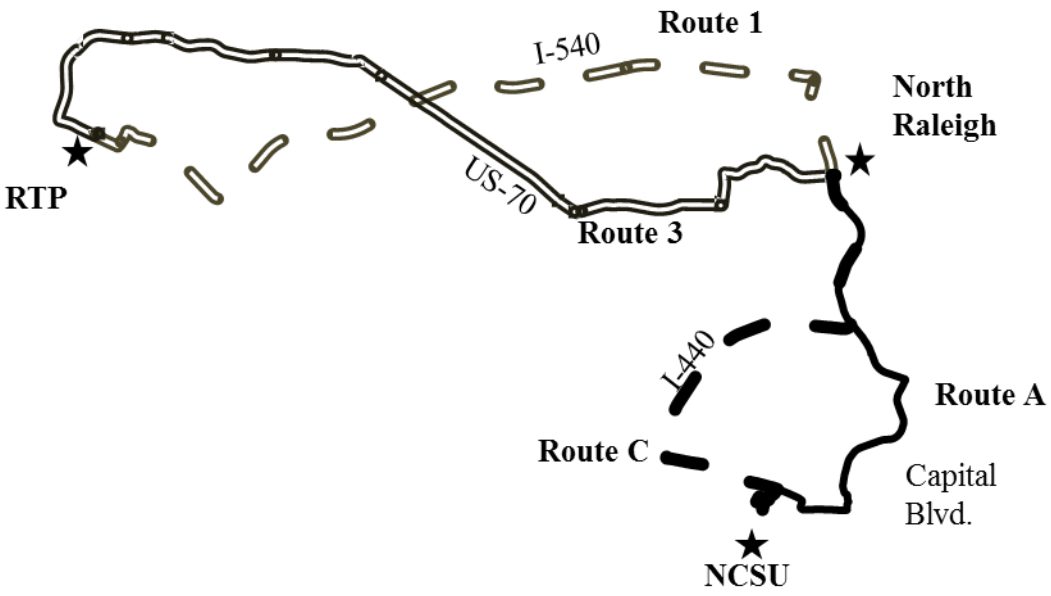

Figure 0-1 Map of the Selected Routes in Raleigh and Research Triangle Park (RTP) Area.

Instruments

The following instruments were used during the measurements:

- An OBD scan tool
- A portable emission measurement systems (PEMS)
- Multiple Garmin 76CSx global position system (GPS) receivers.

More details on each of the key instruments are given below.

On-Board Diagnostic Scantool

An OBD scantool, OBD Pro hardware and ScanPro software, was used to obtain OBD parameters at approximately 1 Hz frequency, including MAP, RPM, intake air temperature (IAT), vehicle speed, mass air flow (MAF) and mass fuel flow (MFF) for the 10 selected vehicles. The OBD scantool was connected to the vehicle OBD-II port and read selected OBD parameters via the vehicle electronic control unit. A laptop was used to record the data. Figure 2-2 shows the OBD scantool.

Portable Emission Measurement System

The OEM-2100 Axion PEMS manufactured by GlobalMRV was used to measure the exhaust composition. The Axion system is comprised of two parallel five-gas analyzers and an on-board computer. The two parallel gas analyzers simultaneously measure the exhaust volume percentage of CO, carbon dioxide (CO_2), and HC using non-dispersive infrared (NDIR) , and nitric oxide (NO) and oxygen (O_2) using electrochemical cell.

The measured exhaust emission concentrations for the same type of PEMS were compared to a reference method by Battelle (2003) using a chassis dynamometer. The measured concentrations for CO_2, CO, and NO from PEMS were within 10% of the reference method. For HC, the concentrations from PEMS were biased low by a factor of approximately 2 due to difference in detection methods.

Prior to each measurement, the Axion System gas analyzers were calibrated using a BAR-97 high concentration calibration gas mixture. During measurement, the gas analyzers were "zeroed" using ambient air every 10 minutes to prevent instrument drift (Frey *et al*., 2008).

The Axion System is designed to measure emissions during the actual use of the vehicle or equipment in its regular daily operation. The monitoring system weighs approximately 35 lbs. The system typically runs on 12V DC vehicle electricity. The power consumption is 5 to 8 Amps. Figure 2-3 shows the deployment of the Axion PEMS in the vehicle, and the connection of the Axion PEMS exhaust sampling line to the vehicle exhaust.

(a) Vehicle OBD-II Connection

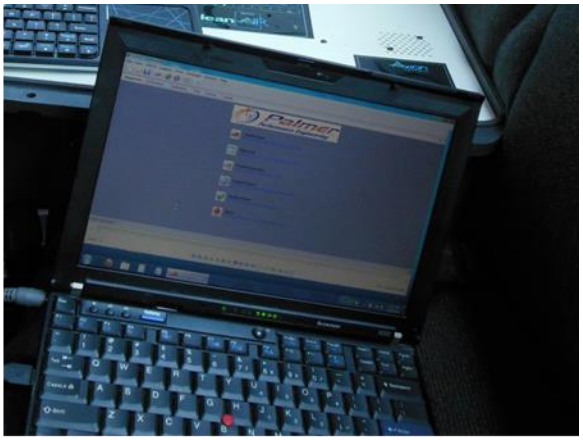

(b) OBD Laptop

Figure 0-2 Pictures of On-Board Diagnostics Connection and Data Acquisition Laptop.

(a) PEMS Inside the Vehicle

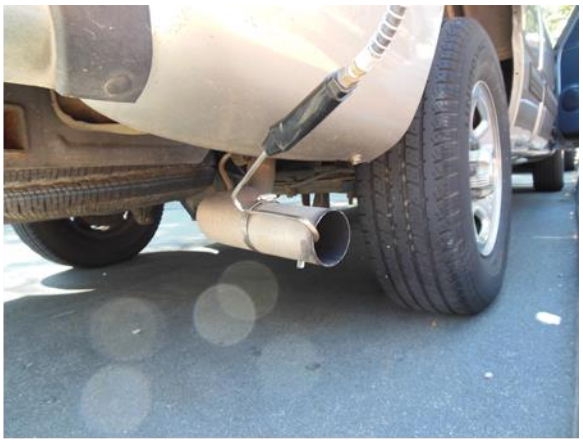

(b) PEMS Exhaust Sampling Line Connected to the Vehicle Exhaust Pipe

Figure 0-3 Pictures of Portable Emission Measurement System (PEMS).

Garmin Global Position System Receivers

Garmin 76CSx GPS receivers with barometric altimeter were used to record vehicle position and elevation. The GPS receivers measure position to within ±3 meters. Relative changes in elevation are measured within ±1 meter. Road grades for every non-overlapping consecutive 0.1 mile segment were inferred based on the method demonstrated elsewhere (Boroujeni and Frey, 2014). Figure 2-4 shows the deployment of GPS receivers during measurements.

Figure 0-4 Pictures of Garmin Global Position System (GPS) Receivers.

Data Collection

Preparation for field data collection included verification of the status of the PEMS, verification that all the parts and equipment were available, and laboratory calibration of the PEMS. Taking field measurements consisted of the installation of the instrumentation into a vehicle, data collection, and decommissioning.

Typically a vehicle started from NCSU, and was driven along Route A to North Raleigh and then along Route 1 to RTP. Afterwards, the vehicle returned to North Raleigh and NCSU following Route 1 and A. The vehicle then was driven to North Raleigh and RTP again following Route C and 3, and returned via Route 3 and C. The entire measurement took about 4 hours per vehicle.

Quality Assurance

The data measured from the PEMS, OBD, and GPS receivers were synchronized and combined. For quality assurance purposes, the combined data set was screened to check for errors or possible problems (Sandhu and Frey, 2013). Typical errors include unusual air-to-fuel ratio and negative emissions values. The errors were either corrected or the errant data records were not used for data analysis.

Data Analysis

For all vehicles, MFF was reported by the OBD. The 1 Hz exhaust mass flow rate was estimated based on carbon balance using MFF, exhaust mole fractions of CO_2, CO, and HC, molecular weight of fuel, and weight percent of carbon in the fuel. Based on exhaust flow rate and pollutant concentrations in the exhaust, time-based emission rates of each pollutant were estimated (Frey *et al.*, 2008).

For the purpose of evaluating the concordance between IOVs and EOVs as indicators of engine power demand, the relationship between $P_{M\times R}$ and VSP was assessed. For light-duty vehicles, VSP is estimated based on vehicle speed, vehicle acceleration, and road grade:

$$VSP = v(1.1a + 9.81r + 0.132) + 0.000302v^3 \quad (2\text{-}1)$$

Where: *VSP* is vehicle specific power (kW/ton); *v* is vehicle speed (m/s); *a* is vehicle acceleration (m/s^2); and *r* is road grade (slope). The relationship between $P_{M\times R}$ and VSP was evaluated.

A previously developed VSP-based modelling approach (Frey *et al*., 2002; Zhang, 2006) was used to estimate vehicle exhaust emissions. In this approach, VSP values were stratified into 14 bins and the average fuel use and emission rates were estimated for each of the 14 VSP bins. For each VSP value, the average fuel use and emission rates were compared with the measured rates. A linear regression between the estimated average rates and the measured rates was used to evaluate the performance of the VSP-based model.

The relationship between fuel flow and engine variables for a stoichiometric gasoline engine can be inferred based on factors that affect engine air flow. Engine air flow is proportional to $P_{M\times R}$, as indicated by the commonly used "speed-density" method (Taylor, 1985; Vojtisek-Lom and Cobb, 1998). Engine air flow is also influenced by engine displacement, number of strokes per cycle, IAT, and engine volumetric efficiency. However, for a given engine with fixed engine displacement and number of strokes per cycle, IAT and engine volumetric efficiency tend to have much less relative variability than MAP and RPM; thus, the 1 Hz variability in engine air flow is mostly influenced by variability in MAP and RPM.

Conventional gasoline engines typically run at stoichiometric combustion conditions with a few exceptions related to cold starts and high power demand during a trip (Heywood, 1998). A cold start typically lasts for only a few minutes (Sentoff *et al*., 2010). High power demand can occur in association with travel at high speed, at high acceleration, during hill climbing, or combinations of these but typically lasts only for a few seconds (Frey *et al*., 2008). Thus, for most periods during a trip the engine runs stoichiometric and the fuel flow rate is proportional to engine air flow, which in turn is proportional to $P_{M\times R}$. Therefore, relationships between fuel use rates and each of MAP, RPM, and $P_{M\times R}$ were investigated.

In previous work, various model function forms were evaluated for predicting fuel use and emission rates based on OBD data (Frey *et al*., 2010). However, based on the data collected for the 10 measured vehicles, the fuel use and emission rates of CO, HC, and NO_x typically follow a power trend over $P_{M\times R}$, as shown later. Therefore, a multiplicative model was used:

$$m_{i,pred}^{(2)} = b(P_{M\times R})^n \quad (2\text{-}2)$$

Where: $m_{i,pred}^{(2)}$ is a mass flow rate of species *i* predicted by Equation (2-2); *i* is either fuel use, CO, HC, or NO_x; and *b* and *n* are fitted scaling and power parameters, respectively.

For models based on Equation (2-2), a log-transformation technique was used to estimate the scaling and power parameters. However, bias is introduced when transforming back from the logarithm unit to the original arithmetic unit. Therefore, a log-transformation bias correction factor, C_{log}, was used per the method demonstrated in (Newman, 1993):

$$m_{i,pred}^{(3)} = b(P_{M\times R})^n \times C_{\log} \tag{2-3}$$

Where: $m_{i,pred}^{(3)}$ is a mass flow rate of species *i* predicted by Equation (2-3); and C_{log} is the log-transformation bias correction factor. After log-transformation bias correction, the fuel use and emission rates at 1 Hz rate were predicted based on Equation (2-3). However, because a log-transformation in effect leads to an estimate of the median value, rather than mean values, an additional bias correction is needed (Frey *et al*., 2010). For the purpose of bias correction, a linear regression was conducted between the Equation (2-3) predicted fuel use and emission rates and measured rates. The form of this bias correction, including the bias correction slope a' and bias correction intercept b', is:

$$m_{i,pred}^{(3)} = a' \times m_{i,measure} + b' \tag{2-4}$$

Where: $m_{i,measure}$ is the measured mass flow rate of species *i*; and a' and b' are fitted slope and intercept, respectively. Taken into account the analysis steps of Equations (2-3) and (2-4), Equation (2-3) may be written as:

$$m_{i,pred}^{(5)} = b(P_{M\times R})^n \times C_{\log}^{'} - C'' \tag{2-5}$$

Where: $m_{i,pred}^{(5)}$ is the predicted mass flow rate of species *i* based on Equation (5); $C_{\log}^{'}$ is the ratio of C_{log} over a'; and C'' is the ratio of b' over a'. Thus, Equation (2-5) is a bias corrected version of Equation (2-3). Equation (2-5) was used as the final form in predicting fuel use and emission rates based on $P_{M\times R}$.

As an evaluation of goodness-of-fit, the predicted value from Equation (2-5) was compared to the measured value using a parity plot, in which each second of predicted value is plotted versus the corresponding measured value. A linear trend line was fit to the parity plot to assess goodness-of-fit. If the fit is ideal, then the trend line would have a slope of 1 and an intercept of 0. Thus, the goodness-of-fit was evaluated, in part, based on the R^2 and standard error of the following:

$$m_{i,pred}^{(5)} = 1 \times m_{i,measure} + 0 \tag{2-6}$$

As described later, a substantial portion of the 1 Hz exhaust concentrations were below the gas analyzer detection limit, especially for CO and HC, for some vehicles. As long as the mean value of the emission factor is for a concentration that is above the detection limit, the mean value is usually robust to the presence of non-detected measurements (Frey and Zhao, 2004). However, if the mean emission rate is associated with a measured concentration below the detection limit, then

the resulting regression model will be subject to large relative random errors and will typically have a poor predictive capability, low R^2, and high residual standard error. Thus, as will be shown later, models with very poor goodness-of-fit are typically associated with a high proportion of very low exhaust concentrations. Conversely, models fit to data with a high proportion of measured exhaust concentrations above the detection limit are expected to be statistically significant and to have better explanatory capability.

Results

For each of the 10 vehicles, typically more than 12,500 seconds of valid data were collected, which account for more than 95 percent of raw data from the field measurements. Errant data, primarily due to unusual air-to-fuel ratio, were excluded from the analysis.

The results section includes an example of a 2005 Chevrolet Tahoe to demonstrate development of the models, and a synthesis summary of the evaluation of the models based on all 10 vehicles.

Example Detailed Results for a 2005 Chevrolet Tahoe

A 2005 Chevrolet Tahoe is taken as an example to demonstrate the relationship between IOVs versus EOVs, and the relationship between fuel use and emission rates versus $P_{M\times R}$.

Internally versus Externally Observable Variables

The relationship between $P_{M\times R}$ versus VSP is illustrated in Figure 3-1. Average $P_{M\times R}$ values are plotted versus VSP ranging from -30 to 30 kW/ton with a 1 kW/ton interval. This range accounts for over 99% of measured vehicle activity. At negative VSP, there is no load on the engine and, thus, $P_{M\times R}$ is approximately constant. For increasing positive VSP, $P_{M\times R}$ typically increases monotonically.

A regression analysis was conducted for $P_{M\times R}$ versus VSP for positive VSP values, as shown in Figure 3-1(b):

$$P_{M\times R} = 38100 \times VSP^{0.42}, \text{ for VSP>0, } R^2 = 0.97 \qquad (2\text{-}7)$$

$P_{M\times R}$ is 32,000 kPa-rev/min for negative VSP, and is corrected to no less than 32,000 kPa-rev/min for positive VSP. The p-values for the estimated scaling parameter of 38,100 and power parameter of 0.42 are both less than 0.001, indicating statistical significance. $P_{M\times R}$ is highly correlated with VSP. Thus, $P_{M\times R}$ is a good surrogate for engine power demand for this vehicle.

Fuel Use and Emission Rates versus Externally Observable Variables

The VSP-based approach for predicting fuel use and emission rates is illustrated in Figures 3-2(a) through 3-2(d). For each VSP bin, there is substantial variability in fuel use and emission rates, as described in the box and whiskers based on the 2.5-percentile, 25-percentile, 75-percentile, and 97.5-percentile of one second values within each VSP bin. The R^2 for fuel use and emissions of CO, HC, and NO_x are 0.75, 0.32, 0.54, and 0.51, respectively. Thus, VSP is shown to be a good basis for estimating fuel use, and is able to explain some of the variability in 1 Hz emission rates. Furthermore, VSP is accurate in quantifying the mean trend in these rates.

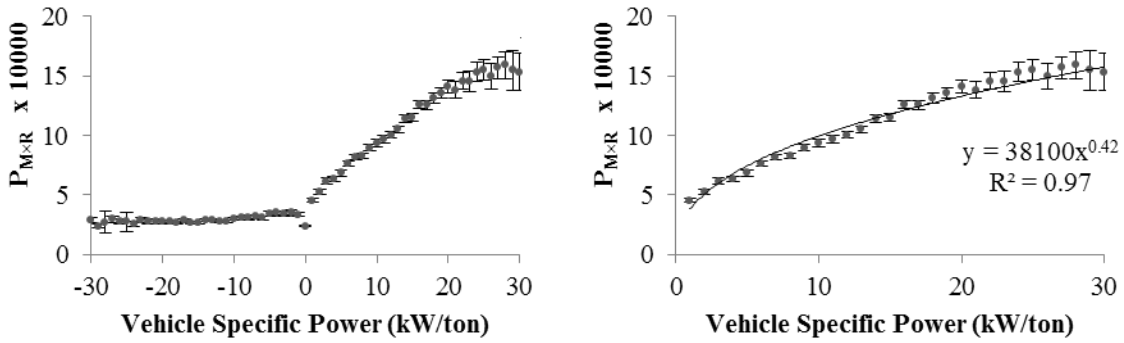

(a) Product of MAP and RPM versus Vehicle Specific Power

(b) Product of MAP and RPM versus Positive Vehicle Specific Power

Figure 2-5 Measured product of Manifold Absolute Pressure (MAP) and engine Revolutions per Minute (RPM) versus Vehicle Specific Power (VSP) for a 2005 Chevrolet Tahoe. Error bars indicate 95 percent confidence intervals.

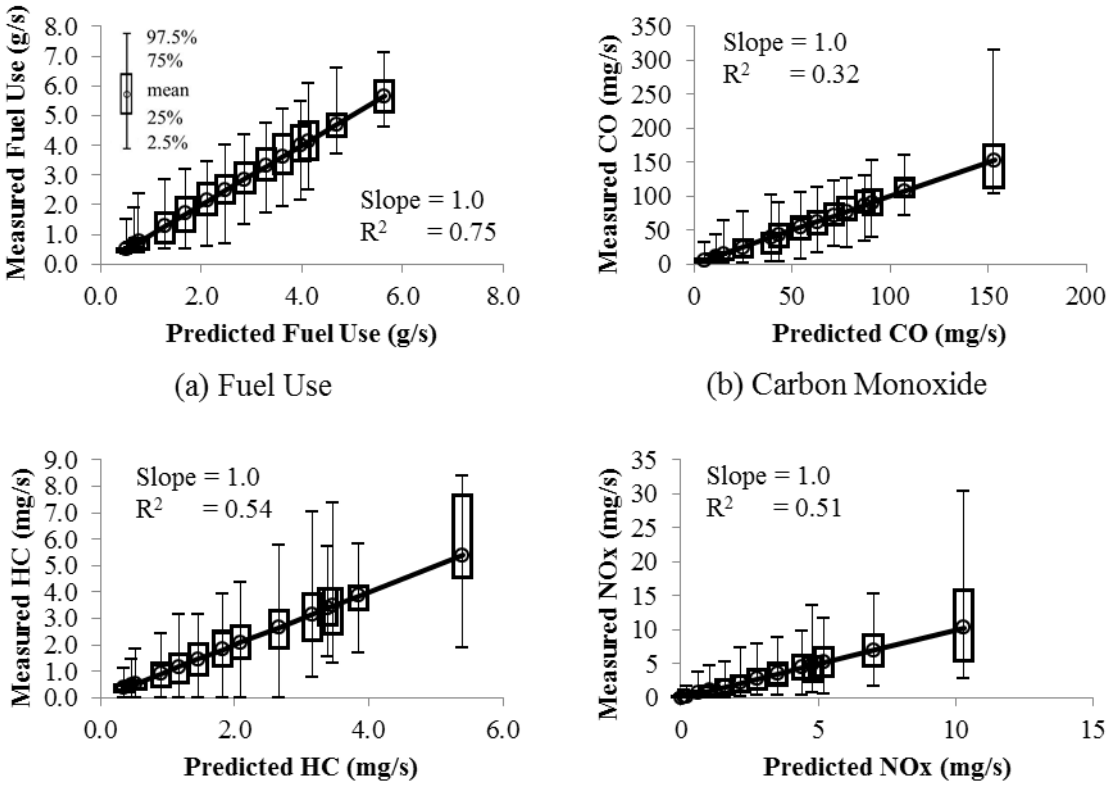

(a) Fuel Use

(b) Carbon Monoxide

(c) Hydrocarbon

(d) Nitrogen Oxides

Figure 2-6 Comparison between measured and predicted fuel use and emission rates based on the Vehicle Specific Power-based model for a 2005 Chevrolet Tahoe measured during 110 miles of driving in the Raleigh, NC area.

Fuel Use versus Internally Observable Variables

Fuel use rates are proportional to each of MAP and RPM, as illustrated in Figures 3-3(a) and 3-3(b), respectively. The coefficients of determination for fuel use as a power function of MAP and RPM are 0.66 and 0.76, respectively. The p-values for the scaling and power parameters for both power regressions were less than 0.001, indicating statistical significance. Therefore, each of MAP and RPM can be an explanatory variable for fuel use, explaining a substantial amount of the variation in fuel use.

However, although fuel use rate is influenced by each of RPM and MAP, the variability in fuel use rate is better explained by $P_{M\times R}$, as shown in Figure 3-3(c). Based on Equation (2), and as shown in Figure 3-3(c), the fitted equation for fuel use rate versus $P_{M\times R}$ is:

$$m_{Fuel,pred}^{(2)} = 5.1\times10^{-6}\times(P_{M\times R})^{1.14},\ R^2 = 0.98 \quad (2\text{-}8)$$

The p-values for both the scaling parameter of 5.1×10^{-6} and power parameter of 1.14 are less than 0.001, indicating statistical significance. After log-transformation bias correction, the model in the form of Equation (2-3) is:

$$m_{Fuel,pred}^{(3)} = 5.1\times10^{-6}\times(P_{M\times R})^{1.14}\times1.01 \quad (2\text{-}9)$$

The numerical value of "1.01" is the log-transformation bias correction factor. The fuel use rates predicted by Equation (2-9) versus measured rates are compared and a linear regression fit is conducted based on Equation (2-4):

$$m_{Fuel,pred}^{(3)} = 1.01\times m_{Fuel,measure} - 0.001 \quad (2\text{-}10)$$

Based on the fitted slope of 1.01 and intercept of –0.001 in Equation (2-10), and by substitution of Equation (2-9) into Equation (2-10), the predicted fuel use with bias corrections in terms of $P_{M\times R}$ in the form of Equation (2-5) is:

$$m_{Fuel,pred}^{(5)} = 5.1\times10^{-6}\times(P_{M\times R})^{1.14}\times1.00-(-0.001) \quad (2\text{-}11)$$

The numerical values of "1.00" and "–0.001" are the correction factors. Equation (2-11) is used for predicting fuel use rates based on $P_{M\times R}$ for this vehicle.

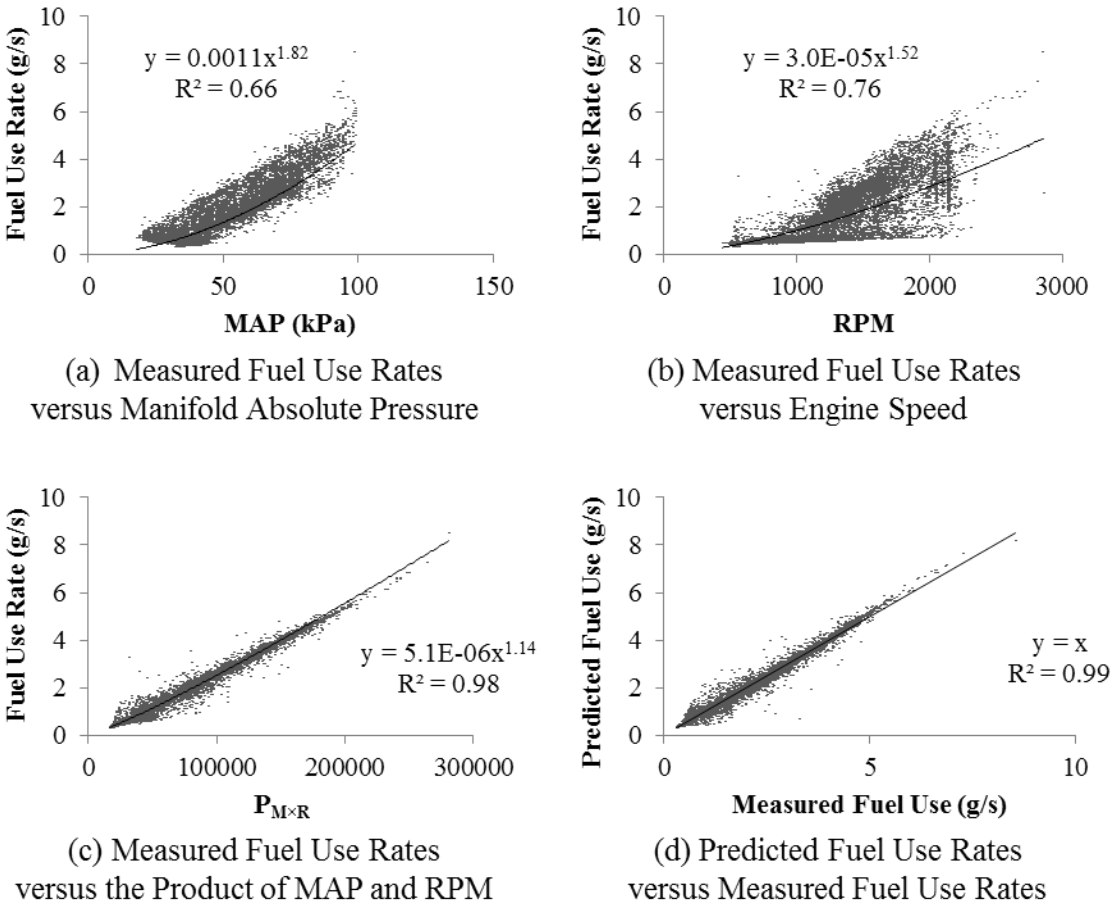

Figure 2-7 Measured fuel use rates versus (a) Manifold Absolute Pressure (MAP) (b) engine Revolutions Per Minute (RPM), (c) the product of MAP and RPM, and (d) the predicted versus measured fuel use rates for a 2005 Chevrolet Tahoe measured during 110 miles of driving in the Raleigh, NC area.

A parity plot comparison between the Equation (2-11) predicted versus measured fuel use rates is shown in Figure 3-3(d), based on Equation (2-6). The data points follow a linear trend. The slope is 1 and the intercept is 0. The standard deviation of the residuals is 0.14 mg/s, which is small compared to mean fuel use rates of 1.5 mg/s. The R^2 for the linear fit is 0.99. The R^2 value of 0.99 is a significant improvement compared to the R^2 value of 0.75 based on the VSP-based approach. Therefore, the IOV-based model performs better than the EOV-based modal. There are some artifacts of the scatter plot that imply that the residual error may have non-constant variance with respect to the magnitude of fuel use rate. For very high fuel use rate the sample size is very small. Therefore, the "fit" for fuel use rates higher than about 6 g/s may not seem as "good" as for smaller values. However, from a practical perspective, this model is highly effective in predicting fuel use rate without any average bias.

Emission Rates versus Internally Observable Variables

The relationships between emission rates of CO, HC, and NO_x versus and $P_{M\times R}$ are shown in Figures 3-4(a), 3-4(c), and 3-4(e), respectively. For CO, most of the data points follow a power trend. A small portion of data has much higher CO emission rates compared to the fitted model. For this vehicle, some of the CO emission rates were relatively high, ranging up to approximately 1,000 mg/sec. However, CO emission rates were higher than 200 mg/sec only 0.7% of time. These very high emission rates are likely to be from short duration events in which the air-to-fuel ratio was commanded by the ECU to run fuel rich to prevent the catalytic converter from overheating, also known as "open-loop" operation, and thus this cluster of data is a different operating condition than the vast majority of the entire dataset. A regression model based solely on $P_{M\times R}$ is not able to predict this cluster of very high emitting values as a distinct emissions event from the main trend for over 99% of the data set. Thus, the data are stratified. For measured CO emission rates of less than 200 mg/s, the IOV model based on $P_{M\times R}$ for CO emission rates is developed similarly to the model for fuel use rates. The model in the form of Equation (2-5) is:

$$m_{CO,pred}^{(5)} = 3.0\times10^{-7}\times(P_{M\times R})^{1.64}\times1.11-0.78,\ R^2 = 0.75 \qquad (2\text{-}12)$$

The numerical values of "1.11" and "0.78" are the bias correction factors. Both the fitted scaling parameter of 3.0×10^{-7} and the power parameter of 1.64 have p-values of less than 0.001, indicating statistically significance.

For the cluster of high emitting "open-loop" data that were separated from the main data set, the model is:

$$m_{CO-OL,pred}^{(5)} = 0.034\times(P_{M\times R})^{0.84}\times2.6-640,\ R^2 = 0.48 \qquad (2\text{-}13)$$

Where: $m_{CO-OL,pred}^{(5)}$ is the predicted CO emission rate for "open-loop" data based on Equation (2-5). The parity plot for this model had an R^2 of 0.47 and a standard error of 220 mg/sec, which is approximately 49% of the mean emission rate for this stratum of data. The model of Equation (2-13) would be selected based on an IOV that indicates "open-loop" events. Such IOVs are available internally in the ECU although they are not typically broadcast via the OBD interface.

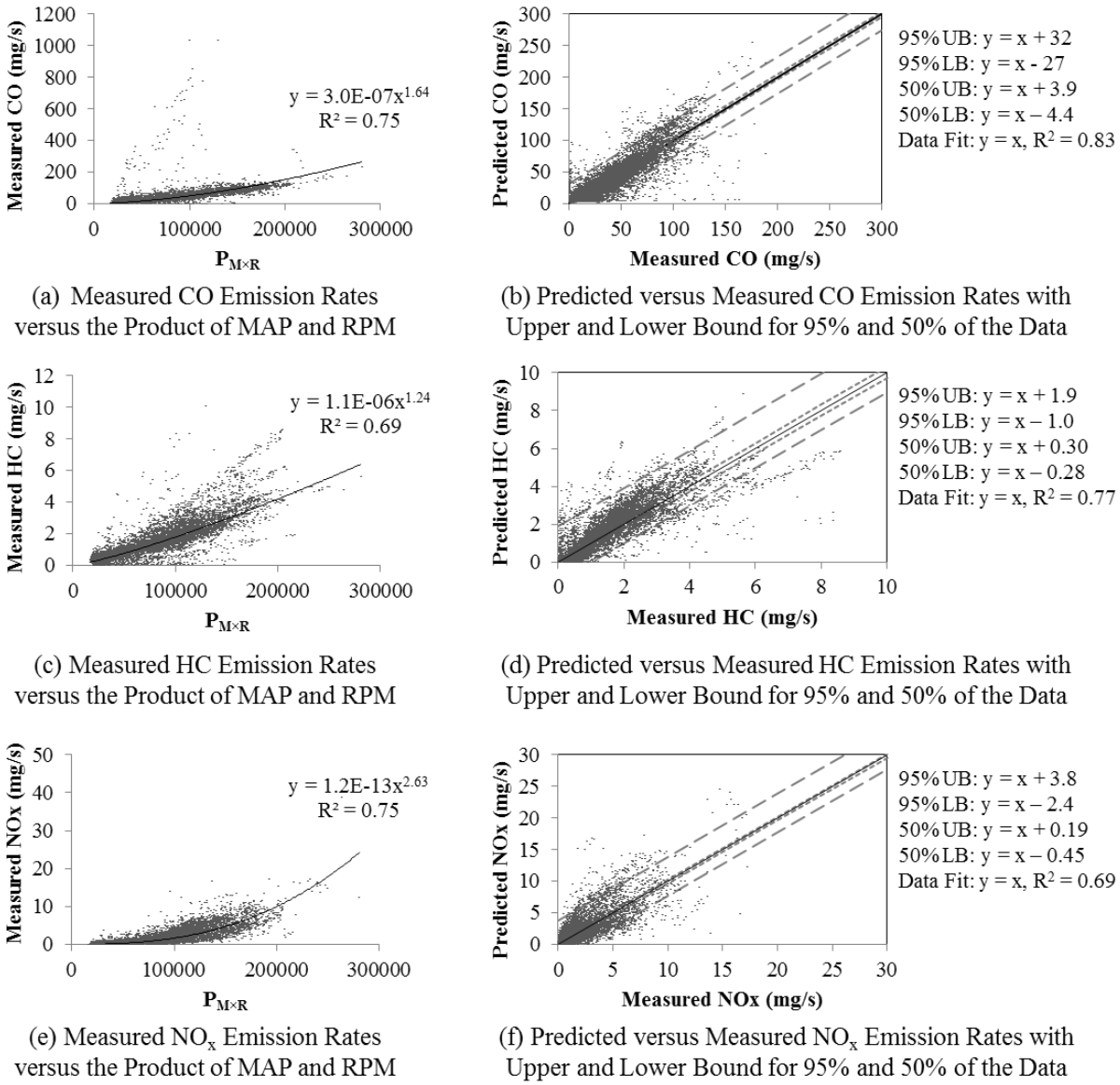

(a) Measured CO Emission Rates versus the Product of MAP and RPM

(b) Predicted versus Measured CO Emission Rates with Upper and Lower Bound for 95% and 50% of the Data

(c) Measured HC Emission Rates versus the Product of MAP and RPM

(d) Predicted versus Measured HC Emission Rates with Upper and Lower Bound for 95% and 50% of the Data

(e) Measured NO_x Emission Rates versus the Product of MAP and RPM

(f) Predicted versus Measured NO_x Emission Rates with Upper and Lower Bound for 95% and 50% of the Data

Figure 2-8 Relationship between emission rates and the product of Manifold Absolute Pressure (MAP) and engine Revolutions Per Minute (RPM) and comparison between predicted and measured emission rates for a 2005 Chevrolet Tahoe measured during 110 miles of driving in the Raleigh, NC area.

A comparison of Equation (2-12) predicted versus measured CO emission rates is shown in Figure 3-4(b). The data fit a line with slope of 1 and the intercept of 0. The R^2 value of 0.83 is a significant improvement compared to the R^2 value of 0.32 for the VSP-based model shown in Figure 3-2(b). The VSP model includes the high emitting portion of the data set that was excluded from the regression model of Equation (2-12). However, Equation (2-13) also has a good fit and thus the IOV-based approach, coupled with an IOV to distinguish between closed-loop and open-loop control of the air-to-fuel ratio, would cover the same overall data as the VSP model. Although the

scatter plot gives the impression that the fitted model may not be very good, this impression is somewhat misleading. In fact, a large proportion of the data are clustered very close to the fitted line. As shown in Figure 3-4(b), the 50 percent frequency range of the residuals of the parity plot are so close to the parity line that the upper and lower bound of this 50 percent frequency range is barely different than the parity line, and the 50 percent range is approximately ±4 mg/s. This is a very small range compared to the mean emission rates of 30 mg/s. The 95 percent frequency range is also shown. The standard deviation of the residuals is 14 mg/s. Thus, the high R^2 of this model reflects that most of the predicted values are closely clustered toward the measured values.

Figure 3-4(c) illustrates the relationship between measured HC emission rates versus $P_{M\times R}$. There appear to be several clusters in this scatter plot. The majority of HC emission rates ranging from 0 to approximately 6 mg/s follow a power trend versus $P_{M\times R}$. There also appear approximately 3 more clusters each containing a small portion of data. Two clusters have higher HC emission rates than the fitted model, such as about 6 to 8 mg/s and about 4.5 to 6 mg/s at $P_{M\times R}$ of 150,000 to 200,000 kPa-rev/min. There is also a cluster of data with lower HC emission rates than the fitted model, such as approximately 1 to 2 mg/s at $P_{M\times R}$ of 150,000 to 200,000 kPa-rev/min. Therefore, at $P_{M\times R}$ higher than 150,000 kPa-rev/min, four clusters of data appear. This vehicle has 4-gear automatic transmission. These clusters might be associated with gear selection. For example, an exploration analysis is conducted for data with $P_{M\times R}$ ranging from 150,000 to 200,000 kPa-rev/min. The HC emission rates are stratified into four sub-groups: from 0 to 2 mg/s, from 2 to 4.5 mg/s, from 4.5 to 6 mg/s, and higher than 6 mg/s. The average values of MAP decrease and the average values of RPM increase for the four sub-groups with increasing HC emission rates. Therefore, higher HC emission rates might be associated with higher RPM with lower gear. Although stratification of these data might be possible based on additional IOVs, these clusters cannot be discriminated based on $P_{M\times R}$ alone. For all data, the fitted model is:

$$m_{HC,pred}^{(5)} = 1.1\times10^{-6}\times(P_{M\times R})^{1.24}\times1.43-0.35,\ R^2 = 0.69 \qquad (2\text{-}14)$$

The numerical values of "1.43" and "0.35" are the bias correction factors. Both the fitted scaling parameter of 1.1×10^{-6} and the power parameter of 1.24 have p-values of less than 0.001, indicating statistical significance. This R^2 is sufficiently high to imply that the clusters identified above are not substantially compromising the mean explanatory capability of this fitted model.

A comparison of Equation (14) predicted versus measured HC emission rates is shown in Figure 3-4(d). The R^2 is 0.77 and is a significant improvement compared to the R^2 of 0.54 based on the VSP-based model, as illustrated in Figure 3-2(c). Therefore, the IOV-based model describes the HC emission rates well, and is better than the EOV-based model. The standard deviation of the residuals of this model is 0.71 mg/sec, which is 60 percent of the mean measured emission rate of 1.2 mg/sec. The 50 percent frequency range of the residuals is very close to the parity line, ranging within only ±0.3 mg/sec of the predicted value. The 95 percent frequency range of the residuals is also shown.

The relationship between measured NO_x emission rates versus $P_{M\times R}$ is illustrated in Figure 3-4(e). The data appear to follow a power trend. The fitted model is:

$$m_{NOx,\,pred}^{(5)} = 1.2\times10^{-13}\times(P_{M\times R})^{2.63}\times1.39-0.32\,,\ R^2 = 0.75 \qquad (2\text{-}15)$$

The numerical values of "1.39" and "0.32" are the bias correction factors. Both the fitted scaling parameter of 1.2×10^{-13} and the power parameter of 2.63 have p-values of less than 0.001, indicating statistical significance.

A comparison of Equation (2-15) predicted and measured NO_x emission rates is shown in Figure 3-4(f). The R^2 is 0.69, which is better than the R^2 of 0.51 of the VSP-based model illustrated in Figure 3-2(d). Therefore, the IOV-based model is better than the EOV-based model in predicting NO_x emission rates. The 50 percent frequency range of the residuals is within ±0.5 mg/s, compared to a mean measured emission rate of 1.6 mg/sec. The standard deviation of the residuals is 1.4 mg/s. The apparent broad clustering of the scatter plot for values less than about 8 mg/sec is a visual artifact, since scatter plots are not effective at depicting the relative frequency of clustering for overlapping data. The data are in fact highly clustered around the fitted model.

Synthesis Summary for All Vehicles

Each of the 10 measured vehicles has been analyzed similar to the Chevrolet Tahoe demonstrated above. Table 3-1 shows a synthesis summary of the coefficients of determination for the fitted models for IOVs versus EOVs, and for the fit between each of the IOV-based and EOV-based predicted rates versus measured rates for each of fuel use and emissions. For all 10 vehicles, the coefficients of determination for the power regression between $P_{M\times R}$ and VSP are 0.94 or higher. For all vehicles, the p-values for both the fitted scaling and power parameters are less than 0.001, indicating statistical significance. Therefore, $P_{M\times R}$ and VSP are closely related. For negative VSP values, $P_{M\times R}$ is approximately constant, but varies depending among vehicles from 32,000 kPa-rev/min to 45,100 kPa-rev/min.

For fuel use, the coefficients of determination for the IOV-based model predicted versus measured rates are 0.92 or higher. For the EOV-based models, the coefficients of determination for the relationship between predicted and measured fuel use rates range from 0.53 to 0.75. Therefore, in predicting fuel use rates, the models using IOVs as explanatory variables perform better than the models using EOVs as explanatory variables.

Table 2-2 Coefficients of Determination (R^2) for Internally Observable Variable (IOV) versus Externally Observable Variable (EOV) and for Each of IOV-Based and EOV-Based Model Predicted versus Measured Fuel Use and Emission Rates for 10 Measured Vehicles

Vehicle	$P_{M\times R}$ vs. Positive VSP[a]	Fuel Use		CO		HC		NO_x	
		IOV Based Model[b] vs. Measured	EOV Based Model[c] vs. Measured	IOV Based Model vs. Measured	EOV Based Model vs. Measured	IOV Based Model vs. Measured	EOV Based Model vs. Measured	IOV Based Model vs. Measured	EOV Based Model vs. Measured
		Coefficients of Determination (R^2)							
2005 Mazda 6	0.98	0.97	0.61	0.15	0.09	0.58	0.35	0.04	0.08
2008 Chevrolet Impala	0.97	0.92	0.62	0.02	0.01	0.32	0.20	0.10	0.14
2004 Pontiac Grand Am GT	0.99	0.98	0.74	0.03	0.02	0.49	0.22	0.05	0.13
2001 Volvo S40	0.99	0.97	0.66	0.13	0.11	0.001	0.10	0.30	0.27
2009 Honda Civic	0.98	0.95	0.71	0.03	0.04	0.51	0.34	0.18	0.18
1998 Buick Century	0.94	0.99	0.53	0.05	0.13	0.10	0.15	0.39	0.22
2002 Chevrolet Silverado	0.96	0.99	0.72	0.39	0.32	0.91	0.66	0.77	0.46
2010 Ford F150	0.95	0.99	0.68	0.06	0.03	0.67	0.43	0.24	0.16
1998 Chevrolet S10	0.97	0.98	0.68	0.04	0.03	0.23	0.10	0.26	0.20
2005 Chevrolet Tahoe	0.97	0.99	0.75	0.83	0.32	0.77	0.54	0.69	0.51

[a] *$P_{M\times R}$ is the product of Manifold Absolute Pressure (MAP) and engine Revolutions Per Minute (RPM), VSP is vehicle specific power.*
[b] *IOV based model uses $P_{M\times R}$ as explanatory variables.*
[c] *EOV based model uses VSP as explanatory variables.*

For CO, the coefficients of determination for the IOV-based models range from 0.02 to 0.83, with substantial variability among vehicles. For the EOV-based models, the coefficients of determination range from 0.01 to 0.32. For 8 out of 10 vehicles, the IOV-based models have higher R^2 compared to the EOV-based models, indicating that the IOV-based models would be better in predicting CO emission rates. However, for 8 vehicles, the IOV-based models have R^2 less than 0.15, indicating poor fit. One reason for this is that the measured CO concentrations are below the instrument detection limit for typically 40% to 80% of the 1 Hz emission rates for these vehicles. The high proportion of measurements below detection limit leads to random variability in the data, especially when the mean emission rate is associated with measured concentrations below the detection limit.

For HC, the coefficients of determination for the IOV-based models range from 0.23 to 0.91, except for a 2001 Volvo S40 and a 1998 Buick Century, for which the R^2 values are 0.001 and 0.10, respectively. The measured HC concentrations are below the detection limit for 54% and 96% of time for the Volvo and the Buick, respectively. The high proportion of data below detection limit leads to random variability. For the other eight vehicles, the IOV-based models perform better than the EOV-based models.

For NO_x, the coefficients of determination for the IOV-based models range from 0.18 to 0.77, except for a 2005 Mazda 6, a 2008 Chevrolet Impala, and a 2004 Pontiac Grand Am GT, for which the R^2 values are 0.04, 0.10, and 0.05, respectively. For the Mazda, the Chevrolet, and the Pontiac, 81%, 77%, and 87%, respectively, of the measured NO_x concentrations are below the detection limit. For the other seven vehicles, the IOV-based models have higher R^2 than the EOV-based models.

Overall, in terms of coefficients of determination, the models using IOVs as explanatory variables are typically better than the modals using EOVs as explanatory variables in predicting fuel use and emission rates. However, there are some limitations in the IOV-based models. The models are not predicting CO, HC, and NOx emission rates as well as fuel use rates. One reason is that a substantial proportion of the measured concentrations is below the detection limit, which leads to random variability (Sandhu and Frey, 2013). Another reason is that the models are developed based on tailpipe emissions, which are also influenced by the catalytic converter. Though such influence has been taking into account in the Comprehensive Modal Emissions Model (CMEM) developed by University of California Riverside (Barth *et al*., 1996), future exploration of an IOV modeling approach that might make use of additional IOVs, such as related to commanded fuel rich operation or catalyst temperature can be conducted, but such exploration would require addition in-use measurements.

Conclusions

IOV-based predictors of engine load, in particular $P_{M\times R}$, are highly correlated and concordant with EOV-based predictions, such as VSP, over a wide range of VSP. Furthermore, they are better predictors of fuel use and are typically better predictors of emission rates.

A method is demonstrated to predict fuel use and emission rates based on the use of IOVs, such as $P_{M\times R}$. Fuel use rates can be accurately estimated using the IOV-based model based on $P_{M\times R}$, and such models performs better than models using EOVs as explanatory variables. For CO, HC, and NO_x emission rates, the IOV-based model typically provides similar or better prediction than the EOV-based model, but the goodness-of-fit is subject to substantial variability among vehicles. Usually, the best fits are obtained for vehicles that have exhaust concentrations above the detection limit of the gas analyzer. Thus, models for low emitting vehicles tend not to be as good. However, from a policy perspective, there is typically more interest in how to identify and manage high emission rates. Thus, the trade-off between detection limit and goodness-of-fit is not a substantial problem in that there would be less need to manage emissions from vehicles that have low emission rates compared to vehicles that have high emission rates. IOV-based models of emission rates could be incorporated into the ECU to enable reporting feedback to drivers regarding their emission rates.

The product of MAP and RPM is shown to be highly predictive of CO, HC, and NO_x emission rates for the majority of measured vehicles. However, the detailed evaluation of model goodness-of-fit also indicates that there are opportunities to extend this work to improve model performance by incorporating other IOVs. For examples, IOVs related to open loop operation would help to explain episodic high CO emission rates. IOVs related to the choice of gear might also improve explanatory power, such as for HC emission rates. Nonetheless, models based on the readily available IOVs of MAP and RPM are shown to be effective in predicting fuel use with high precision and in predicting emission rates with high precision for emission rates above the gas analyzer detection limit. The models shown here will be incorporated into a new traffic simulation model. Further development of IOV-based models of emissions on a vehicle specific basis is recommended.

References

Barth, M., F. An, J. Norbeck, and M. Ross. Modal Emissions Modeling: a Physical Approach. Transportation Research Record: Journal of the Transportation Research Board, 1996, 1520: 81-88.

Battelle. Environmental Technology Verification Report: Clean Air Technologies International, Inc., Remote On-Board Emissions Monitor. Prepared by Battelle for U.S. Environmental Protection Agency, Ann Arbor, MI, 2003.

Boroujeni, B.Y. and H.C. Frey. Road Grade Quantification Based on Global Positioning System Data Obtained from Real-World Vehicle Fuel Use and Emissions Measurements. Atmospheric Environment, 2014, 85: 179-186.

Frey, H.C., A. Unal, J. Chen, S. Li, and C. Xuan. Methodology for Developing Modal Emission Rates for EPA's Multi-scale Motor Vehicle & Equipment Emission System. EPA420-R-02-02, Prepared by North Carolina State University for Office of Transportation and Air Quality, U.S. Environmental Protection Agency, Ann Arbor, MI, 2002.

Frey, H.C. and Y. Zhao. Quantification of Variability and Uncertainty for Air Toxic Emission Inventories With Censored Emission Factor Data. Environmental Science & Technology, 2004, 38(22):6094-6100.

Frey, H.C., K. Zhang, and N.M. Rouphail. Fuel Use and Emissions Comparisons for Alternative Routes, Time of Day, Road Grade, and Vehicles Based on In-Use Measurements. Environmental Science & Technology, 2008, 42(7): 2483-2489.

Frey, H.C., K. Zhang, and N.M. Rouphail. Vehicle-Specific Emissions Modeling Based Upon On-Road Measurements. Environmental Science & Technology, 2010, 44(9): 3594-3600.

Heywood, J.B. Internal Combustion Engine Fundamentals. Vol.930, McGraw-Hill, New York, 1998.

Jimenez-Palacios, J. Understanding and Quantifying Motor Vehicle Emissions and Vehicle Specific Power with TILDAS Remote Sensing. Doctoral Dissertation, Massachusetts Institute of Technology, Cambridge, MA, 1999.

McTrans Center, TSIS-CORSIM Software Package and Users Guides. Copyright 2007-2012, University of Florida, Portions Copyright 1995-2005, ITT Industries, Inc., Gainesville, FL.

Newman, M.C. Regression Analysis of Log-Transformed Data: Statistical Bias and Its Correction. Environmental Toxicology and Chemistry, 1993, 12: 1129-1133.

Sandhu, G.S. and H.C. Frey. Effects of Errors on Vehicle Emission Rates from Portable Emission Measurement Systems. Transportation Research Record: Journal of the Transportation Research Board, 2013, 2340: 10-19.

Sentoff, K.M., M.K. Robinson, and B.A. Holmen. Second-by-Second Characterization of Cold-Start Gas-Phase and Air Toxic Emissions from a Light-Duty Vehicle, Transportation Research Record: Journal of the Transportation Research Board, 2010, 2158: 95-104.

Taylor, C.F. The Internal-Combustion Engine in Theory and Practice. Vol.1, M.I.T. Press, Cambridge, Massachusetts, 1985.

U.S. EIA. Annual Energy Review, Energy Consumption Estimates by Sector, 1949-2012. U.S. Energy Information Administration, Washington, D.C., 2015.

U.S. EPA. The 2011 National Emissions Inventory. U.S. Environmental Protection Agency, Washington, D.C., 2015.

Vojtisek-Lom, M. and J.T. Cobb. On-road Light-duty Vehicle Emissions Measurements Using a Novel Inexpensive On-board Portable System. Proceedings of the 8th Coordinating Research Council (CRC) On-road Vehicle Emissions Workshop, San Diego, CA, April 20-22, 1998.

Washburn, S.S., N.M. Rouphail, and H.C., Frey. Emissions Modelling and Integration into Traffic Micro-Simulations. Southeastern Transportation Research, Innovation, Development and Education Center (STRIDE) Project 2012-014 Annual Report, Gainesville, FL, 2013.

Zhang, K. Micro-Scale On-Road Vehicle-Specific Emissions Measurements and Modeling. Doctoral Dissertation, North Carolina State University, Raleigh, NC, 2006.

Appendix A. Results for Measured Vehicles

A1 2005 Mazda 6

For the 2005 Mazda 6, more than 12,200 seconds of valid data were collected, which account for more than 95 percent of raw data from the field measurements.

A1.1 Internally versus Externally Observable Variables

The relationship between $P_{M\times R}$ versus VSP is illustrated in Figure A-1. Average $P_{M\times R}$ values are plotted versus VSP ranging from -30 to 30 kW/ton with a 1 kW/ton interval. This range accounts for over 99% of measured vehicle activity. At negative VSP, there is no load on the engine and, thus, $P_{M\times R}$ is approximately constant. For increasing positive VSP, $P_{M\times R}$ typically increases monotonically.

A regression analysis was conducted for $P_{M\times R}$ versus VSP for positive VSP values, as shown in Figure A-1(b):

$$P_{M\times R} = 58700 \times VSP^{0.39}, \text{ for VSP>0, } R^2 = 0.98 \qquad \text{(A1-1)}$$

$P_{M\times R}$ is 45,000 kPa-rev/min for negative VSP, and is corrected to no less than 45,000 kPa-rev/min for positive VSP. The p-values for the estimated scaling parameter of 58,700 and power parameter of 0.39 are both less than 0.001, indicating statistical significance. $P_{M\times R}$ is highly correlated with VSP. Thus, $P_{M\times R}$ is a good surrogate for engine power demand for this vehicle.

A1.2 Fuel Use and Emission Rates versus Externally Observable Variables

The VSP-based approach for predicting fuel use and emission rates is illustrated in Figures A-2(a) through A-2(d). For each VSP bin, there is substantial variability in fuel use and emission rates, as described in the box and whiskers based on the 2.5-percentile, 25-percentile, 75-percentile, and 97.5-percentile of one second values within each VSP bin. The R^2 for fuel use and emissions of CO, HC, and NO_x are 0.61, 0.09, 0.35, and 0.08, respectively. Thus, VSP is shown to be a good basis for estimating fuel use, and is able to explain some of the variability in 1 Hz emission rates. Furthermore, VSP is accurate in quantifying the mean trend in these rates.

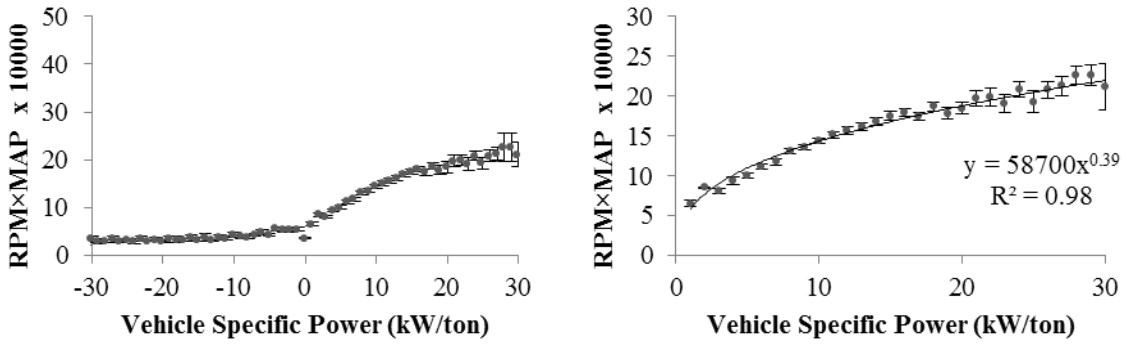

(a) Product of MAP and RPM versus Vehicle Specific Power

(b) Product of MAP and RPM versus Positive Vehicle Specific Power

Figure A-1 Measured product of Manifold Absolute Pressure (MAP) and engine Revolutions per Minute (RPM) versus Vehicle Specific Power (VSP) for a 2005 Mazda 6. Error bars indicate 95 percent confidence intervals.

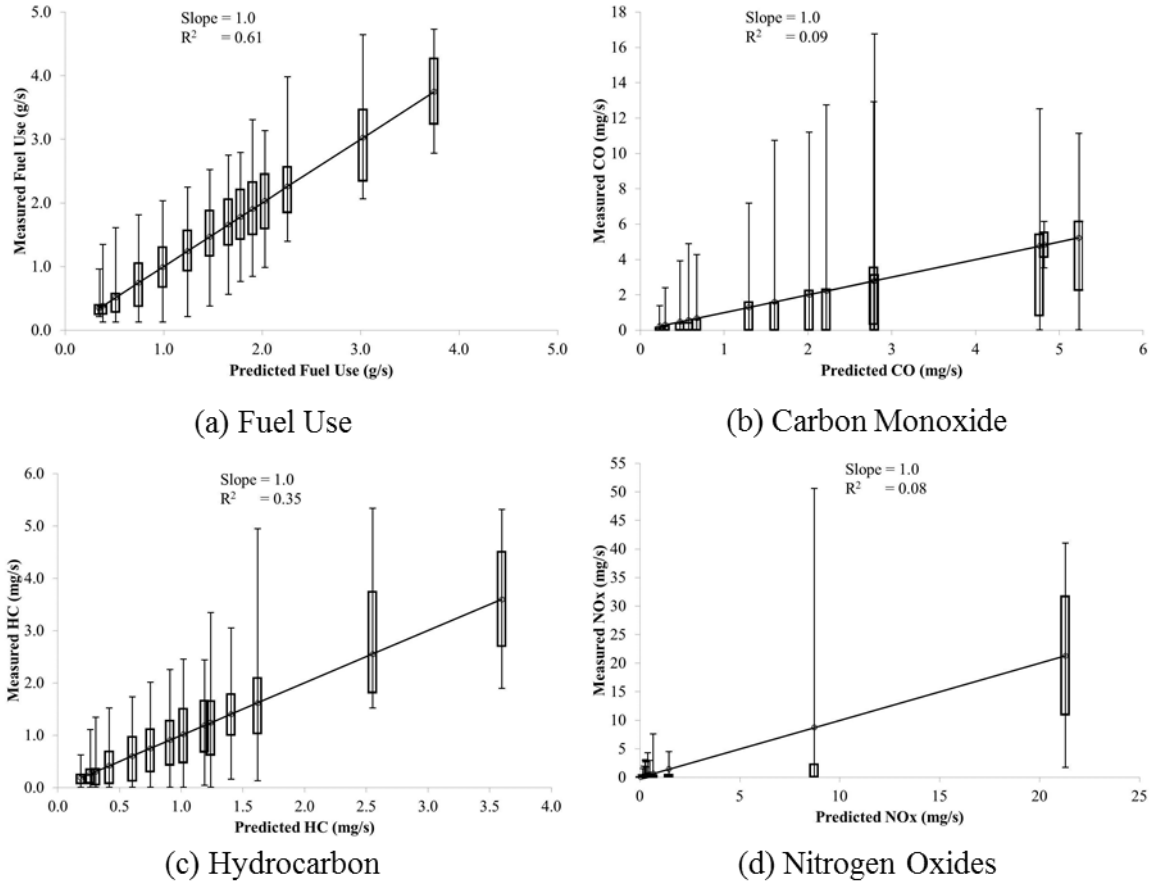

(a) Fuel Use

(b) Carbon Monoxide

(c) Hydrocarbon

(d) Nitrogen Oxides

Figure A-2 Comparison between measured and predicted fuel use and emission rates based on the Vehicle Specific Power-based model for a 2005 Mazda 6.

A1.3 Fuel Use versus Internally Observable Variables

Fuel use rates are proportional to each of MAP and RPM, as illustrated in Figures A-3(a) and A-3(b), respectively. The coefficients of determination for fuel use as a power function of MAP and RPM are 0.77 and 0.52, respectively. The p-values for the scaling and power parameters for both power regressions were less than 0.001, indicating statistical significance. Therefore, each of MAP and RPM can be an explanatory variable for fuel use, explaining a substantial amount of the variation in fuel use.

However, although fuel use rate is influenced by each of RPM and MAP, the variability in fuel use rate is better explained by $P_{M\times R}$, as shown in Figure A-3(c). The predicted fuel use with bias corrections in terms of $P_{M\times R}$ in the form of Equation (5) is:

$$m_{Fuel,pred}^{(5)} = 3.2\times10^{-6}\times(P_{M\times R})^{1.09}\times1.04-0.027\text{ , } R^2 = 0.92 \qquad \text{(A1-2)}$$

The numerical values of "1.04" and "0.027" are the correction factors. Equation (A1-2) is used for predicting fuel use rates based on $P_{M\times R}$ for this vehicle.

A parity plot comparison between the Equation (A1-2) predicted versus measured fuel use rates is shown in Figure A-3(d), based on Equation (6). The data points follow a linear trend. The slope is 1 and the intercept is 0. The standard deviation of the residuals is 0.13 mg/s, which is small compared to mean fuel use rates of 0.95 mg/s. The R^2 for the linear fit is 0.97. The R^2 value of 0.97 is a significant improvement compared to the R^2 value of 0.61 based on the VSP-based approach. Therefore, the IOV-based model performs better than the EOV-based modal. There are some artifacts of the scatter plot that imply that the residual error may have non-constant variance with respect to the magnitude of fuel use rate. For very high fuel use rate the sample size is very small. However, from a practical perspective, this model is highly effective in predicting fuel use rate without any average bias.

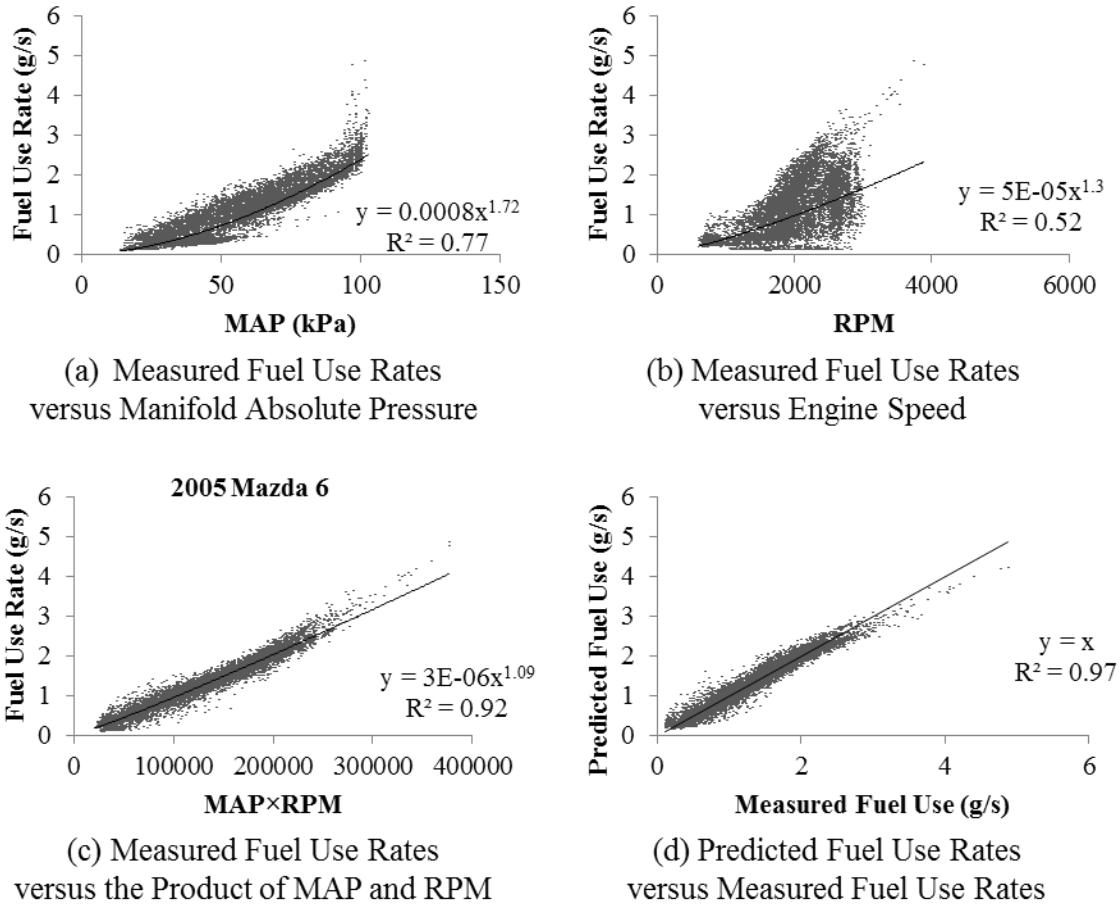

(a) Measured Fuel Use Rates versus Manifold Absolute Pressure

(b) Measured Fuel Use Rates versus Engine Speed

(c) Measured Fuel Use Rates versus the Product of MAP and RPM

(d) Predicted Fuel Use Rates versus Measured Fuel Use Rates

Figure A-3 Measured fuel use rates versus (a) Manifold Absolute Pressure (MAP) (b) engine Revolutions Per Minute (RPM), (c) the product of MAP and RPM, and (d) the predicted versus measured fuel use rates for a 2005 Mazda 6 measured during 110 miles of driving in the Raleigh, NC area.

A1.4 Emission Rates versus Internally Observable Variables

The relationships between emission rates of CO, HC, and NO_x versus and $P_{M\times R}$ are shown in Figures A-4(a), A-4(c), and A-4(e), respectively. For CO, most of the data points follow a power trend. A small portion of data has much higher CO emission rates compared to the fitted model. the IOV model based on $P_{M\times R}$ for CO emission rates is developed similarly to the model for fuel use rates. The model in the form of Equation (5) is:

$$m_{CO,pred}^{(5)} = 3.5\times10^{-7}\times(P_{M\times R})^{1.27}\times13-9.6,\ R^2 = 0.39 \qquad \text{(A1-3)}$$

The numerical values of "13" and "9.6" are the bias correction factors. Both the fitted scaling parameter of 3.5×10^{-7} and the power parameter of 1.27 have p-values of less than 0.001, indicating statistically significance.

A comparison of Equation (A1-3) predicted versus measured CO emission rates is shown in Figure A-4(b). The data fit a line with slope of 1 and the intercept of 0. The R^2 value of 0.15 is higher compared to the R^2 value of 0.09 for the VSP-based model shown in Figure A-2(b).

Figure A-4(c) illustrates the relationship between measured HC emission rates versus $P_{M\times R}$. There appear to be some clusters in this scatter plot. The majority of HC emission rates ranging from 0 to approximately 6 mg/s follow a power trend versus $P_{M\times R}$. There also appear other clusters each containing a small portion of data. Two clusters have lower HC emission rates than the fitted model, such as about 0 to 0.5 mg/s and about 0.5 to 1 mg/s at $P_{M\times R}$ of 150,000 to 250,000 kPa-rev/min. This vehicle has 4-gear automatic transmission. These clusters might be associated with gear selection. Although stratification of these data might be possible based on additional IOVs, these clusters cannot be discriminated based on $P_{M\times R}$ alone. For all data, the fitted model is:

$$m_{HC,pred}^{(5)} = 1.2\times10^{-6}\times(P_{M\times R})^{1.13}\times 2.1 - 0.45,\ R^2 = 0.50 \qquad \text{(A1-4)}$$

The numerical values of "2.1" and "0.45" are the bias correction factors. Both the fitted scaling parameter of 1.2×10^{-6} and the power parameter of 1.13 have p-values of less than 0.001, indicating statistical significance.

A comparison of Equation (A1-4) predicted versus measured HC emission rates is shown in Figure A-4(d). The R^2 is 0.58 and is a significant improvement compared to the R^2 of 0.35 based on the VSP-based model, as illustrated in Figure A-2(c). Therefore, the IOV-based model describes the HC emission rates well, and is better than the EOV-based model.

The relationship between measured NO_x emission rates versus $P_{M\times R}$ is illustrated in Figure A-4(e). The data appear to follow a power trend. The fitted model is:

$$m_{NOx,pred}^{(5)} = 1.0\times10^{-6}\times(P_{M\times R})^{0.97}\times 181 - 13,\ R^2 = 0.17 \qquad \text{(A1-5)}$$

The numerical values of "181" and "13" are the bias correction factors. Both the fitted scaling parameter of 1.0×10^{-6} and the power parameter of 0.97 have p-values of less than 0.001, indicating statistical significance.

A comparison of Equation (A1-5) predicted and measured NO_x emission rates is shown in Figure A-4(f). The R^2 is 0.05, which is slightly lower than the R^2 of 0.08 of the VSP-based model illustrated in Figure A-2(d). Both the IOV- and EOV- based models are not well explaining the variation in NO_x emission rates.

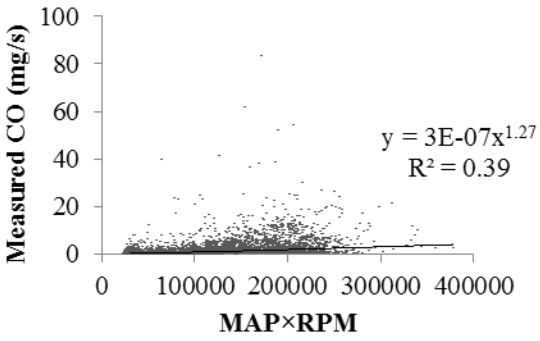

(a) Measured CO Emission Rates versus the Product of MAP and RPM

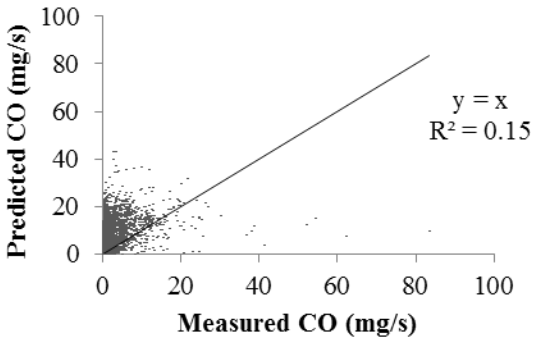

(b) Predicted versus Measured CO Emission Rates

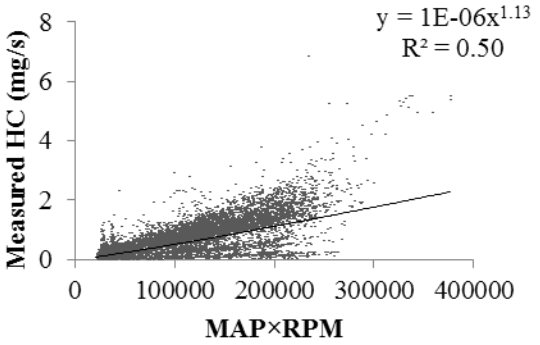

(c) Measured HC Emission Rates versus the Product of MAP and RPM

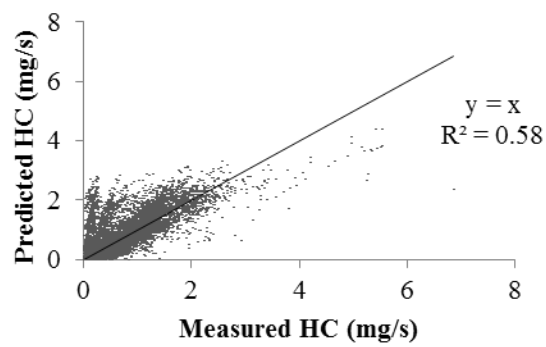

(d) Predicted versus Measured HC Emission Rates

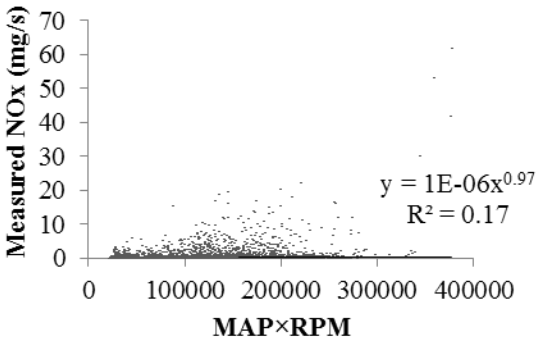

(e) Measured NO_x Emission Rates versus the Product of MAP and RPM

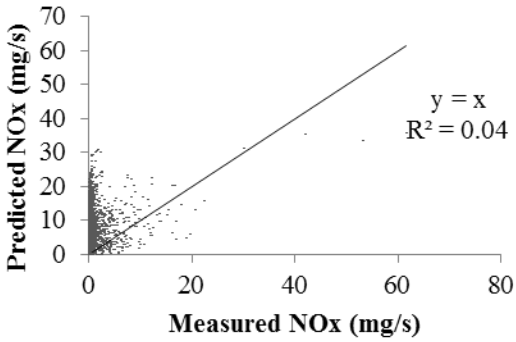

(f) Predicted versus Measured NO_x Emission Rates

Figure A-4 Relationship between emission rates and the product of Manifold Absolute Pressure (MAP) and engine Revolutions Per Minute (RPM) and comparison between predicted and measured emission rates for a 2005 Mazda 6 measured during 110 miles of driving in the Raleigh, NC area.

A2 2008 Chevrolet Impala

For the 2008 Chevrolet Impala, more than 11,500 seconds of valid data were collected, which account for more than 98 percent of raw data from the field measurements.

A2.1 Internally versus Externally Observable Variables

The relationship between $P_{M\times R}$ versus VSP is illustrated in Figure A-5. Average $P_{M\times R}$ values are plotted versus VSP ranging from -30 to 30 kW/ton with a 1 kW/ton interval. This range accounts for over 99% of measured vehicle activity. At negative VSP, there is no load on the engine and, thus, $P_{M\times R}$ is approximately constant. For increasing positive VSP, $P_{M\times R}$ typically increases monotonically.

A regression analysis was conducted for $P_{M\times R}$ versus VSP for positive VSP values, as shown in Figure A5(b):

$$P_{M\times R} = 44800\times VSP^{0.42}, \text{ for VSP>0, } R^2 = 0.97 \qquad \text{(A2-1)}$$

$P_{M\times R}$ is 40,000 kPa-rev/min for negative VSP, and is corrected to no less than 40,000 kPa-rev/min for positive VSP. The p-values for the estimated scaling parameter of 44,800 and power parameter of 0.42 are both less than 0.001, indicating statistical significance. $P_{M\times R}$ is highly correlated with VSP. Thus, $P_{M\times R}$ is a good surrogate for engine power demand for this vehicle.

A2.2 Fuel Use and Emission Rates versus Externally Observable Variables

The VSP-based approach for predicting fuel use and emission rates is illustrated in Figures A-6(a) through A-6(d). For each VSP bin, there is substantial variability in fuel use and emission rates, as described in the box and whiskers based on the 2.5-percentile, 25-percentile, 75-percentile, and 97.5-percentile of one second values within each VSP bin. The R^2 for fuel use and emissions of CO, HC, and NO_x are 0.62, 0.01, 0.20, and 0.14, respectively. Thus, VSP is shown to be a good basis for estimating fuel use, and is able to explain some of the variability in 1 Hz emission rates. Furthermore, VSP is accurate in quantifying the mean trend in these rates.

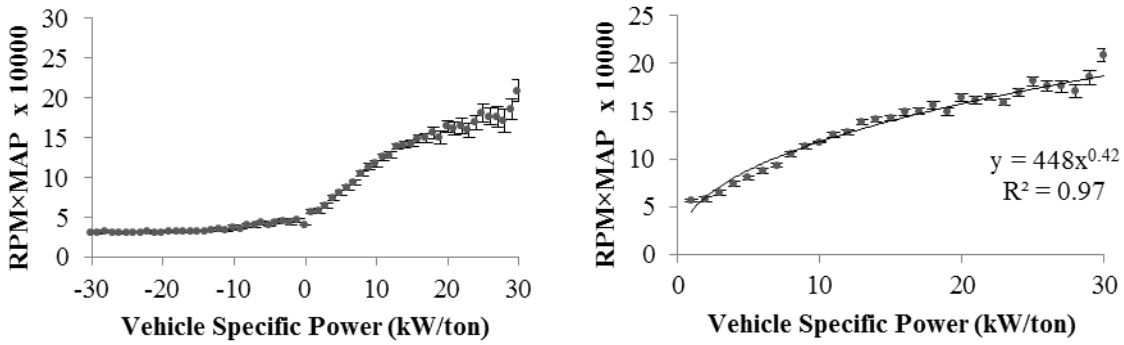

(a) Product of MAP and RPM versus Vehicle Specific Power

(b) Product of MAP and RPM versus Positive Vehicle Specific Power

Figure A-5 Measured product of Manifold Absolute Pressure (MAP) and engine Revolutions per Minute (RPM) versus Vehicle Specific Power (VSP) for a 2008 Chevrolet Impala. Error bars indicate 95 percent confidence intervals.

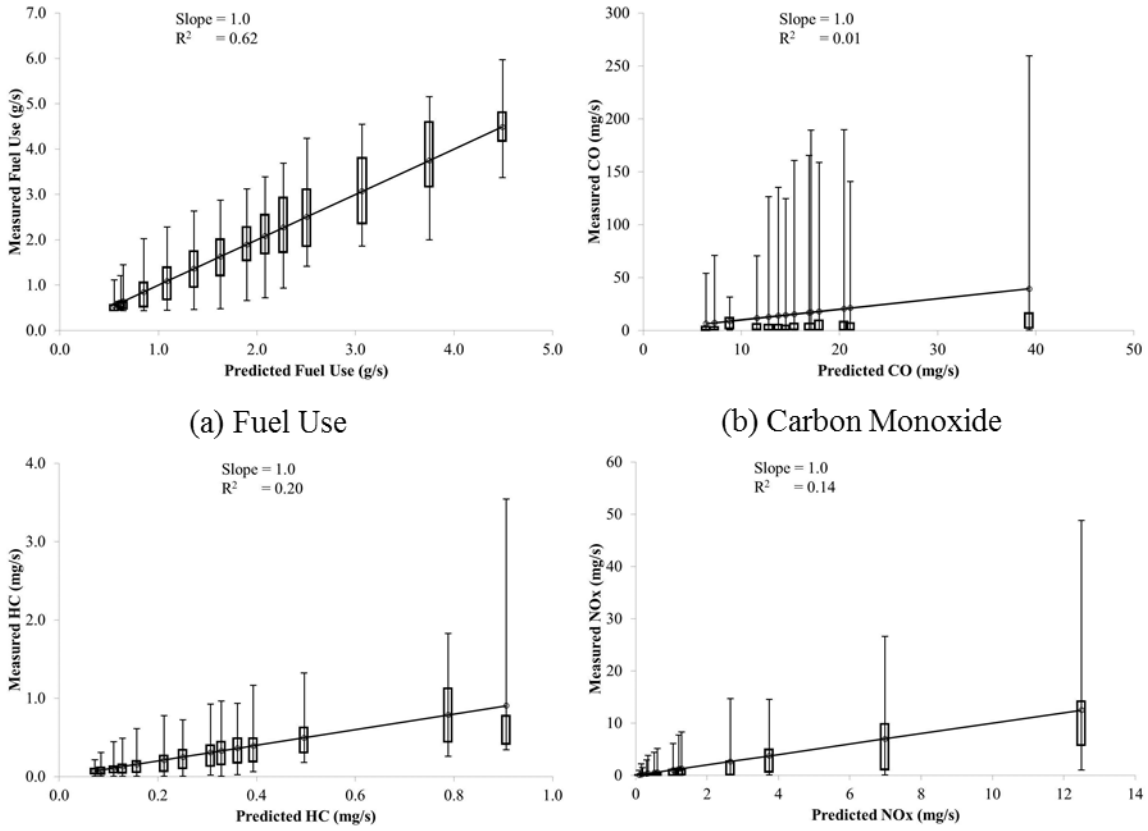

(a) Fuel Use

(b) Carbon Monoxide

(c) Hydrocarbon

(d) Nitrogen Oxides

Figure A-6 Comparison between measured and predicted fuel use and emission rates based on the Vehicle Specific Power-based model for a 2008 Chevrolet Impala.

A2.3 Fuel Use versus Internally Observable Variables

Fuel use rates are proportional to each of MAP and RPM, as illustrated in Figures A-7(a) and A-7(b), respectively. The coefficients of determination for fuel use as a power function of MAP and RPM are 0.84 and 0.71, respectively. The p-values for the scaling and power parameters for both power regressions were less than 0.001, indicating statistical significance. Therefore, each of MAP and RPM can be an explanatory variable for fuel use, explaining a substantial amount of the variation in fuel use.

However, although fuel use rate is influenced by each of RPM and MAP, the variability in fuel use rate is better explained by $P_{M\times R}$, as shown in Figure A-7(c). The predicted fuel use with bias corrections in terms of $P_{M\times R}$ in the form of Equation (5) is:

$$m_{Fuel,pred}^{(5)} = 2.6\times10^{-5}\times(P_{M\times R})^{0.94}\times1.18-0.18,\ R^2 = 0.95 \qquad \text{(A2-2)}$$

The numerical values of "1.18" and "0.18" are the correction factors. Equation (A2-2) is used for predicting fuel use rates based on $P_{M\times R}$ for this vehicle.

A parity plot comparison between the Equation (A2-2) predicted versus measured fuel use rates is shown in Figure A7(d), based on Equation (6). The data points follow a linear trend. The slope is 1 and the intercept is 0. The standard deviation of the residuals is 0.23 mg/s, which is small compared to mean fuel use rates of 1.2 mg/s. The R^2 for the linear fit is 0.92. The R^2 value of 0.92 is a significant improvement compared to the R^2 value of 0.62 based on the VSP-based approach. Therefore, the IOV-based model performs better than the EOV-based modal. There are some artifacts of the scatter plot that imply that the residual error may have non-constant variance with respect to the magnitude of fuel use rate. For very high fuel use rate the sample size is very small. However, from a practical perspective, this model is highly effective in predicting fuel use rate without any average bias.

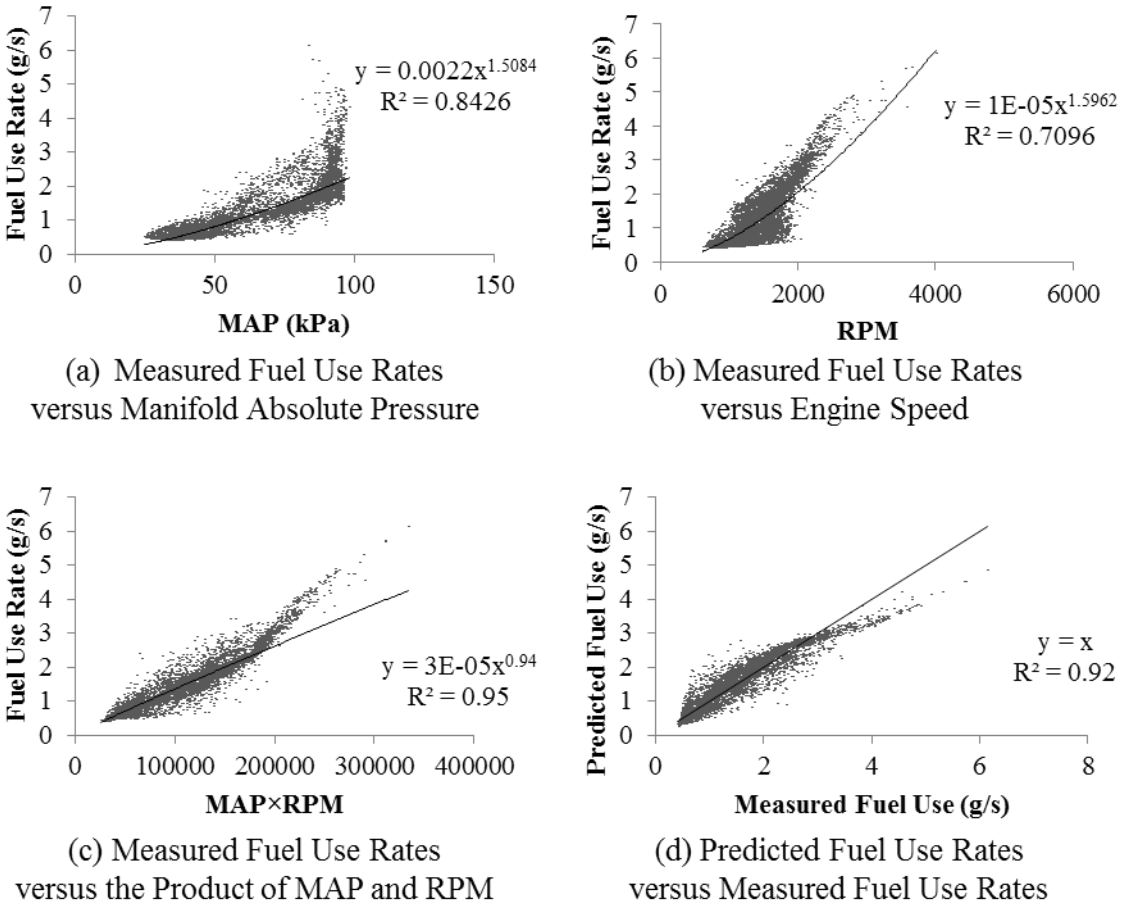

(a) Measured Fuel Use Rates versus Manifold Absolute Pressure

(b) Measured Fuel Use Rates versus Engine Speed

(c) Measured Fuel Use Rates versus the Product of MAP and RPM

(d) Predicted Fuel Use Rates versus Measured Fuel Use Rates

Figure A-7 Measured fuel use rates versus (a) Manifold Absolute Pressure (MAP) (b) engine Revolutions Per Minute (RPM), (c) the product of MAP and RPM, and (d) the predicted versus measured fuel use rates for a 2008 Chevrolet Impala measured during 110 miles of driving in the Raleigh, NC area.

A2.4 Emission Rates versus Internally Observable Variables

The relationships between emission rates of CO, HC, and NO_x versus and $P_{M\times R}$ are shown in Figures A-8(a), A-8(c), and A-8(e), respectively. For CO, most of the data points follow a power trend. A small portion of data has much higher CO emission rates compared to the fitted model. the IOV model based on $P_{M\times R}$ for CO emission rates is developed similarly to the model for fuel use rates. The model in the form of Equation (5) is:

$$m_{CO,pred}^{(5)} = 8.5\times10^{-4}\times(P_{M\times R})^{0.70}\times370-87,\ R^2 = 0.05 \qquad \text{(A2-3)}$$

The numerical values of "370" and "87" are the bias correction factors. Both the fitted scaling parameter of 8.5×10^{-4} and the power parameter of 0.70 have p-values of less than 0.001, indicating statistically significance.

A comparison of Equation (A2-3) predicted versus measured CO emission rates is shown in Figure A-8(b). The data fit a line with slope of 1 and the intercept of 0. The R^2 value of 0.02 is similar compared to the R^2 value of 0.01 for the VSP-based model shown in Figure A-6(b). Both the IOV- and EOV- based models are not well explaining the variation in CO emission rates

Figure A-8(c) illustrates the relationship between measured HC emission rates versus $P_{M\times R}$. There appear to be some clusters in this scatter plot. The majority of HC emission rates ranging from 0 to approximately 6 mg/s follow a power trend versus $P_{M\times R}$. For all data, the fitted model is:

$$m_{HC,pred}^{(5)} = 1.8\times10^{-6}\times(P_{M\times R})^{0.99}\times 4.6 - 0.46,\ R^2 = 0.39 \qquad \text{(A2-4)}$$

The numerical values of "4.6" and "0.46" are the bias correction factors. Both the fitted scaling parameter of 1.8×10^{-6} and the power parameter of 0.99 have p-values of less than 0.001, indicating statistical significance.

A comparison of Equation (A2-4) predicted versus measured HC emission rates is shown in Figure A-8(d). The R^2 is 0.32 and is a significant improvement compared to the R^2 of 0.20 based on the VSP-based model, as illustrated in Figure A-6(c). Therefore, the IOV-based model describes the HC emission rates well, and is better than the EOV-based model.

The relationship between measured NO_x emission rates versus $P_{M\times R}$ is illustrated in Figure A-8(e). The data appear to follow a power trend. The fitted model is:

$$m_{NOx,pred}^{(5)} = 1.3\times10^{-8}\times(P_{M\times R})^{1.46}\times 43 - 11,\ R^2 = 0.23 \qquad \text{(A2-5)}$$

The numerical values of "43" and "11" are the bias correction factors. Both the fitted scaling parameter of 1.3×10^{-8} and the power parameter of 1.46 have p-values of less than 0.001, indicating statistical significance.

A comparison of Equation (A2-5) predicted and measured NO_x emission rates is shown in Figure A-8(f). The R^2 is 0.10, which is slightly lower than the R^2 of 0.14 of the VSP-based model illustrated in Figure A-6(d). Both the IOV- and EOV- based models are not well explaining the variation in NO_x emission rates.

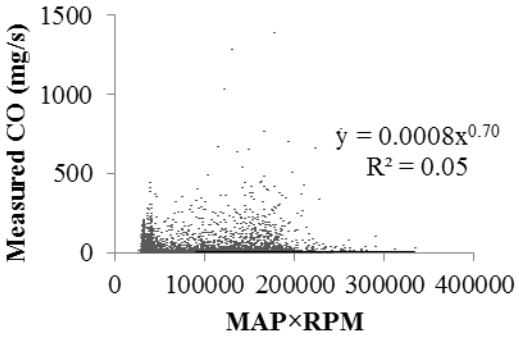

(a) Measured CO Emission Rates versus the Product of MAP and RPM

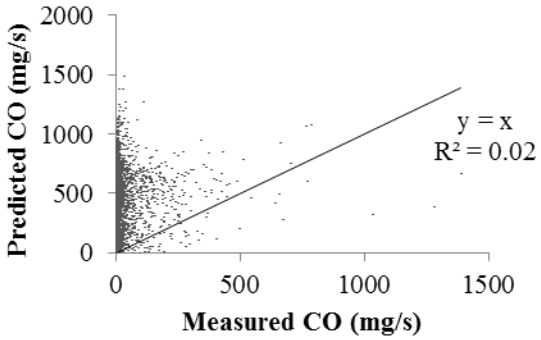

(b) Predicted versus Measured CO Emission Rates

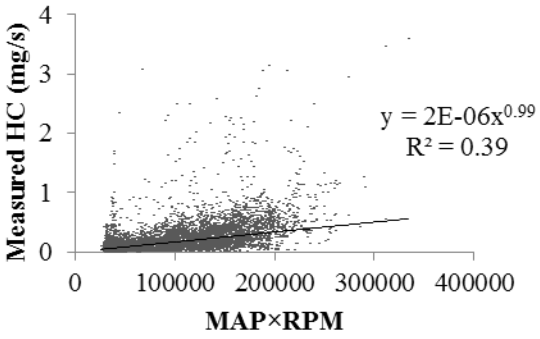

(c) Measured HC Emission Rates versus the Product of MAP and RPM

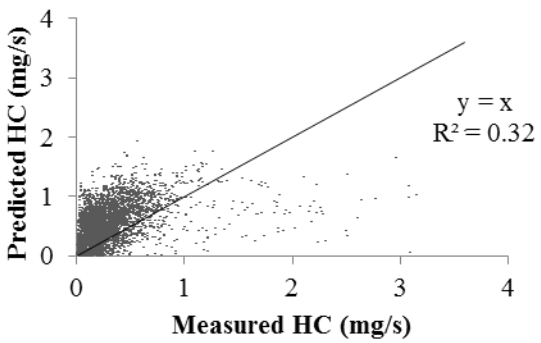

(d) Predicted versus Measured HC Emission Rates

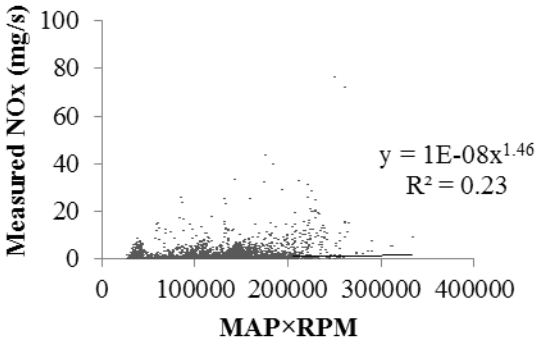

(e) Measured NO_x Emission Rates versus the Product of MAP and RPM

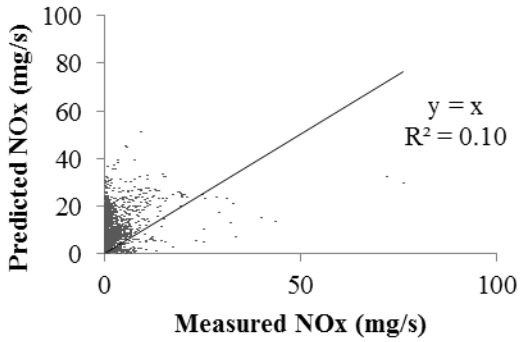

(f) Predicted versus Measured NO_x Emission Rates

Figure A-8 Relationship between emission rates and the product of Manifold Absolute Pressure (MAP) and engine Revolutions Per Minute (RPM) and comparison between predicted and measured emission rates for a 2008 Chevrolet Impala measured during 110 miles of driving in the Raleigh, NC area.

A3 2004 Pontiac Grand Am GT

For the 2004 Pontiac Grand Am GT, more than 13,400 seconds of valid data were collected, which account for more than 96 percent of raw data from the field measurements.

A3.1 Internally versus Externally Observable Variables

The relationship between $P_{M\times R}$ versus VSP is illustrated in Figure A-9. Average $P_{M\times R}$ values are plotted versus VSP ranging from -30 to 30 kW/ton with a 1 kW/ton interval. This range accounts for over 99% of measured vehicle activity. At negative VSP, there is no load on the engine and, thus, $P_{M\times R}$ is approximately constant. For increasing positive VSP, $P_{M\times R}$ typically increases monotonically.

A regression analysis was conducted for $P_{M\times R}$ versus VSP for positive VSP values, as shown in Figure A-9(b):

$$P_{M\times R} = 44300 \times VSP^{0.42}, \text{ for VSP>0, } R^2 = 0.99 \quad \text{(A3-1)}$$

$P_{M\times R}$ is 36,300 kPa-rev/min for negative VSP, and is corrected to no less than 36,300 kPa-rev/min for positive VSP. The p-values for the estimated scaling parameter of 44,300 and power parameter of 0.42 are both less than 0.001, indicating statistical significance. $P_{M\times R}$ is highly correlated with VSP. Thus, $P_{M\times R}$ is a good surrogate for engine power demand for this vehicle.

A3.2 Fuel Use and Emission Rates versus Externally Observable Variables

The VSP-based approach for predicting fuel use and emission rates is illustrated in Figures A-10(a) through A-10(d). For each VSP bin, there is substantial variability in fuel use and emission rates, as described in the box and whiskers based on the 2.5-percentile, 25-percentile, 75-percentile, and 97.5-percentile of one second values within each VSP bin. The R^2 for fuel use and emissions of CO, HC, and NO_x are 0.74, 0.02, 0.22, and 0.13, respectively. Thus, VSP is shown to be a good basis for estimating fuel use, and is able to explain some of the variability in 1 Hz emission rates. Furthermore, VSP is accurate in quantifying the mean trend in these rates.

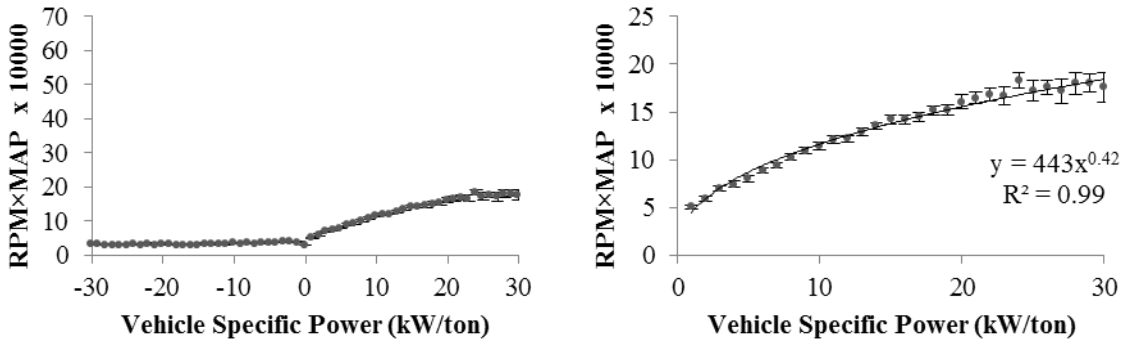

(a) Product of MAP and RPM versus Vehicle Specific Power

(b) Product of MAP and RPM versus Positive Vehicle Specific Power

Figure A-9 Measured product of Manifold Absolute Pressure (MAP) and engine Revolutions per Minute (RPM) versus Vehicle Specific Power (VSP) for a 2004 Pontiac Grand Am GT. Error bars indicate 95 percent confidence intervals.

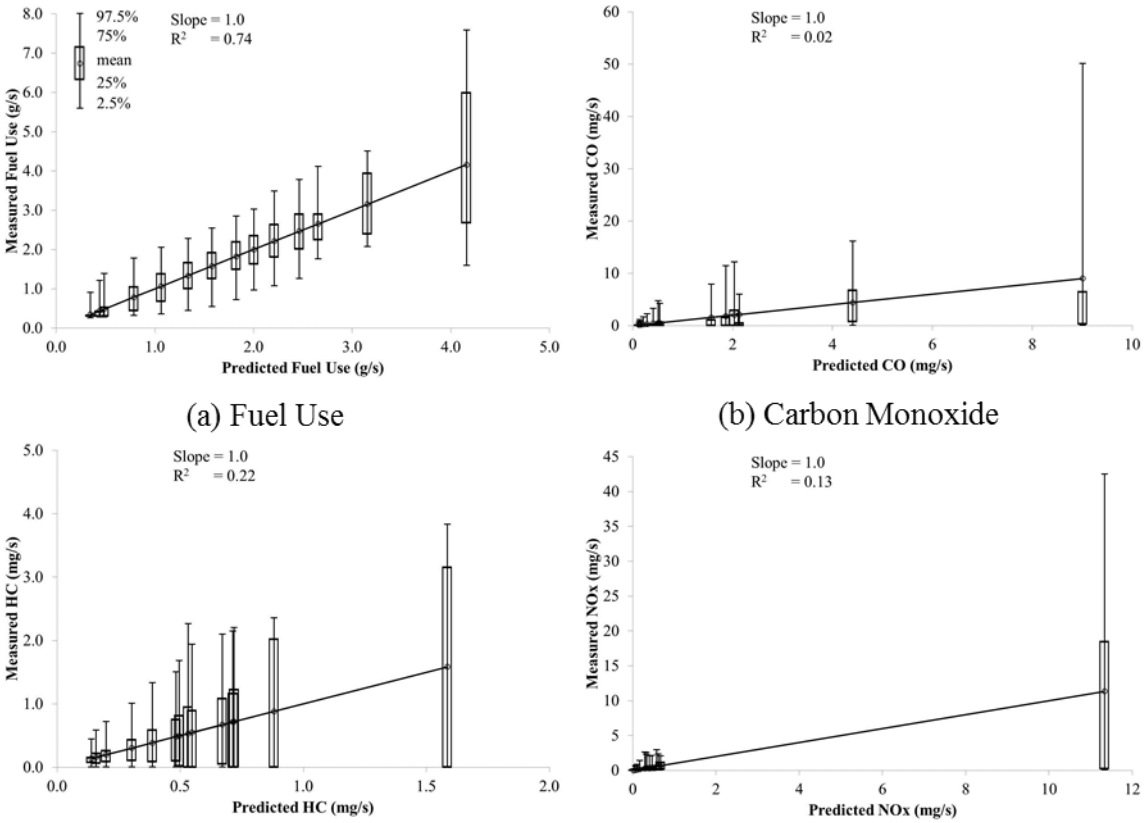

(a) Fuel Use

(b) Carbon Monoxide

(c) Hydrocarbon

(d) Nitrogen Oxides

Figure A-10 Comparison between measured and predicted fuel use and emission rates based on the Vehicle Specific Power-based model for a 2004 Pontiac Grand Am GT.

A3.3 Fuel Use versus Internally Observable Variables

Fuel use rates are proportional to each of MAP and RPM, as illustrated in Figures A-11(a) and A-11(b), respectively. The coefficients of determination for fuel use as a power function of MAP and RPM are 0.69 and 0.79, respectively. The p-values for the scaling and power parameters for both power regressions were less than 0.001, indicating statistical significance. Therefore, each of MAP and RPM can be an explanatory variable for fuel use, explaining a substantial amount of the variation in fuel use.

However, although fuel use rate is influenced by each of RPM and MAP, the variability in fuel use rate is better explained by $P_{M\times R}$, as shown in Figure A-11(c). The predicted fuel use with bias corrections in terms of $P_{M\times R}$ in the form of Equation (5) is:

$$m_{Fuel,pred}^{(5)} = 4.5\times10^{-6}\times(P_{M\times R})^{1.09}\times1.03-0.027\ ,\ R^2 = 0.98 \qquad \text{(A3-2)}$$

The numerical values of "1.03" and "0.027" are the correction factors. Equation (A3-2) is used for predicting fuel use rates based on $P_{M\times R}$ for this vehicle.

A parity plot comparison between the Equation (A3-2) predicted versus measured fuel use rates is shown in Figure A-11(d), based on Equation (6). The data points follow a linear trend. The slope is 1 and the intercept is 0. The standard deviation of the residuals is 0.12 mg/s, which is small compared to mean fuel use rates of 0.94 mg/s. The R^2 for the linear fit is 0.98. The R^2 value of 0.98 is a significant improvement compared to the R^2 value of 0.74 based on the VSP-based approach. Therefore, the IOV-based model performs better than the EOV-based modal. There are some artifacts of the scatter plot that imply that the residual error may have non-constant variance with respect to the magnitude of fuel use rate. For very high fuel use rate the sample size is very small. However, from a practical perspective, this model is highly effective in predicting fuel use rate without any average bias.

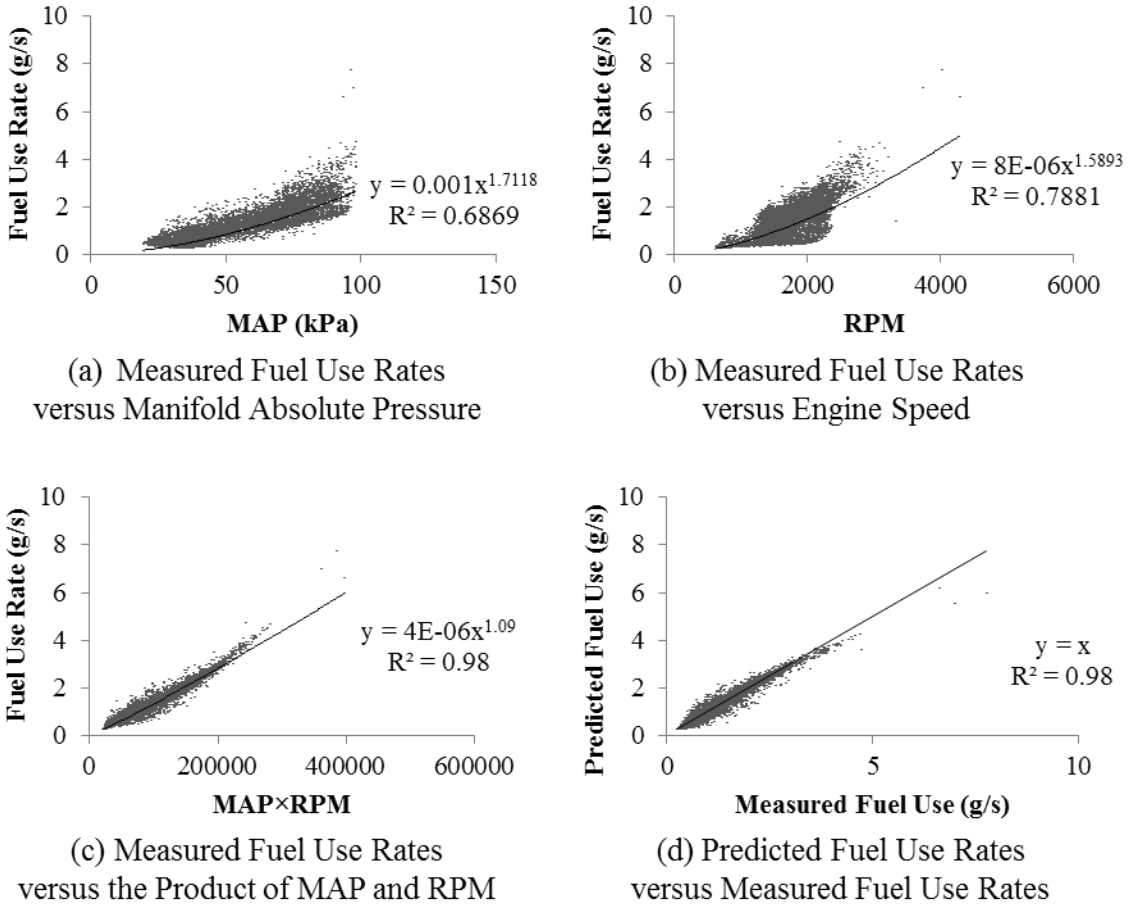

(a) Measured Fuel Use Rates versus Manifold Absolute Pressure

(b) Measured Fuel Use Rates versus Engine Speed

(c) Measured Fuel Use Rates versus the Product of MAP and RPM

(d) Predicted Fuel Use Rates versus Measured Fuel Use Rates

Figure A-11 Measured fuel use rates versus (a) Manifold Absolute Pressure (MAP) (b) engine Revolutions Per Minute (RPM), (c) the product of MAP and RPM, and (d) the predicted versus measured fuel use rates for a 2005 Mazda 6 measured during 110 miles of driving in the Raleigh, NC area.

A3.4 Emission Rates versus Internally Observable Variables

The relationships between emission rates of CO, HC, and NO_x versus and $P_{M\times R}$ are shown in Figures A-12(a), A-12(c), and A-12(e), respectively. For CO, most of the data points follow a power trend. A small portion of data has much higher CO emission rates compared to the fitted model. the IOV model based on $P_{M\times R}$ for CO emission rates is developed similarly to the model for fuel use rates. The model in the form of Equation (5) is:

$$m_{CO,pred}^{(5)} = 1.3\times10^{-6}\times(P_{M\times R})^{1.15}\times92-57\ ,\ R^2 = 0.38 \qquad \text{(A3-3)}$$

The numerical values of "92" and "57" are the bias correction factors. Both the fitted scaling parameter of 1.3×10^{-6} and the power parameter of 1.15 have p-values of less than 0.001, indicating statistically significance.

A comparison of Equation (A3-3) predicted versus measured CO emission rates is shown in Figure A-12(b). The data fit a line with slope of 1 and the intercept of 0. The R^2 value of 0.03 is similar compared to the R^2 value of 0.02 for the VSP-based model shown in Figure A-12(b). Both the IOV- and EOV-based models are not well predicting the CO emission rates.

Figure A-12(c) illustrates the relationship between measured HC emission rates versus $P_{M\times R}$. There appear to be some clusters in this scatter plot. The majority of HC emission rates ranging from 0 to approximately 6 mg/s follow a power trend versus $P_{M\times R}$. There also appear other clusters each containing a small portion of data. Two clusters have higher HC emission rates than the fitted model, such as about 2 to 4 mg/s and about 1 to 3 mg/s at $P_{M\times R}$ of 100,000 to 200,000 kPa-rev/min. This vehicle has 4-gear automatic transmission. These clusters might be associated with gear selection. Although stratification of these data might be possible based on additional IOVs, these clusters cannot be discriminated based on $P_{M\times R}$ alone. For all data, the fitted model is:

$$m_{HC,pred}^{(5)} = 5.7\times10^{-6}\times(P_{M\times R})^{0.97}\times 2.9 - 0.44,\ R^2 = 0.37 \qquad \text{(A3-4)}$$

The numerical values of "2.9" and "0.44" are the bias correction factors. Both the fitted scaling parameter of 5.7×10^{-6} and the power parameter of 0.97 have p-values of less than 0.001, indicating statistical significance.

A comparison of Equation (A3-4) predicted versus measured HC emission rates is shown in Figure A-12(d). The R^2 is 0.49 and is a significant improvement compared to the R^2 of 0.22 based on the VSP-based model, as illustrated in Figure A-10(c). Therefore, the IOV-based model describes the HC emission rates well, and is better than the EOV-based model.

The relationship between measured NO_x emission rates versus $P_{M\times R}$ is illustrated in Figure A-12(e). The data appear to follow a power trend. The fitted model is:

$$m_{NOx,pred}^{(5)} = 2.5\times10^{-9}\times(P_{M\times R})^{1.51}\times 69 - 5.9,\ R^2 = 0.36 \qquad \text{(A3-5)}$$

The numerical values of "69" and "5.9" are the bias correction factors. Both the fitted scaling parameter of 2.4×10^{-9} and the power parameter of 1.51 have p-values of less than 0.001, indicating statistical significance.

A comparison of Equation (A3-5) predicted and measured NO_x emission rates is shown in Figure A-12(f). The R^2 is 0.05, which is slightly lower than the R^2 of 0.13 of the VSP-based model illustrated in Figure A-10(d). Both the IOV- and EOV- based models are not well explaining the variation in NO_x emission rates.

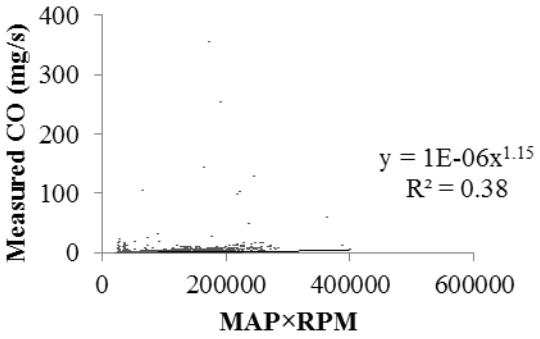

(a) Measured CO Emission Rates versus the Product of MAP and RPM

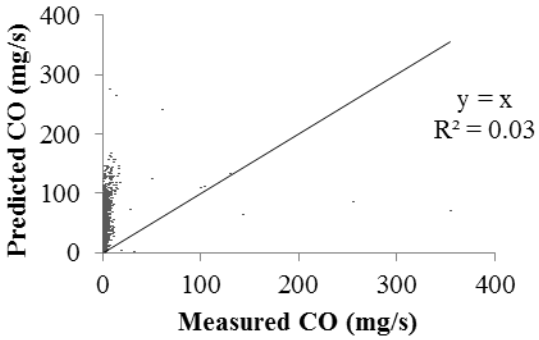

(b) Predicted versus Measured CO Emission Rates

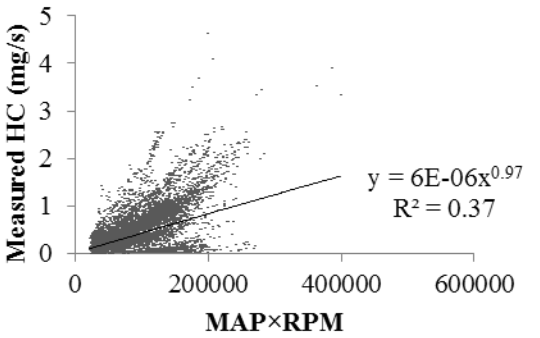

(c) Measured HC Emission Rates versus the Product of MAP and RPM

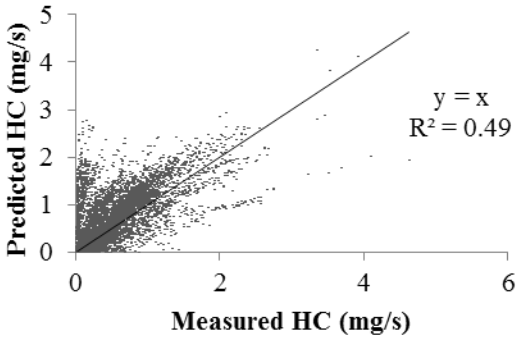

(d) Predicted versus Measured HC Emission Rates

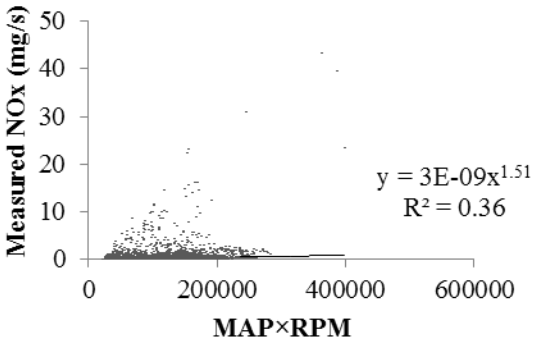

(e) Measured NO_x Emission Rates versus the Product of MAP and RPM

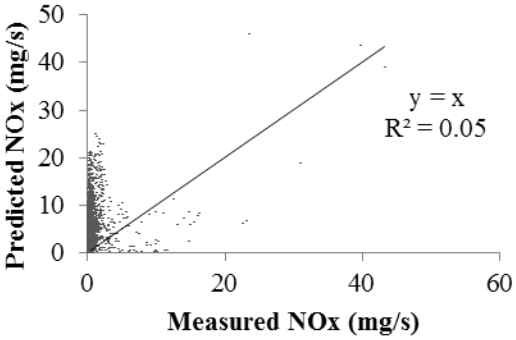

(f) Predicted versus Measured NO_x Emission Rates

Figure A-12 Relationship between emission rates and the product of Manifold Absolute Pressure (MAP) and engine Revolutions Per Minute (RPM) and comparison between predicted and measured emission rates for a 2004 Pontiac Grand Am GT measured during 110 miles of driving in the Raleigh, NC area.

A4 2001 Volvo S40

For the 2001 Volvo S40, more than 13,000 seconds of valid data were collected, which account for more than 99 percent of raw data from the field measurements.

A4.1 Internally versus Externally Observable Variables

The relationship between $P_{M\times R}$ versus VSP is illustrated in Figure A-13. Average $P_{M\times R}$ values are plotted versus VSP ranging from -30 to 30 kW/ton with a 1 kW/ton interval. This range accounts for over 99% of measured vehicle activity. At negative VSP, there is no load on the engine and, thus, $P_{M\times R}$ is approximately constant. For increasing positive VSP, $P_{M\times R}$ typically increases monotonically.

A regression analysis was conducted for $P_{M\times R}$ versus VSP for positive VSP values, as shown in Figure A-13(b):

$$P_{M\times R} = 59900 \times VSP^{0.37}, \text{ for VSP>0, } R^2 = 0.99 \quad \text{(A4-1)}$$

$P_{M\times R}$ is 45,400 kPa-rev/min for negative VSP, and is corrected to no less than 45,400 kPa-rev/min for positive VSP. The p-values for the estimated scaling parameter of 59,900 and power parameter of 0.37 are both less than 0.001, indicating statistical significance. $P_{M\times R}$ is highly correlated with VSP. Thus, $P_{M\times R}$ is a good surrogate for engine power demand for this vehicle.

A4.2 Fuel Use and Emission Rates versus Externally Observable Variables

The VSP-based approach for predicting fuel use and emission rates is illustrated in Figures A-14(a) through A-14(d). For each VSP bin, there is substantial variability in fuel use and emission rates, as described in the box and whiskers based on the 2.5-percentile, 25-percentile, 75-percentile, and 97.5-percentile of one second values within each VSP bin. The R^2 for fuel use and emissions of CO, HC, and NO_x are 0.66, 0.11, 0.10, and 0.27, respectively. Thus, VSP is shown to be a good basis for estimating fuel use, and is able to explain some of the variability in 1 Hz emission rates. Furthermore, VSP is accurate in quantifying the mean trend in these rates.

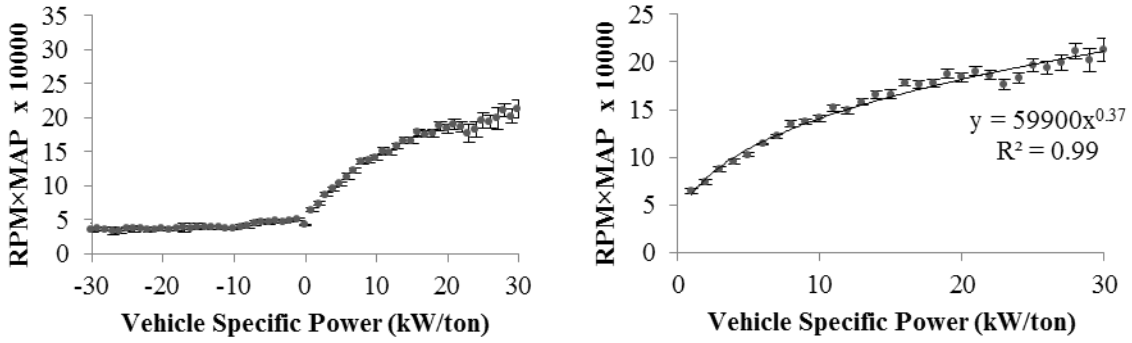

(a) Product of MAP and RPM versus Vehicle Specific Power

(b) Product of MAP and RPM versus Positive Vehicle Specific Power

Figure A-13 Measured product of Manifold Absolute Pressure (MAP) and engine Revolutions per Minute (RPM) versus Vehicle Specific Power (VSP) for a 2001 Volvo S40. Error bars indicate 95 percent confidence intervals.

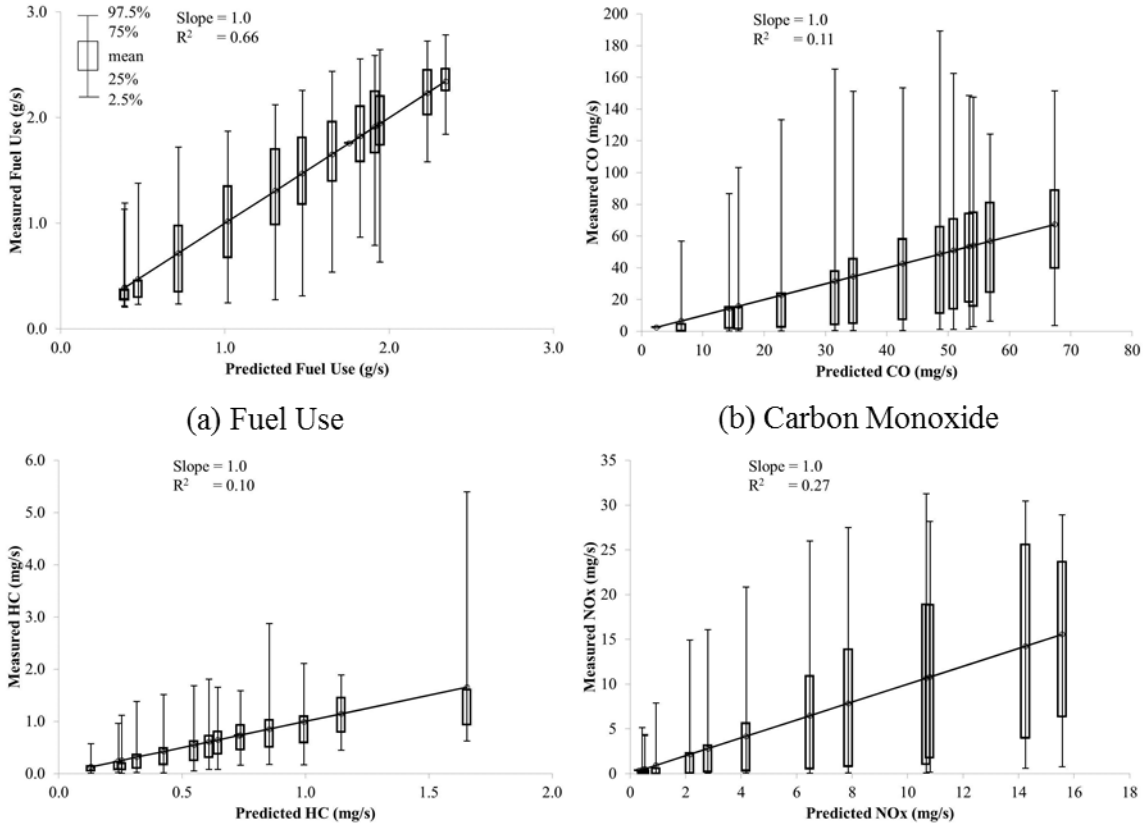

(a) Fuel Use

(b) Carbon Monoxide

(c) Hydrocarbon

(d) Nitrogen Oxides

Figure A-14 Comparison between measured and predicted fuel use and emission rates based on the Vehicle Specific Power-based model for a 2001 Volvo S40.

A4.3 Fuel Use versus Internally Observable Variables

Fuel use rates are proportional to each of MAP and RPM, as illustrated in Figures A-15(a) and A-15(b), respectively. The coefficients of determination for fuel use as a power function of MAP and RPM are 0.74 and 0.55, respectively. The p-values for the scaling and power parameters for both power regressions were less than 0.001, indicating statistical significance. Therefore, each of MAP and RPM can be an explanatory variable for fuel use, explaining a substantial amount of the variation in fuel use.

However, although fuel use rate is influenced by each of RPM and MAP, the variability in fuel use rate is better explained by $P_{M\times R}$, as shown in Figure A-15(c). The predicted fuel use with bias corrections in terms of $P_{M\times R}$ in the form of Equation (5) is:

$$m_{Fuel,pred}^{(5)} = 2.6\times10^{-6}\times(P_{M\times R})^{1.11}\times1.08-0.027,\ R^2 = 0.95 \qquad \text{(A4-2)}$$

The numerical values of "1.08" and "0.027" are the correction factors. Equation (A4-2) is used for predicting fuel use rates based on $P_{M\times R}$ for this vehicle.

A parity plot comparison between the Equation (A4-2) predicted versus measured fuel use rates is shown in Figure A-15(d), based on Equation (6). The data points follow a linear trend. The slope is 1 and the intercept is 0. The standard deviation of the residuals is 0.12 mg/s, which is small compared to mean fuel use rates of 0.89 mg/s. The R^2 for the linear fit is 0.97. The R^2 value of 0.97 is a significant improvement compared to the R^2 value of 0.66 based on the VSP-based approach. Therefore, the IOV-based model performs better than the EOV-based modal. There are some artifacts of the scatter plot that imply that the residual error may have non-constant variance with respect to the magnitude of fuel use rate. For very high fuel use rate the sample size is very small. However, from a practical perspective, this model is highly effective in predicting fuel use rate without any average bias.

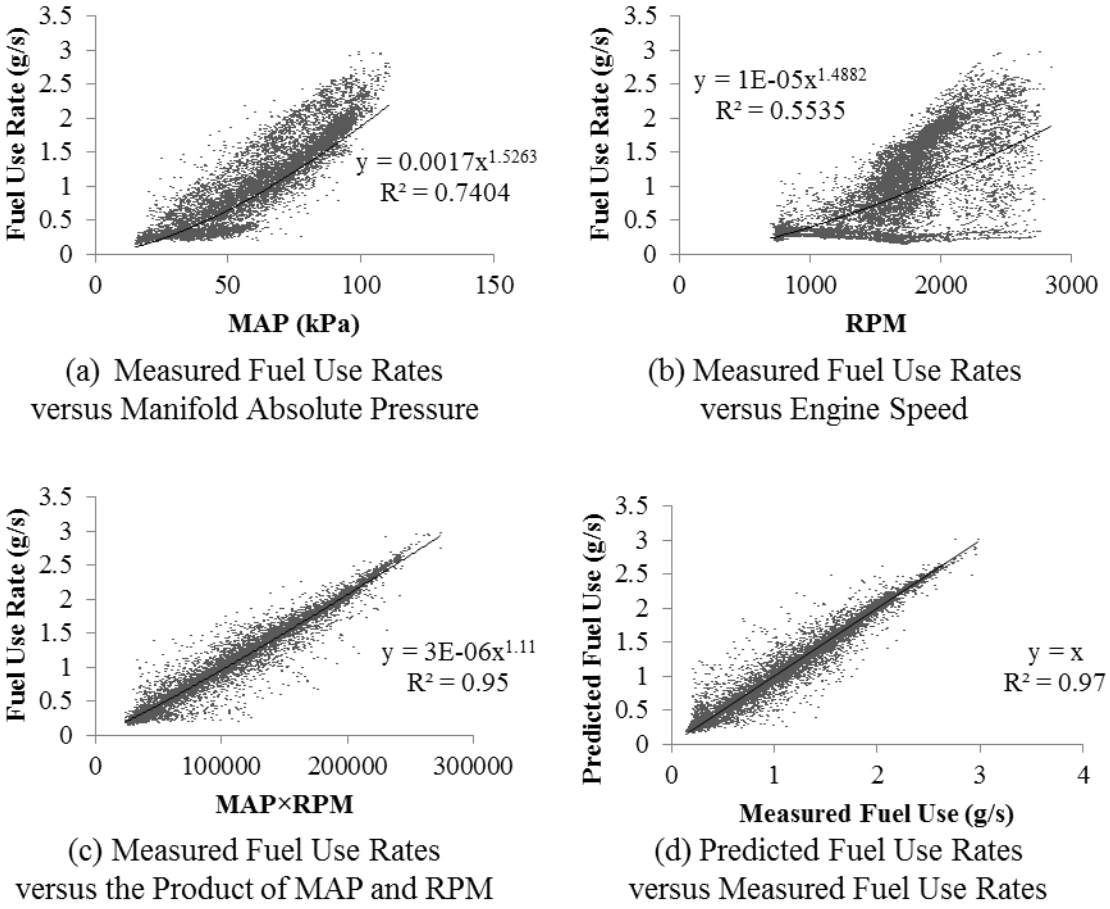

(a) Measured Fuel Use Rates versus Manifold Absolute Pressure

(b) Measured Fuel Use Rates versus Engine Speed

(c) Measured Fuel Use Rates versus the Product of MAP and RPM

(d) Predicted Fuel Use Rates versus Measured Fuel Use Rates

Figure A-15 Measured fuel use rates versus (a) Manifold Absolute Pressure (MAP) (b) engine Revolutions Per Minute (RPM), (c) the product of MAP and RPM, and (d) the predicted versus measured fuel use rates for a 2001 Volvo S40 measured during 110 miles of driving in the Raleigh, NC area.

A4.4 Emission Rates versus Internally Observable Variables

The relationships between emission rates of CO, HC, and NO_x versus and $P_{M\times R}$ are shown in Figures A-16(a), A-16(c), and A-16(e), respectively. For CO, most of the data points follow a power trend. A small portion of data has much higher CO emission rates compared to the fitted model. the IOV model based on $P_{M\times R}$ for CO emission rates is developed similarly to the model for fuel use rates. The model in the form of Equation (5) is:

$$m_{CO,pred}^{(5)} = 4.6\times10^{-7}\times(P_{M\times R})^{1.49}\times11-119,\ R^2 = 0.30 \qquad \text{(A4-3)}$$

The numerical values of "11" and "119" are the bias correction factors. Both the fitted scaling parameter of 4.6×10^{-7} and the power parameter of 1.49 have p-values of less than 0.001, indicating statistically significance.

A comparison of Equation (A4-3) predicted versus measured CO emission rates is shown in Figure A-16(b). The data fit a line with slope of 1 and the intercept of 0. The R^2 value of 0.13 is slightly higher compared to the R^2 value of 0.11 for the VSP-based model shown in Figure A-14(b).

Figure A-16(c) illustrates the relationship between measured HC emission rates versus $P_{M\times R}$. There appear to be some clusters in this scatter plot. The majority of HC emission rates ranging from 0 to approximately 6 mg/s follow a power trend versus $P_{M\times R}$. Although stratification of these data might be possible based on additional IOVs, these clusters cannot be discriminated based on $P_{M\times R}$ alone. For all data, the fitted model is:

$$m_{HC,pred}^{(5)} = 0.30\times(P_{M\times R})^{-0.03}\times 6100 - 1320,\ R^2 = 0.0003 \qquad \text{(A4-4)}$$

The numerical values of "6,100" and "1,320" are the bias correction factors. Both the fitted scaling parameter of 0.30 and the power parameter of -0.03 have p-values of less than 0.001, indicating statistical significance.

A comparison of Equation (A4-4) predicted versus measured HC emission rates is shown in Figure A-16(d). The R^2 is 0.0.001 and is lower compared to the R^2 of 0.10 based on the VSP-based model, as illustrated in Figure A-14(c). Both the IOV- and EOV-based models are not well predicting the HC emission rates.

The relationship between measured NO_x emission rates versus $P_{M\times R}$ is illustrated in Figure A-16(e). The data appear to follow a power trend. The fitted model is:

$$m_{NOx,pred}^{(5)} = 6.1\times10^{-12}\times(P_{M\times R})^{2.2}\times 11 - 6.8,\ R^2 = 0.39 \qquad \text{(A4-5)}$$

The numerical values of "11" and "6.8" are the bias correction factors. Both the fitted scaling parameter of 6.1×10^{-12} and the power parameter of 2.2 have p-values of less than 0.001, indicating statistical significance.

A comparison of Equation (A4-5) predicted and measured NO_x emission rates is shown in Figure A-16(f). The R^2 is 0.30, which is slightly higher than the R^2 of 0.27 of the VSP-based model illustrated in Figure A-14(d). Therefore, the IOV-based model is better than the EOV-based model in predicting NO_x emission rates.

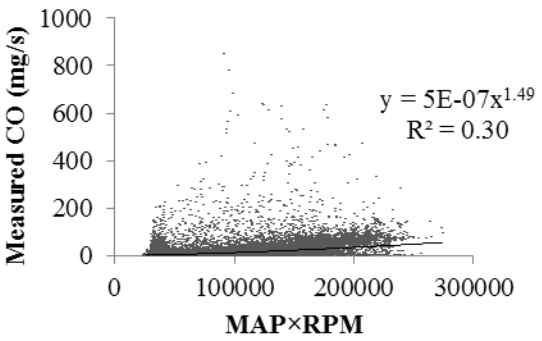

(a) Measured CO Emission Rates versus the Product of MAP and RPM

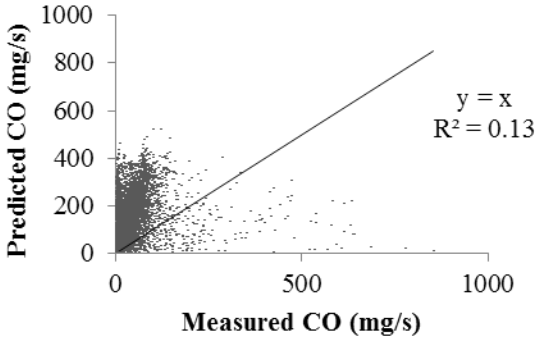

(b) Predicted versus Measured CO Emission Rates

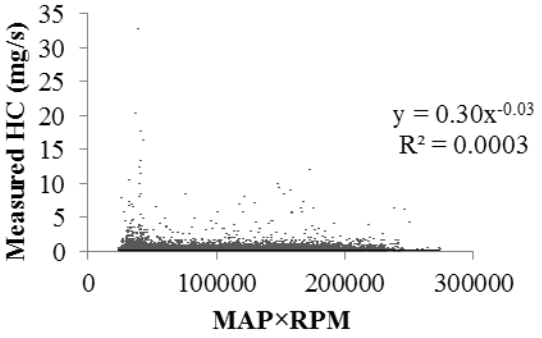

(c) Measured HC Emission Rates versus the Product of MAP and RPM

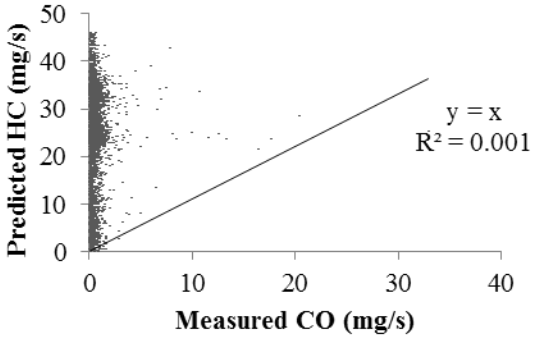

(d) Predicted versus Measured HC Emission Rates

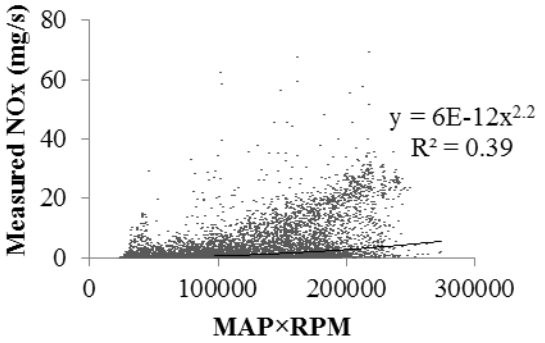

(e) Measured NO_x Emission Rates versus the Product of MAP and RPM

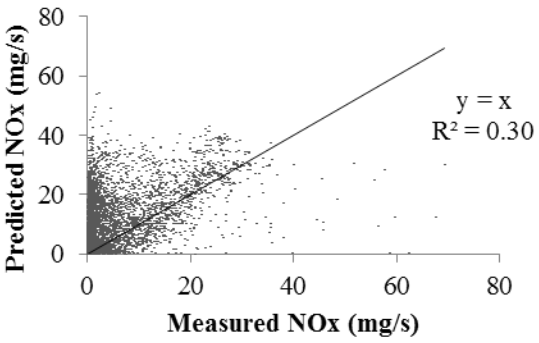

(f) Predicted versus Measured NO_x Emission Rates

Figure A-16 Relationship between emission rates and the product of Manifold Absolute Pressure (MAP) and engine Revolutions Per Minute (RPM) and comparison between predicted and measured emission rates for a 2001 Volvo S40 measured during 110 miles of driving in the Raleigh, NC area.

A5 2009 Honda Civic

For the 2009 Honda Civic, more than 12,100 seconds of valid data were collected, which account for more than 97 percent of raw data from the field measurements.

A5.1 Internally versus Externally Observable Variables

The relationship between $P_{M\times R}$ versus VSP is illustrated in Figure A-17. Average $P_{M\times R}$ values are plotted versus VSP ranging from -30 to 30 kW/ton with a 1 kW/ton interval. This range accounts for over 99% of measured vehicle activity. At negative VSP, there is no load on the engine and, thus, $P_{M\times R}$ is approximately constant. For increasing positive VSP, $P_{M\times R}$ typically increases monotonically.

A regression analysis was conducted for $P_{M\times R}$ versus VSP for positive VSP values, as shown in Figure A-17(b):

$$P_{M\times R} = 59100 \times VSP^{0.43}, \text{ for VSP>0, } R^2 = 0.98 \quad \text{(A5-1)}$$

$P_{M\times R}$ is 37,800 kPa-rev/min for negative VSP, and is corrected to no less than 37,800 kPa-rev/min for positive VSP. The p-values for the estimated scaling parameter of 59,100 and power parameter of 0.43 are both less than 0.001, indicating statistical significance. $P_{M\times R}$ is highly correlated with VSP. Thus, $P_{M\times R}$ is a good surrogate for engine power demand for this vehicle.

A5.2 Fuel Use and Emission Rates versus Externally Observable Variables

The VSP-based approach for predicting fuel use and emission rates is illustrated in Figures A-18(a) through A-18(d). For each VSP bin, there is substantial variability in fuel use and emission rates, as described in the box and whiskers based on the 2.5-percentile, 25-percentile, 75-percentile, and 97.5-percentile of one second values within each VSP bin. The R^2 for fuel use and emissions of CO, HC, and NO_x are 0.71, 0.04, 0.34, and 0.18, respectively. Thus, VSP is shown to be a good basis for estimating fuel use, and is able to explain some of the variability in 1 Hz emission rates. Furthermore, VSP is accurate in quantifying the mean trend in these rates.

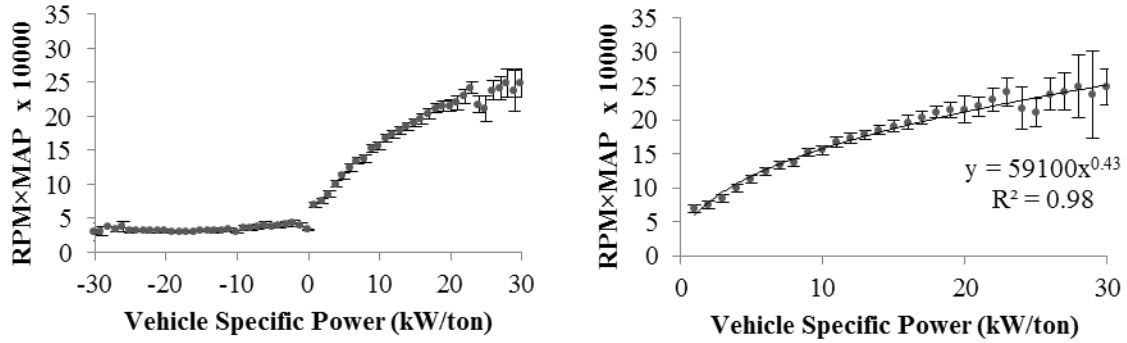

(a) Product of MAP and RPM versus Vehicle Specific Power

(b) Product of MAP and RPM versus Positive Vehicle Specific Power

Figure A-17 Measured product of Manifold Absolute Pressure (MAP) and engine Revolutions per Minute (RPM) versus Vehicle Specific Power (VSP) for a 2009 Honda Civic. Error bars indicate 95 percent confidence intervals.

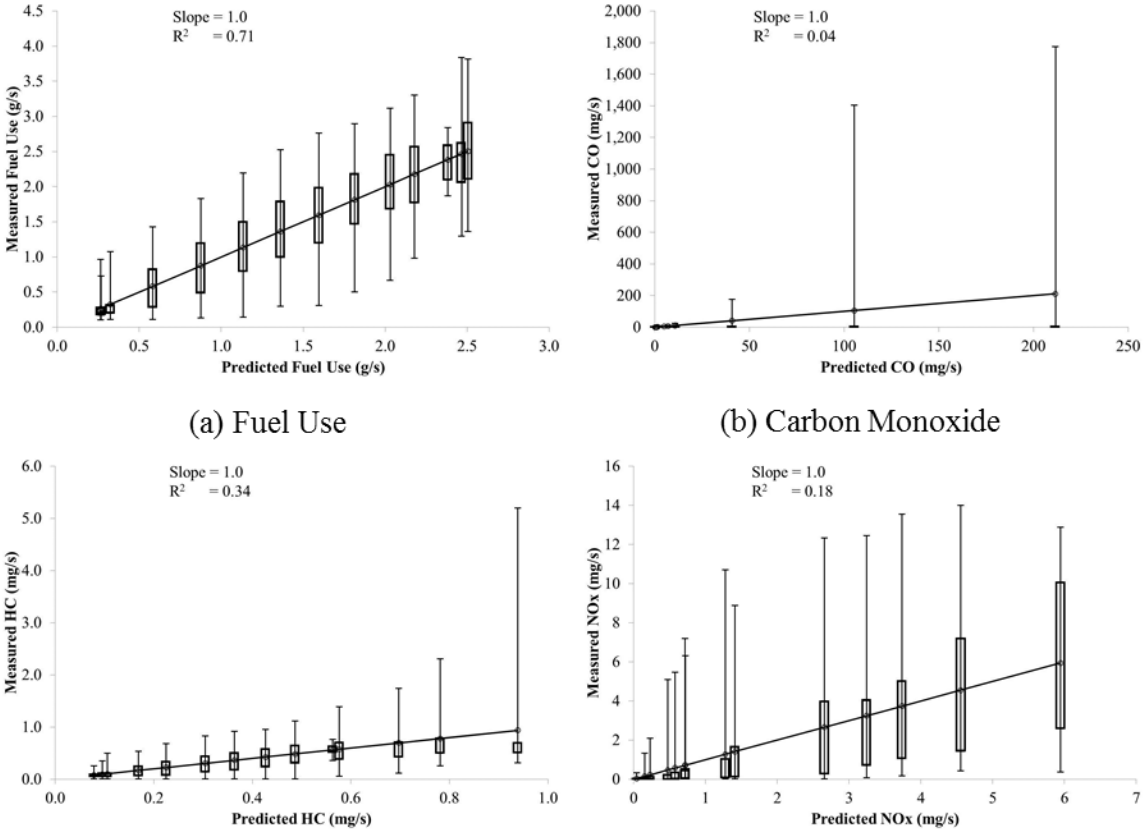

(a) Fuel Use

(b) Carbon Monoxide

(c) Hydrocarbon

(d) Nitrogen Oxides

Figure A-18 Comparison between measured and predicted fuel use and emission rates based on the Vehicle Specific Power-based model for a 2009 Honda Civic.

A5.3 Fuel Use versus Internally Observable Variables

Fuel use rates are proportional to each of MAP and RPM, as illustrated in Figures A-19(a) and A-19(b), respectively. The coefficients of determination for fuel use as a power function of MAP and RPM are 0.83 and 0.61, respectively. The p-values for the scaling and power parameters for both power regressions were less than 0.001, indicating statistical significance. Therefore, each of MAP and RPM can be an explanatory variable for fuel use, explaining a substantial amount of the variation in fuel use.

However, although fuel use rate is influenced by each of RPM and MAP, the variability in fuel use rate is better explained by $P_{M\times R}$, as shown in Figure A-19(c). The predicted fuel use with bias corrections in terms of $P_{M\times R}$ in the form of Equation (5) is:

$$m_{Fuel,pred}^{(5)} = 3.6\times10^{-6}\times(P_{M\times R})^{1.07}\times1.13-0.087\ ,\ R^2 = 0.91 \qquad \text{(A5-2)}$$

The numerical values of "1.13" and "0.087" are the correction factors. Equation (A5-2) is used for predicting fuel use rates based on $P_{M\times R}$ for this vehicle.

A parity plot comparison between the Equation (A5-2) predicted versus measured fuel use rates is shown in Figure A-19(d), based on Equation (6). The data points follow a linear trend. The slope is 1 and the intercept is 0. The standard deviation of the residuals is 0.17 mg/s, which is small compared to mean fuel use rates of 0.78 mg/s. The R^2 for the linear fit is 0.95. The R^2 value of 0.95 is a significant improvement compared to the R^2 value of 0.71 based on the VSP-based approach. Therefore, the IOV-based model performs better than the EOV-based modal. There are some artifacts of the scatter plot that imply that the residual error may have non-constant variance with respect to the magnitude of fuel use rate. For very high fuel use rate the sample size is very small. However, from a practical perspective, this model is highly effective in predicting fuel use rate without any average bias.

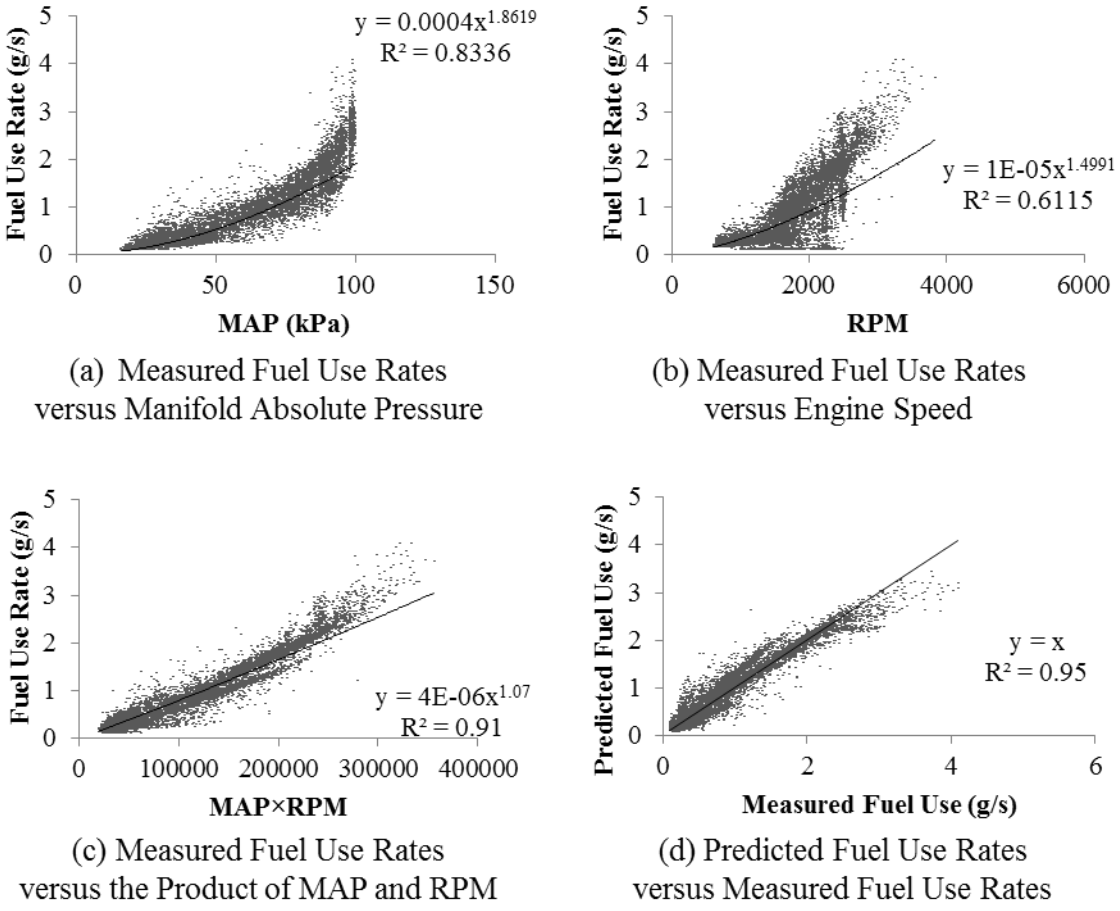

(a) Measured Fuel Use Rates versus Manifold Absolute Pressure

(b) Measured Fuel Use Rates versus Engine Speed

(c) Measured Fuel Use Rates versus the Product of MAP and RPM

(d) Predicted Fuel Use Rates versus Measured Fuel Use Rates

Figure A-19 Measured fuel use rates versus (a) Manifold Absolute Pressure (MAP) (b) engine Revolutions Per Minute (RPM), (c) the product of MAP and RPM, and (d) the predicted versus measured fuel use rates for a 2009 Honda Civic measured during 110 miles of driving in the Raleigh, NC area.

A5.4 Emission Rates versus Internally Observable Variables

The relationships between emission rates of CO, HC, and NO_x versus and $P_{M\times R}$ are shown in Figures A-20(a), A-20(c), and A-20(e), respectively. For CO, most of the data points follow a power trend. A small portion of data has much higher CO emission rates compared to the fitted model. the IOV model based on $P_{M\times R}$ for CO emission rates is developed similarly to the model for fuel use rates. The model in the form of Equation (5) is:

$$m_{CO,pred}^{(5)} = 2.1\times10^{-5}\times(P_{M\times R})^{0.90}\times1200-710\,,\ R^2 = 0.23 \qquad \text{(A5-3)}$$

The numerical values of "1,200" and "710" are the bias correction factors. Both the fitted scaling parameter of 2.1×10^{-5} and the power parameter of 0.90 have p-values of less than 0.001, indicating statistically significance.

A comparison of Equation (A5-3) predicted versus measured CO emission rates is shown in Figure A-20(b). The data fit a line with slope of 1 and the intercept of 0. The R^2 value of 0.03 is similar compared to the R^2 value of 0.04 for the VSP-based model shown in Figure A-18(b). Both the IOV- and EOV-based models are not well predicting the CO emission rates.

Figure A-20(c) illustrates the relationship between measured HC emission rates versus $P_{M\times R}$. There appear to be some clusters in this scatter plot. The majority of HC emission rates ranging from 0 to approximately 6 mg/s follow a power trend versus $P_{M\times R}$. There also appear another cluster containing a small portion of data, which have higher HC emission rates than the fitted model, such as about 1 to 2 mg/s at $P_{M\times R}$ of 150,000 to 300,000 kPa-rev/min. This vehicle has 4-gear automatic transmission. These clusters might be associated with gear selection. Although stratification of these data might be possible based on additional IOVs, these clusters cannot be discriminated based on $P_{M\times R}$ alone. For all data, the fitted model is:

$$m_{HC,pred}^{(5)} = 3.1\times10^{-6}\times(P_{M\times R})^{0.97}\times 2.6 - 0.28\,,\ R^2 = 0.74 \qquad \text{(A5-4)}$$

The numerical values of "2.6" and "0.28" are the bias correction factors. Both the fitted scaling parameter of 3.1×10^{-6} and the power parameter of 0.97 have p-values of less than 0.001, indicating statistical significance.

A comparison of Equation (A5-4) predicted versus measured HC emission rates is shown in Figure A-20(d). The R^2 is 0.51 and is a significant improvement compared to the R^2 of 0.34 based on the VSP-based model, as illustrated in Figure A-18(c). Therefore, the IOV-based model describes the HC emission rates well, and is better than the EOV-based model.

The relationship between measured NO_x emission rates versus $P_{M\times R}$ is illustrated in Figure A-20(e). The data appear to follow a power trend. The fitted model is:

$$m_{NOx,pred}^{(5)} = 3.1\times10^{-9}\times(P_{M\times R})^{1.55}\times 20 - 4.1,\ R^2 = 0.41 \qquad \text{(A5-5)}$$

The numerical values of "20" and "4.1" are the bias correction factors. Both the fitted scaling parameter of 3.1×10^{-9} and the power parameter of 1.55 have p-values of less than 0.001, indicating statistical significance.

A comparison of Equation (A5-5) predicted and measured NO_x emission rates is shown in Figure A-20(f). The R^2 is 0.18, which is the same as the R^2 of 0.18 of the VSP-based model illustrated in Figure A-18(d).

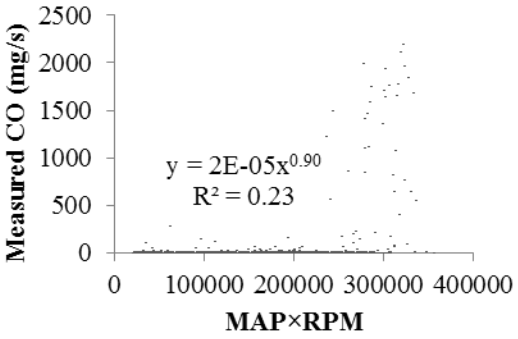

(a) Measured CO Emission Rates versus the Product of MAP and RPM

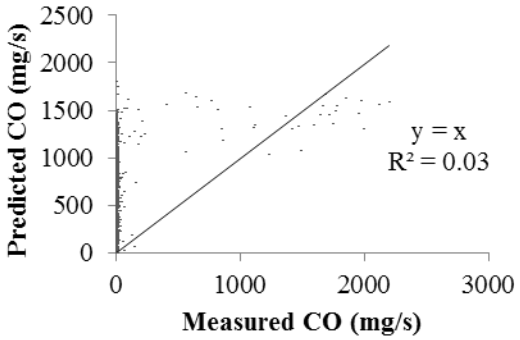

(b) Predicted versus Measured CO Emission Rates

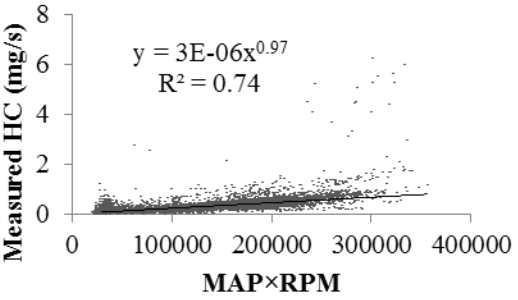

(c) Measured HC Emission Rates versus the Product of MAP and RPM

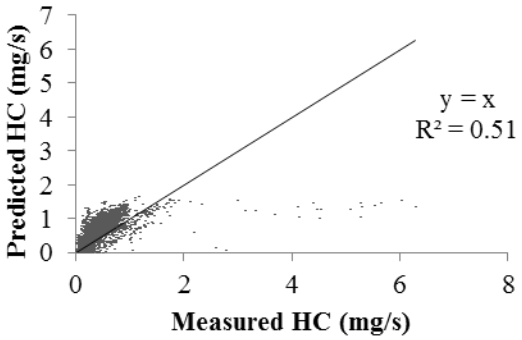

(d) Predicted versus Measured HC Emission Rates

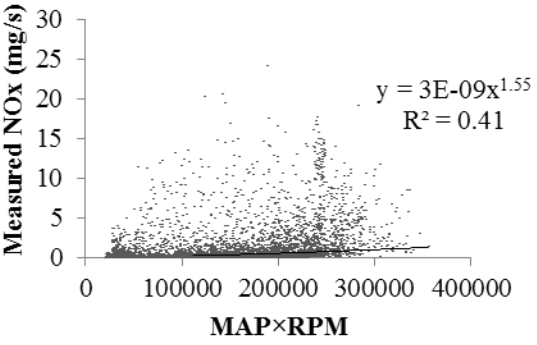

(e) Measured NO_x Emission Rates versus the Product of MAP and RPM

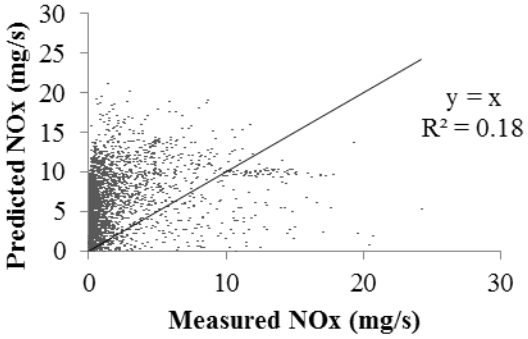

(f) Predicted versus Measured NO_x Emission Rates

Figure A-20 Relationship between emission rates and the product of Manifold Absolute Pressure (MAP) and engine Revolutions Per Minute (RPM) and comparison between predicted and measured emission rates for a 2009 Honda Civic measured during 110 miles of driving in the Raleigh, NC area.

A6 1998 Buick Century

For the 1998 Buick Century, more than 12,900 seconds of valid data were collected, which account for more than 99 percent of raw data from the field measurements.

A6.1 Internally versus Externally Observable Variables

The relationship between $P_{M\times R}$ versus VSP is illustrated in Figure A-21. Average $P_{M\times R}$ values are plotted versus VSP ranging from -30 to 30 kW/ton with a 1 kW/ton interval. This range accounts for over 99% of measured vehicle activity. At negative VSP, there is no load on the engine and, thus, $P_{M\times R}$ is approximately constant. For increasing positive VSP, $P_{M\times R}$ typically increases monotonically.

A regression analysis was conducted for $P_{M\times R}$ versus VSP for positive VSP values, as shown in Figure A-21(b):

$$P_{M\times R} = 55200\times VSP^{0.35}, \text{ for VSP>0, } R^2 = 0.94 \quad \text{(A6-1)}$$

$P_{M\times R}$ is 43,600 kPa-rev/min for negative VSP, and is corrected to no less than 43,600 kPa-rev/min for positive VSP. The p-values for the estimated scaling parameter of 55,200 and power parameter of 0.35 are both less than 0.001, indicating statistical significance. $P_{M\times R}$ is highly correlated with VSP. Thus, $P_{M\times R}$ is a good surrogate for engine power demand for this vehicle.

A6.2 Fuel Use and Emission Rates versus Externally Observable Variables

The VSP-based approach for predicting fuel use and emission rates is illustrated in Figures A-22(a) through A-22(d). For each VSP bin, there is substantial variability in fuel use and emission rates, as described in the box and whiskers based on the 2.5-percentile, 25-percentile, 75-percentile, and 97.5-percentile of one second values within each VSP bin. The R^2 for fuel use and emissions of CO, HC, and NO_x are 0.53, 0.13, 0.15, and 0.22, respectively. Thus, VSP is shown to be a good basis for estimating fuel use, and is able to explain some of the variability in 1 Hz emission rates. Furthermore, VSP is accurate in quantifying the mean trend in these rates.

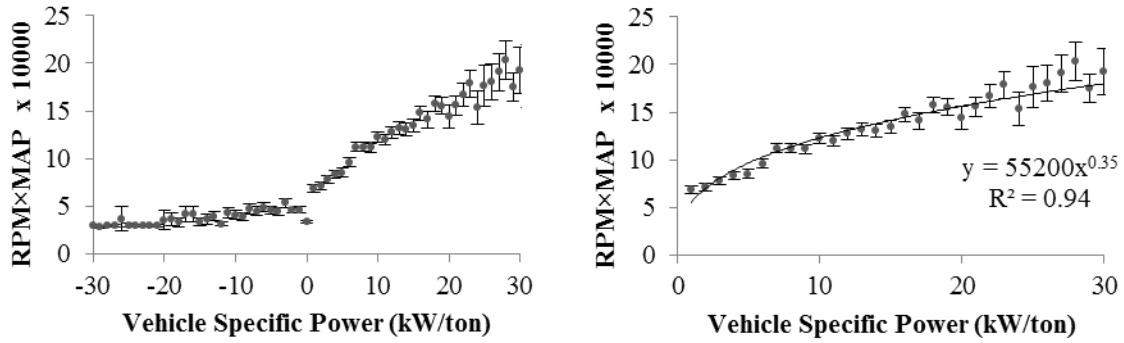

(a) Product of MAP and RPM versus Vehicle Specific Power

(b) Product of MAP and RPM versus Positive Vehicle Specific Power

Figure A-21 Measured product of Manifold Absolute Pressure (MAP) and engine Revolutions per Minute (RPM) versus Vehicle Specific Power (VSP) for a 1998 Buick Century. Error bars indicate 95 percent confidence intervals.

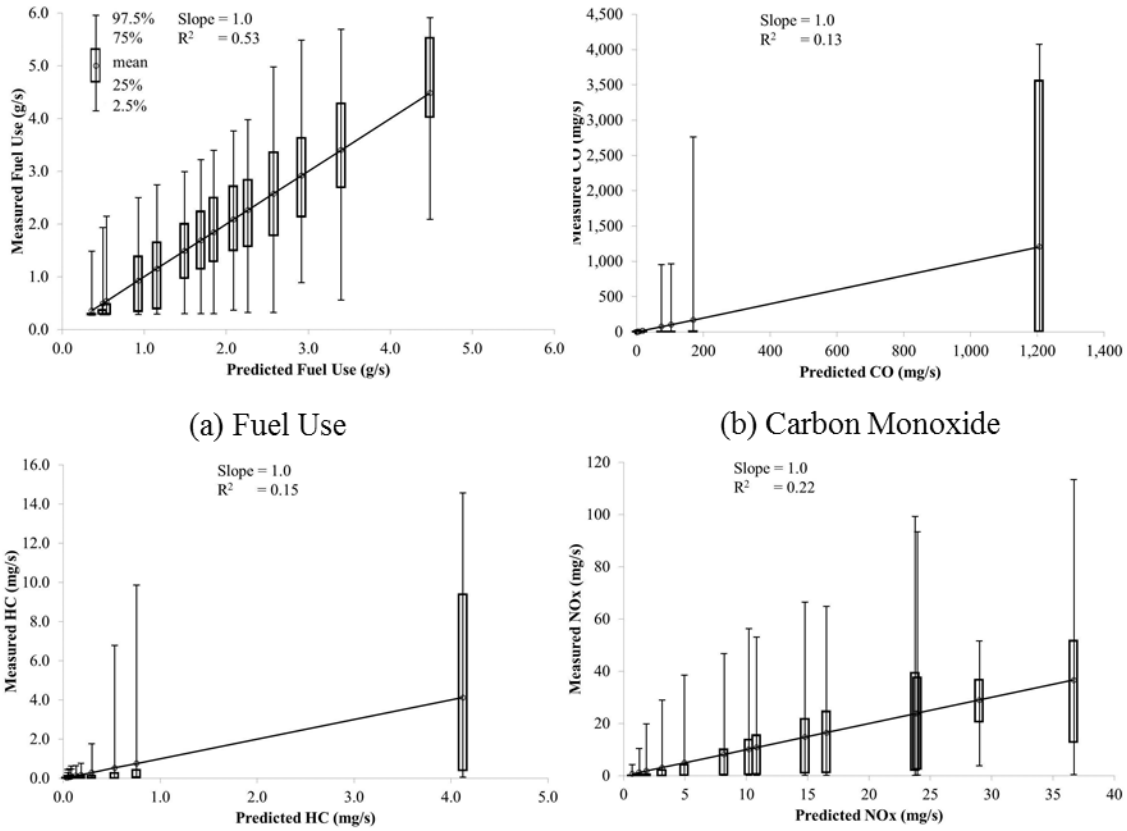

(a) Fuel Use

(b) Carbon Monoxide

(c) Hydrocarbon

(d) Nitrogen Oxides

Figure A-22 Comparison between measured and predicted fuel use and emission rates based on the Vehicle Specific Power-based model for a 1998 Buick Century.

A6.3 Fuel Use versus Internally Observable Variables

Fuel use rates are proportional to each of MAP and RPM, as illustrated in Figures A-23(a) and A-23(b), respectively. The coefficients of determination for fuel use as a power function of MAP and RPM are 0.75 and 0.79, respectively. The p-values for the scaling and power parameters for both power regressions were less than 0.001, indicating statistical significance. Therefore, each of MAP and RPM can be an explanatory variable for fuel use, explaining a substantial amount of the variation in fuel use.

However, although fuel use rate is influenced by each of RPM and MAP, the variability in fuel use rate is better explained by $P_{M\times R}$, as shown in Figure A-23(c). The predicted fuel use with bias corrections in terms of $P_{M\times R}$ in the form of Equation (5) is:

$$m_{Fuel,pred}^{(5)} = 1.4\times10^{-6}\times(P_{M\times R})^{1.19}\times1.02-0.012\text{ , }R^2 = 0.99 \qquad \text{(A6-2)}$$

The numerical values of "1.02" and "0.012" are the correction factors. Equation (A6-2) is used for predicting fuel use rates based on $P_{M\times R}$ for this vehicle.

A parity plot comparison between the Equation (A6-2) predicted versus measured fuel use rates is shown in Figure A-23(d), based on Equation (6). The data points follow a linear trend. The slope is 1 and the intercept is 0. The standard deviation of the residuals is 0.10 mg/s, which is small compared to mean fuel use rates of 1.0 mg/s. The R^2 for the linear fit is 0.99. The R^2 value of 0.99 is a significant improvement compared to the R^2 value of 0.53 based on the VSP-based approach. Therefore, the IOV-based model performs better than the EOV-based modal. There are some artifacts of the scatter plot that imply that the residual error may have non-constant variance with respect to the magnitude of fuel use rate. For very high fuel use rate the sample size is very small. However, from a practical perspective, this model is highly effective in predicting fuel use rate without any average bias.

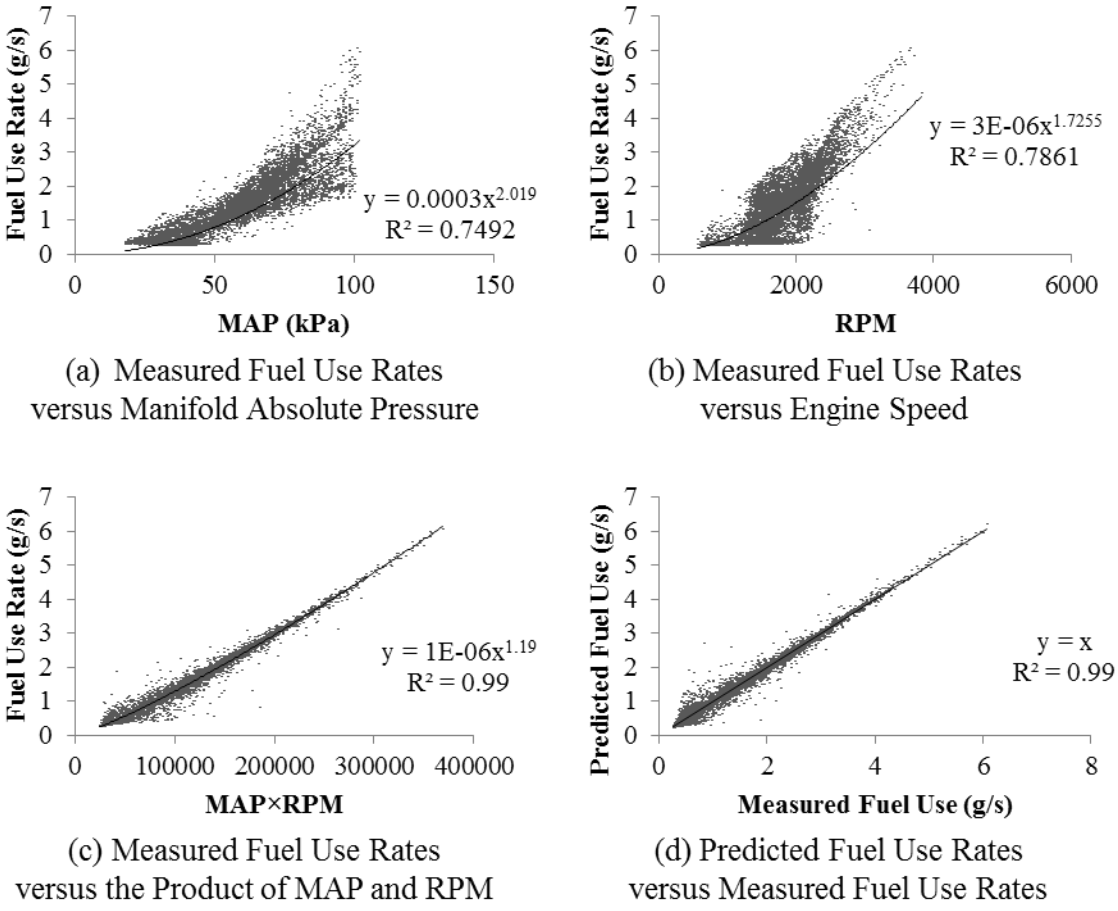

(a) Measured Fuel Use Rates versus Manifold Absolute Pressure

(b) Measured Fuel Use Rates versus Engine Speed

(c) Measured Fuel Use Rates versus the Product of MAP and RPM

(d) Predicted Fuel Use Rates versus Measured Fuel Use Rates

Figure A-23 Measured fuel use rates versus (a) Manifold Absolute Pressure (MAP) (b) engine Revolutions Per Minute (RPM), (c) the product of MAP and RPM, and (d) the predicted versus measured fuel use rates for a 1998 Buick Century measured during 110 miles of driving in the Raleigh, NC area.

A6.4 Emission Rates versus Internally Observable Variables

The relationships between emission rates of CO, HC, and NO_x versus and $P_{M\times R}$ are shown in Figures A-24(a), A-24(c), and A-24(e), respectively. For CO, most of the data points follow a power trend. A small portion of data has much higher CO emission rates compared to the fitted model. the IOV model based on $P_{M\times R}$ for CO emission rates is developed similarly to the model for fuel use rates. The model in the form of Equation (5) is:

$$m_{CO,pred}^{(5)} = 1.3\times10^{-4}\times(P_{M\times R})^{0.79}\times1550-1270,\ R^2 = 0.11 \qquad \text{(A6-3)}$$

The numerical values of "1,550" and "1,270" are the bias correction factors. Both the fitted scaling parameter of 1.3×10^{-4} and the power parameter of 0.79 have p-values of less than 0.001, indicating statistically significance.

A comparison of Equation (A6-3) predicted versus measured CO emission rates is shown in Figure A-24(b). The data fit a line with slope of 1 and the intercept of 0. The R^2 value of 0.05 is lower compared to the R^2 value of 0.13 for the VSP-based model shown in Figure A-22(b). Both the IOV- and EOV-based models are not well predicting the CO emission rates.

Figure A-24(c) illustrates the relationship between measured HC emission rates versus $P_{M\times R}$. There appear to be some clusters in this scatter plot. The majority of HC emission rates ranging from 0 to approximately 2 mg/s follow a power trend versus $P_{M\times R}$. For all data, the fitted model is:

$$m_{HC,pred}^{(5)} = 1.4\times10^{-7}\times(P_{M\times R})^{1.11}\times51-1.9,\ R^2 = 0.36 \qquad \text{(A6-4)}$$

The numerical values of "51" and "1.9" are the bias correction factors. Both the fitted scaling parameter of 1.4×10^{-7} and the power parameter of 1.11 have p-values of less than 0.001, indicating statistical significance.

A comparison of Equation (A6-4) predicted versus measured HC emission rates is shown in Figure A-24(d). The R^2 is 0.10 and is lower compared to the R^2 of 0.15 based on the VSP-based model, as illustrated in Figure A-22(c). Both the IOV- and EOV-based models are not well predicting the HC emission rates.

The relationship between measured NO_x emission rates versus $P_{M\times R}$ is illustrated in Figure A-24(e). The data appear to follow a power trend. The fitted model is:

$$m_{NOx,pred}^{(5)} = 1.2\times10^{-14}\times(P_{M\times R})^{2.83}\times4.2-5.8,\ R^2 = 0.61 \qquad \text{(A6-5)}$$

The numerical values of "4.2" and "5.8" are the bias correction factors. Both the fitted scaling parameter of 1.2×10^{-14} and the power parameter of 2.83 have p-values of less than 0.001, indicating statistical significance.

A comparison of Equation (A6-5) predicted and measured NO_x emission rates is shown in Figure A-24(f). The R^2 is 0.39, which is slightly higher than the R^2 of 0.22 of the VSP-based model illustrated in Figure A-22(d). Therefore, the IOV-based model is better than the EOV-based model in predicting NO_x emission rates.

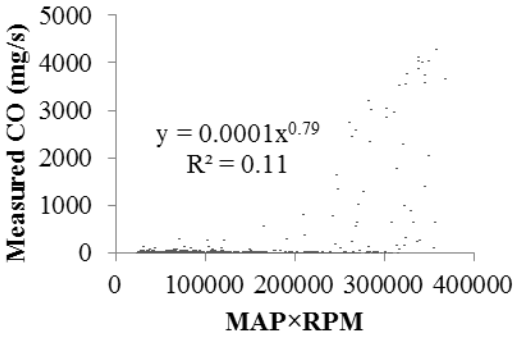

(a) Measured CO Emission Rates versus the Product of MAP and RPM

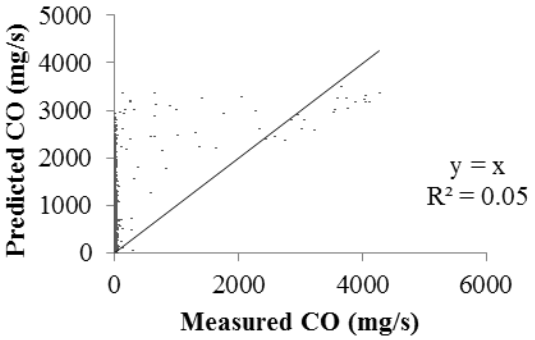

(b) Predicted versus Measured CO Emission Rates

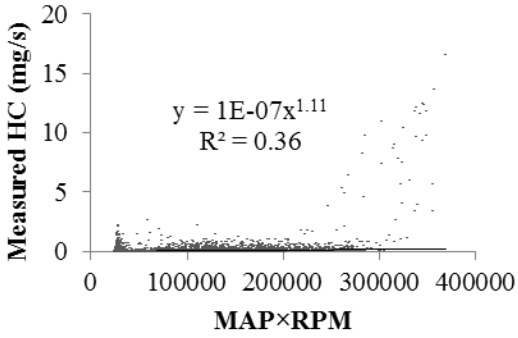

(c) Measured HC Emission Rates versus the Product of MAP and RPM

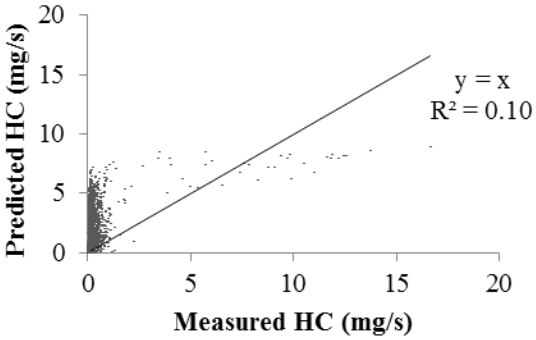

(d) Predicted versus Measured HC Emission Rates

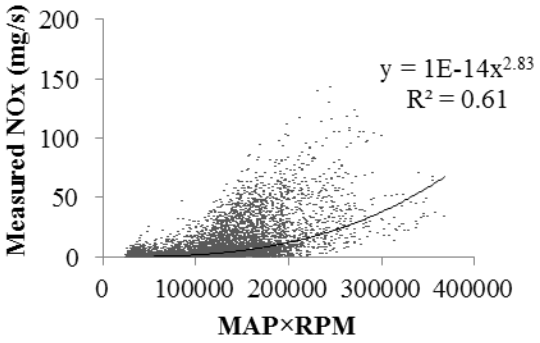

(e) Measured NO_x Emission Rates versus the Product of MAP and RPM

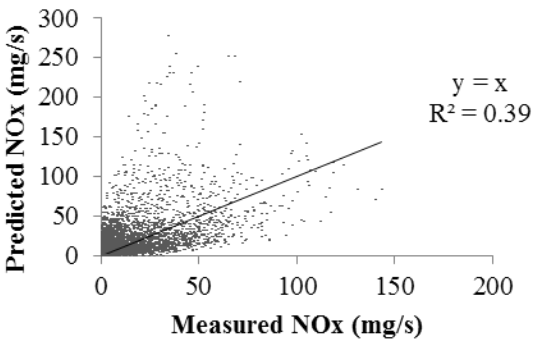

(f) Predicted versus Measured NO_x Emission Rates

Figure A-24 Relationship between emission rates and the product of Manifold Absolute Pressure (MAP) and engine Revolutions Per Minute (RPM) and comparison between predicted and measured emission rates for a 1998 Buick Century measured during 110 miles of driving in the Raleigh, NC area.

A7 2002 Chevrolet Silverado

For the 2002 Chevrolet Silverado, more than 12,800 seconds of valid data were collected, which account for more than 96 percent of raw data from the field measurements.

A7.1 Internally versus Externally Observable Variables

The relationship between $P_{M\times R}$ versus VSP is illustrated in Figure A-25. Average $P_{M\times R}$ values are plotted versus VSP ranging from -30 to 30 kW/ton with a 1 kW/ton interval. This range accounts for over 99% of measured vehicle activity. At negative VSP, there is no load on the engine and, thus, $P_{M\times R}$ is approximately constant. For increasing positive VSP, $P_{M\times R}$ typically increases monotonically.

A regression analysis was conducted for $P_{M\times R}$ versus VSP for positive VSP values, as shown in Figure A-25(b):

$$P_{M\times R} = 37900 \times VSP^{0.44}, \text{ for VSP>0, } R^2 = 0.96 \quad \text{(A7-1)}$$

$P_{M\times R}$ is 34,400 kPa-rev/min for negative VSP, and is corrected to no less than 34,400 kPa-rev/min for positive VSP. The p-values for the estimated scaling parameter of 37,900 and power parameter of 0.44 are both less than 0.001, indicating statistical significance. $P_{M\times R}$ is highly correlated with VSP. Thus, $P_{M\times R}$ is a good surrogate for engine power demand for this vehicle.

A7.2 Fuel Use and Emission Rates versus Externally Observable Variables

The VSP-based approach for predicting fuel use and emission rates is illustrated in Figures A-26(a) through A-26(d). For each VSP bin, there is substantial variability in fuel use and emission rates, as described in the box and whiskers based on the 2.5-percentile, 25-percentile, 75-percentile, and 97.5-percentile of one second values within each VSP bin. The R^2 for fuel use and emissions of CO, HC, and NO_x are 0.72, 0.32, 0.66, and 0.46, respectively. Thus, VSP is shown to be a good basis for estimating fuel use, and is able to explain some of the variability in 1 Hz emission rates. Furthermore, VSP is accurate in quantifying the mean trend in these rates.

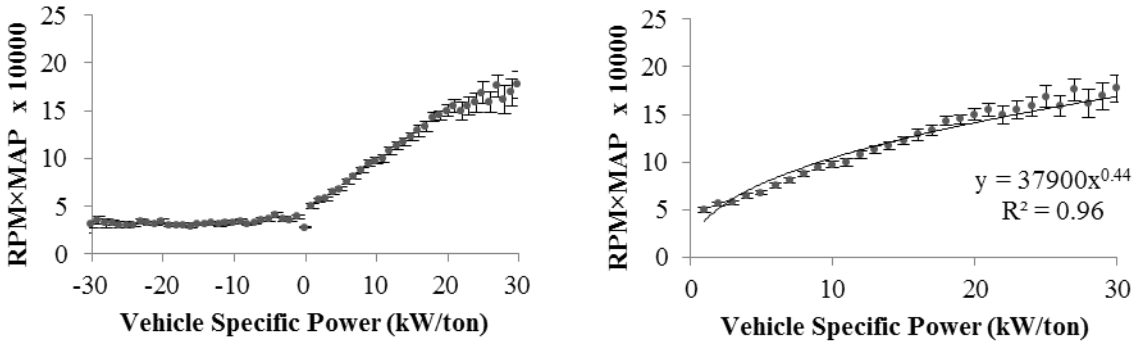

(a) Product of MAP and RPM versus Vehicle Specific Power

(b) Product of MAP and RPM versus Positive Vehicle Specific Power

Figure A-25 Measured product of Manifold Absolute Pressure (MAP) and engine Revolutions per Minute (RPM) versus Vehicle Specific Power (VSP) for a 2002 Chevrolet Silverado. Error bars indicate 95 percent confidence intervals.

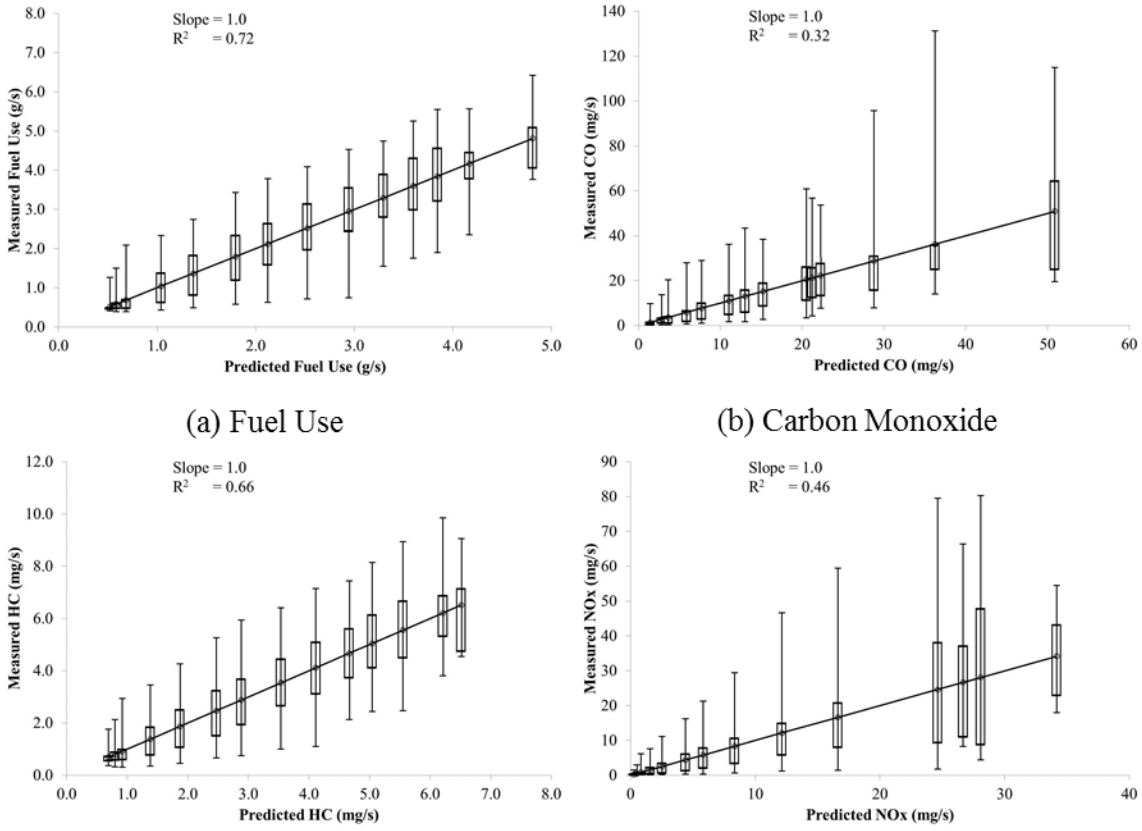

(a) Fuel Use

(b) Carbon Monoxide

(c) Hydrocarbon

(d) Nitrogen Oxides

Figure A-26 Comparison between measured and predicted fuel use and emission rates based on the Vehicle Specific Power-based model for a 2002 Chevrolet Silverado.

A7.3 Fuel Use versus Internally Observable Variables

Fuel use rates are proportional to each of MAP and RPM, as illustrated in Figures A-27(a) and A-27(b), respectively. The coefficients of determination for fuel use as a power function of MAP and RPM are 0.68 and 0.70, respectively. The p-values for the scaling and power parameters for both power regressions were less than 0.001, indicating statistical significance. Therefore, each of MAP and RPM can be an explanatory variable for fuel use, explaining a substantial amount of the variation in fuel use.

However, although fuel use rate is influenced by each of RPM and MAP, the variability in fuel use rate is better explained by $P_{M\times R}$, as shown in Figure A-27(c). The predicted fuel use with bias corrections in terms of $P_{M\times R}$ in the form of Equation (5) is:

$$m_{Fuel,pred}^{(5)} = 6.1\times10^{-6}\times(P_{M\times R})^{1.11}\times1.04-0.031,\ R^2 = 0.99 \qquad \text{(A7-2)}$$

The numerical values of "1.04" and "0.031" are the correction factors. Equation (A7-2) is used for predicting fuel use rates based on $P_{M\times R}$ for this vehicle.

A parity plot comparison between the Equation (A7-2) predicted versus measured fuel use rates is shown in Figure A-27(d), based on Equation (6). The data points follow a linear trend. The slope is 1 and the intercept is 0. The standard deviation of the residuals is 0.07 mg/s, which is small compared to mean fuel use rates of 1.4 mg/s. The R^2 for the linear fit is 0.99. The R^2 value of 0.99 is a significant improvement compared to the R^2 value of 0.72 based on the VSP-based approach. Therefore, the IOV-based model performs better than the EOV-based modal. There are some artifacts of the scatter plot that imply that the residual error may have non-constant variance with respect to the magnitude of fuel use rate. For very high fuel use rate the sample size is very small. However, from a practical perspective, this model is highly effective in predicting fuel use rate without any average bias.

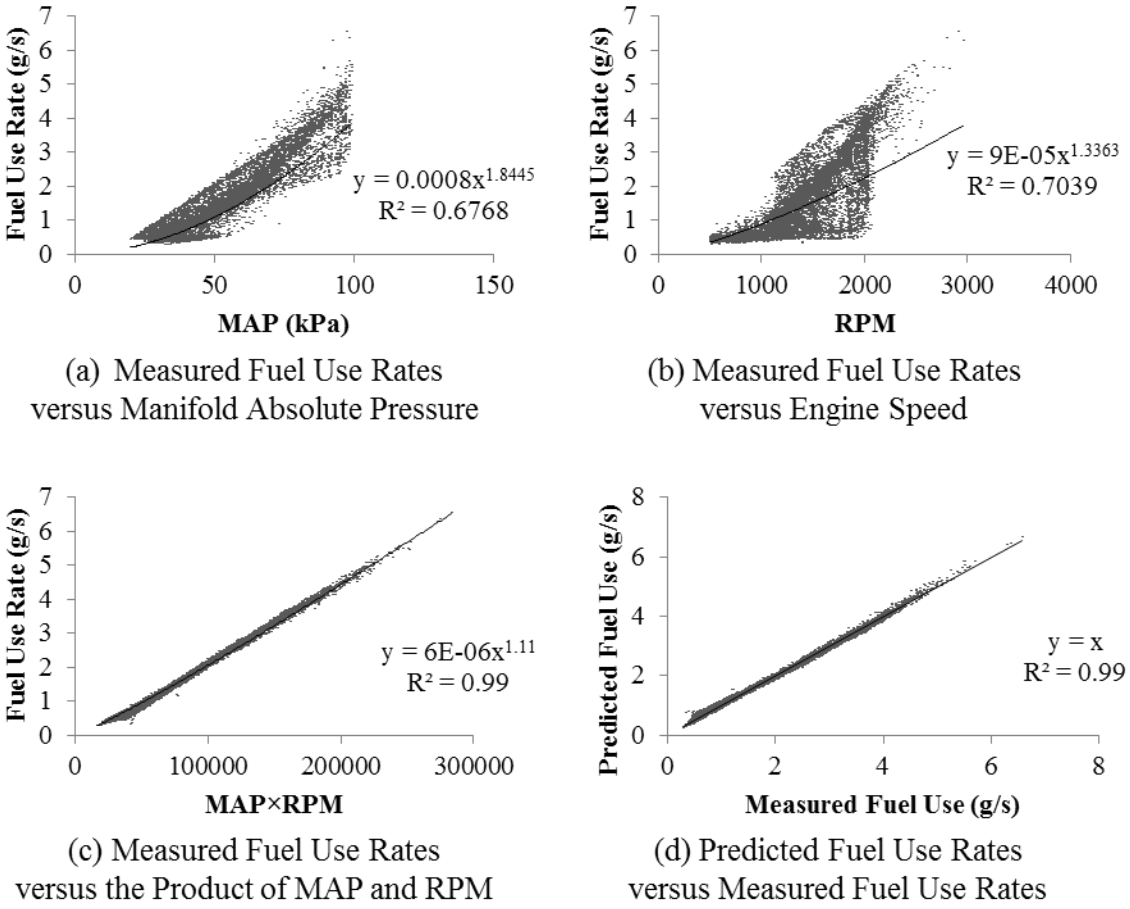

(a) Measured Fuel Use Rates versus Manifold Absolute Pressure

(b) Measured Fuel Use Rates versus Engine Speed

(c) Measured Fuel Use Rates versus the Product of MAP and RPM

(d) Predicted Fuel Use Rates versus Measured Fuel Use Rates

Figure A-27 Measured fuel use rates versus (a) Manifold Absolute Pressure (MAP) (b) engine Revolutions Per Minute (RPM), (c) the product of MAP and RPM, and (d) the predicted versus measured fuel use rates for a 2002 Chevrolet Silverado measured during 110 miles of driving in the Raleigh, NC area.

A7.4 Emission Rates versus Internally Observable Variables

The relationships between emission rates of CO, HC, and NO_x versus and $P_{M\times R}$ are shown in Figures A-28(a), A-28(c), and A-28(e), respectively. For CO, most of the data points follow a power trend. A small portion of data has much higher CO emission rates compared to the fitted model. the IOV model based on $P_{M\times R}$ for CO emission rates is developed similarly to the model for fuel use rates. The model in the form of Equation (5) is:

$$m_{CO,pred}^{(5)} = 1.3\times10^{-11}\times(P_{M\times R})^{1.78}\times 2.4 - 0.008\,,\ R^2 = 0.68 \qquad \text{(A7-3)}$$

The numerical values of "2.4" and "0.008" are the bias correction factors. Both the fitted scaling parameter of 1.3×10^{-11} and the power parameter of 1.78 have p-values of less than 0.001, indicating statistically significance.

A comparison of Equation (A7-3) predicted versus measured CO emission rates is shown in Figure A-28(b). The data fit a line with slope of 1 and the intercept of 0. The R^2 value of 0.39 is higher compared to the R^2 value of 0.32 for the VSP-based model shown in Figure A-26(b).

Figure A-28(c) illustrates the relationship between measured HC emission rates versus $P_{M\times R}$. There appear to be some clusters in this scatter plot. The majority of HC emission rates ranging from 0 to approximately 0.01 mg/s follow a power trend versus $P_{M\times R}$. There also appear other clusters each containing a small portion of data. This vehicle has 4-gear automatic transmission. These clusters might be associated with gear selection. Although stratification of these data might be possible based on additional IOVs, these clusters cannot be discriminated based on $P_{M\times R}$ alone. For all data, the fitted model is:

$$m_{HC,pred}^{(5)} = 5.9\times10^{-9}\times(P_{M\times R})^{1.13}\times1.2-0.0002,\ R^2 = 0.87 \qquad \text{(A7-4)}$$

The numerical values of "1.2" and "0.0002" are the bias correction factors. Both the fitted scaling parameter of 5.9×10^{-9} and the power parameter of 1.13 have p-values of less than 0.001, indicating statistical significance.

A comparison of Equation (A7-4) predicted versus measured HC emission rates is shown in Figure A-28(d). The R^2 is 0.91 and is a significant improvement compared to the R^2 of 0.66 based on the VSP-based model, as illustrated in Figure A-26(c). Therefore, the IOV-based model describes the HC emission rates well, and is better than the EOV-based model.

The relationship between measured NO_x emission rates versus $P_{M\times R}$ is illustrated in Figure A-28(e). The data appear to follow a power trend. The fitted model is:

$$m_{NOx,pred}^{(5)} = 9.5\times10^{-17}\times(P_{M\times R})^{2.73}\times1.6-0.0015,\ R^2 = 0.78 \qquad \text{(A7-5)}$$

The numerical values of "1.6" and "0.0015" are the bias correction factors. Both the fitted scaling parameter of 9.5×10^{-17} and the power parameter of 2.73 have p-values of less than 0.001, indicating statistical significance.

A comparison of Equation (A7-5) predicted and measured NO_x emission rates is shown in Figure A-28(f). The R^2 is 0.77, which is higher than the R^2 of 0.46 of the VSP-based model illustrated in Figure A-26(d). Therefore, the IOV-based model is better than the EOV-based model in predicting NO_x emission rates.

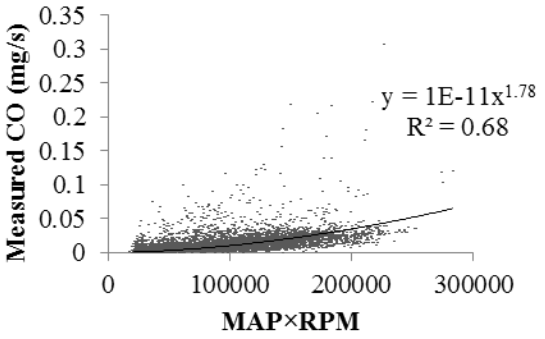

(a) Measured CO Emission Rates versus the Product of MAP and RPM

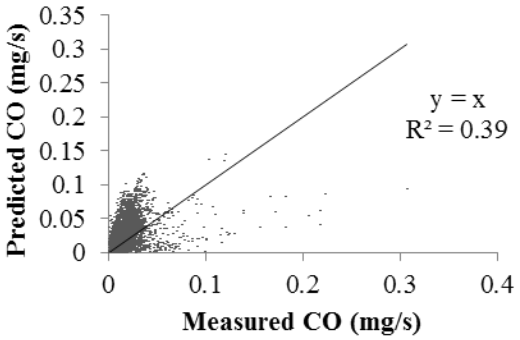

(b) Predicted versus Measured CO Emission Rates

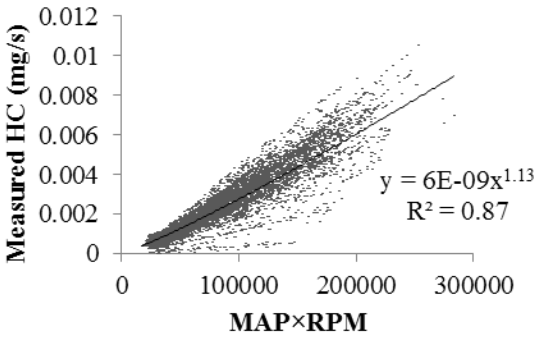

(c) Measured HC Emission Rates versus the Product of MAP and RPM

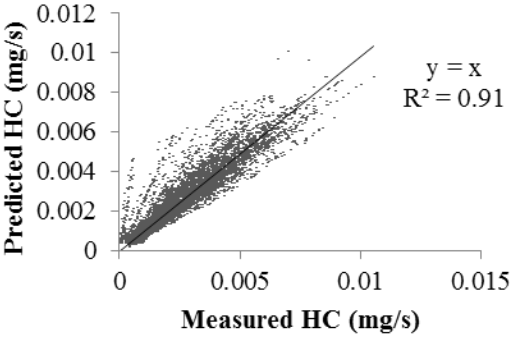

(d) Predicted versus Measured HC Emission Rates

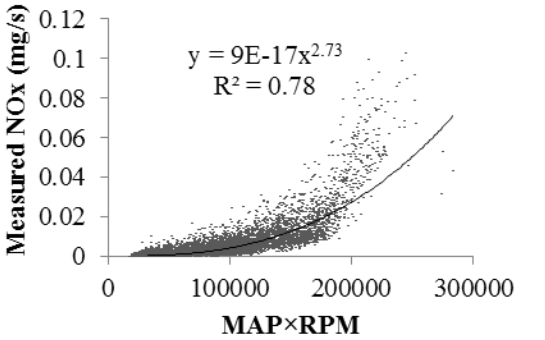

(e) Measured NO_x Emission Rates versus the Product of MAP and RPM

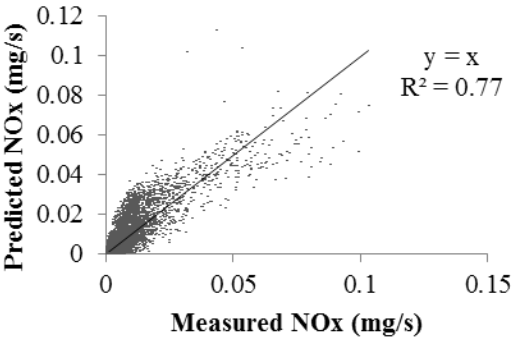

(f) Predicted versus Measured NO_x Emission Rates

Figure A-28 Relationship between emission rates and the product of Manifold Absolute Pressure (MAP) and engine Revolutions Per Minute (RPM) and comparison between predicted and measured emission rates for a 2002 Chevrolet Silverado measured during 110 miles of driving in the Raleigh, NC area.

A8 2010 Ford F150

For the 2010 Ford F150, more than 12,100 seconds of valid data were collected, which account for more than 96 percent of raw data from the field measurements.

A8.1 Internally versus Externally Observable Variables

The relationship between $P_{M\times R}$ versus VSP is illustrated in Figure A-29. Average $P_{M\times R}$ values are plotted versus VSP ranging from -30 to 30 kW/ton with a 1 kW/ton interval. This range accounts for over 99% of measured vehicle activity. At negative VSP, there is no load on the engine and, thus, $P_{M\times R}$ is approximately constant. For increasing positive VSP, $P_{M\times R}$ typically increases monotonically.

A regression analysis was conducted for $P_{M\times R}$ versus VSP for positive VSP values, as shown in Figure A-29(b):

$$P_{M\times R} = 36600 \times VSP^{0.44}, \text{ for VSP>0, } R^2 = 0.95 \quad \text{(A8-1)}$$

$P_{M\times R}$ is 32,100 kPa-rev/min for negative VSP, and is corrected to no less than 32,100 kPa-rev/min for positive VSP. The p-values for the estimated scaling parameter of 36,600 and power parameter of 0.44 are both less than 0.001, indicating statistical significance. $P_{M\times R}$ is highly correlated with VSP. Thus, $P_{M\times R}$ is a good surrogate for engine power demand for this vehicle.

A8.2 Fuel Use and Emission Rates versus Externally Observable Variables

The VSP-based approach for predicting fuel use and emission rates is illustrated in Figures A-30(a) through A-30(d). For each VSP bin, there is substantial variability in fuel use and emission rates, as described in the box and whiskers based on the 2.5-percentile, 25-percentile, 75-percentile, and 97.5-percentile of one second values within each VSP bin. The R^2 for fuel use and emissions of CO, HC, and NO_x are 0.68, 0.03, 0.43, and 0.16, respectively. Thus, VSP is shown to be a good basis for estimating fuel use, and is able to explain some of the variability in 1 Hz emission rates. Furthermore, VSP is accurate in quantifying the mean trend in these rates.

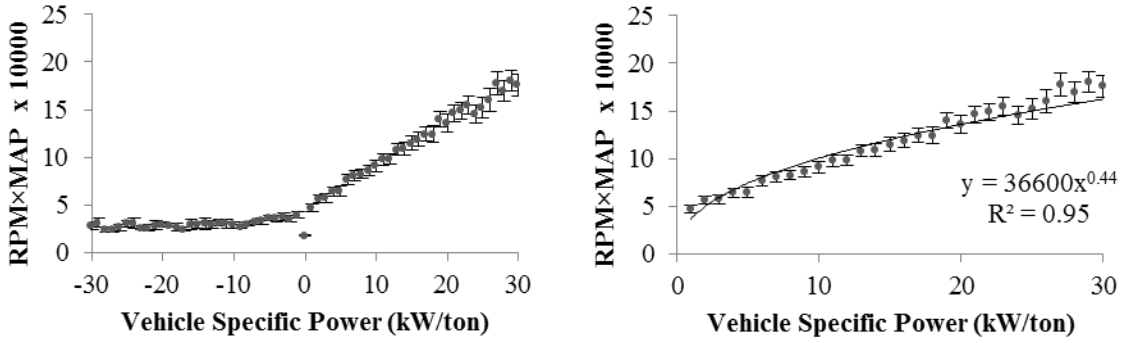

(a) Product of MAP and RPM versus Vehicle Specific Power

(b) Product of MAP and RPM versus Positive Vehicle Specific Power

Figure A-29 Measured product of Manifold Absolute Pressure (MAP) and engine Revolutions per Minute (RPM) versus Vehicle Specific Power (VSP) for a 2010 Ford F150. Error bars indicate 95 percent confidence intervals.

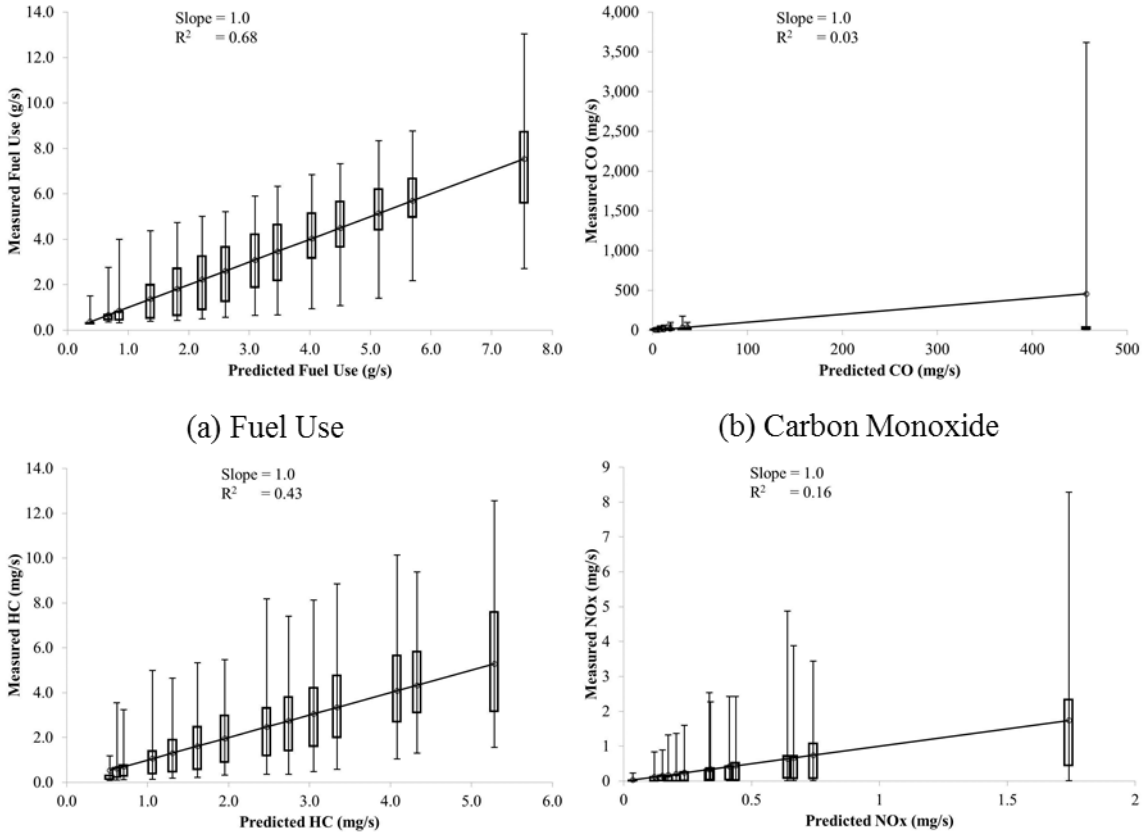

(a) Fuel Use

(b) Carbon Monoxide

(c) Hydrocarbon

(d) Nitrogen Oxides

Figure A-30 Comparison between measured and predicted fuel use and emission rates based on the Vehicle Specific Power-based model for a 2010 Ford F150.

A8.3 Fuel Use versus Internally Observable Variables

Fuel use rates are proportional to each of MAP and RPM, as illustrated in Figures A-31(a) and A-31(b), respectively. The coefficients of determination for fuel use as a power function of MAP and RPM are 0.86 and 0.69, respectively. The p-values for the scaling and power parameters for both power regressions were less than 0.001, indicating statistical significance. Therefore, each of MAP and RPM can be an explanatory variable for fuel use, explaining a substantial amount of the variation in fuel use.

However, although fuel use rate is influenced by each of RPM and MAP, the variability in fuel use rate is better explained by $P_{M\times R}$, as shown in Figure A-31(c). The predicted fuel use with bias corrections in terms of $P_{M\times R}$ in the form of Equation (5) is:

$$m_{Fuel,pred}^{(5)} = 3.8\times10^{-6}\times(P_{M\times R})^{1.17}\times0.99-(-0.022)\text{ , } R^2 = 0.99 \qquad \text{(A8-2)}$$

The numerical values of "0.99" and "-0.022" are the correction factors. Equation (A8-2) is used for predicting fuel use rates based on $P_{M\times R}$ for this vehicle.

A parity plot comparison between the Equation (A8-2) predicted versus measured fuel use rates is shown in Figure A-31(d), based on Equation (6). The data points follow a linear trend. The slope is 1 and the intercept is 0. The standard deviation of the residuals is 0.18 mg/s, which is small compared to mean fuel use rates of 1.8 mg/s. The R^2 for the linear fit is 0.99. The R^2 value of 0.99 is a significant improvement compared to the R^2 value of 0.68 based on the VSP-based approach. Therefore, the IOV-based model performs better than the EOV-based modal. There are some artifacts of the scatter plot that imply that the residual error may have non-constant variance with respect to the magnitude of fuel use rate. For very high fuel use rate the sample size is very small. However, from a practical perspective, this model is highly effective in predicting fuel use rate without any average bias.

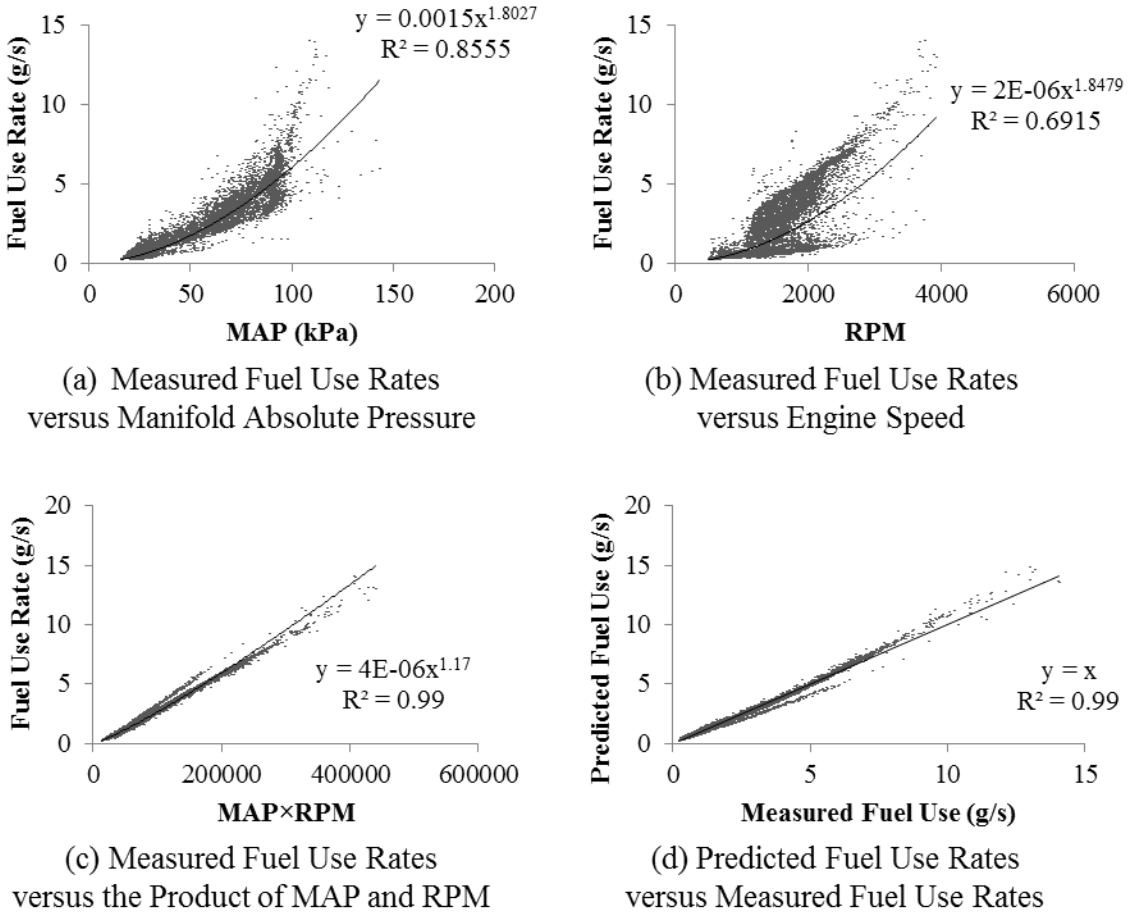

(a) Measured Fuel Use Rates versus Manifold Absolute Pressure

(b) Measured Fuel Use Rates versus Engine Speed

(c) Measured Fuel Use Rates versus the Product of MAP and RPM

(d) Predicted Fuel Use Rates versus Measured Fuel Use Rates

Figure A-31 Measured fuel use rates versus (a) Manifold Absolute Pressure (MAP) (b) engine Revolutions Per Minute (RPM), (c) the product of MAP and RPM, and (d) the predicted versus measured fuel use rates for a 2010 Ford F150 measured during 110 miles of driving in the Raleigh, NC area.

A8.4 Emission Rates versus Internally Observable Variables

The relationships between emission rates of CO, HC, and NO_x versus and $P_{M\times R}$ are shown in Figures A-32(a), A-32(c), and A-32(e), respectively. For CO, most of the data points follow a power trend. A small portion of data has much higher CO emission rates compared to the fitted model. the IOV model based on $P_{M\times R}$ for CO emission rates is developed similarly to the model for fuel use rates. The model in the form of Equation (5) is:

$$m_{CO,pred}^{(5)} = 1.4\times10^{-6}\times(P_{M\times R})^{1.29}\times144-405,\ R^2 = 0.48 \qquad \text{(A8-3)}$$

The numerical values of "144" and "405" are the bias correction factors. Both the fitted scaling parameter of 1.4×10^{-6} and the power parameter of 1.29 have p-values of less than 0.001, indicating statistically significance.

A comparison of Equation (A8-3) predicted versus measured CO emission rates is shown in Figure A-32(b). The data fit a line with slope of 1 and the intercept of 0. The R^2 value of 0.06 is slightly higher compared to the R^2 value of 0.03 for the VSP-based model shown in Figure A-30(b).

Figure A-32(c) illustrates the relationship between measured HC emission rates versus $P_{M\times R}$. There appear to be some clusters in this scatter plot. The majority of HC emission rates ranging from 0 to approximately 6 mg/s follow a power trend versus $P_{M\times R}$. There also appear other clusters each containing a small portion of data. This vehicle has 4-gear automatic transmission. These clusters might be associated with gear selection. Although stratification of these data might be possible based on additional IOVs, these clusters cannot be discriminated based on $P_{M\times R}$ alone. For all data, the fitted model is:

$$m_{HC,pred}^{(5)} = 2.0\times10^{-6}\times(P_{M\times R})^{1.20}\times1.6-0.60,\ R^2 = 0.80 \qquad \text{(A8-4)}$$

The numerical values of "1.6" and "0.60" are the bias correction factors. Both the fitted scaling parameter of 2.0×10^{-6} and the power parameter of 1.20 have p-values of less than 0.001, indicating statistical significance.

A comparison of Equation (A8-4) predicted versus measured HC emission rates is shown in Figure A-32(d). The R^2 is 0.67 and is a significant improvement compared to the R^2 of 0.43 based on the VSP-based model, as illustrated in Figure A-30(c). Therefore, the IOV-based model describes the HC emission rates well, and is better than the EOV-based model.

The relationship between measured NO_x emission rates versus $P_{M\times R}$ is illustrated in Figure A-32(e). The data appear to follow a power trend. The fitted model is:

$$m_{NOx,pred}^{(5)} = 5.0\times10^{-8}\times(P_{M\times R})^{1.33}\times8.4-1.1,\ R^2 = 0.45 \qquad \text{(A8-5)}$$

The numerical values of "8.4" and "1.1" are the bias correction factors. Both the fitted scaling parameter of 5.0×10^{-8} and the power parameter of 1.33 have p-values of less than 0.001, indicating statistical significance.

A comparison of Equation (A8-5) predicted and measured NO_x emission rates is shown in Figure A-32(f). The R^2 is 0.24, which is higher than the R^2 of 0.16 of the VSP-based model illustrated in Figure A-2(d). Therefore, the IOV-based model is better than the EOV-based model in predicting NO_x emission rates.

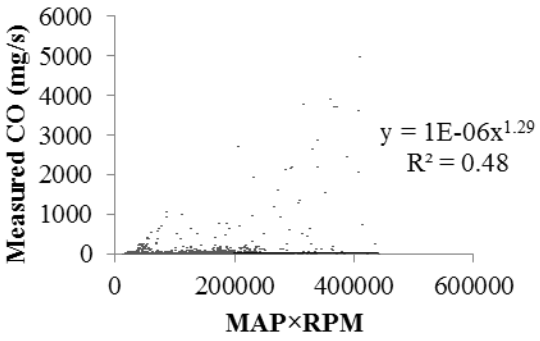

(a) Measured CO Emission Rates versus the Product of MAP and RPM

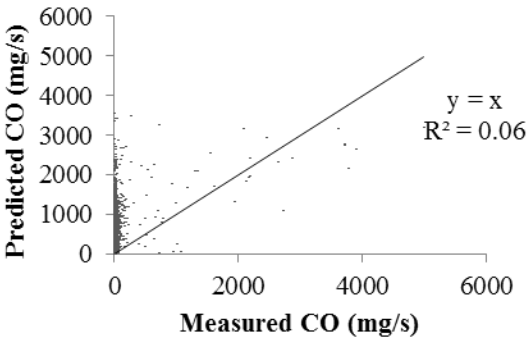

(b) Predicted versus Measured CO Emission Rates

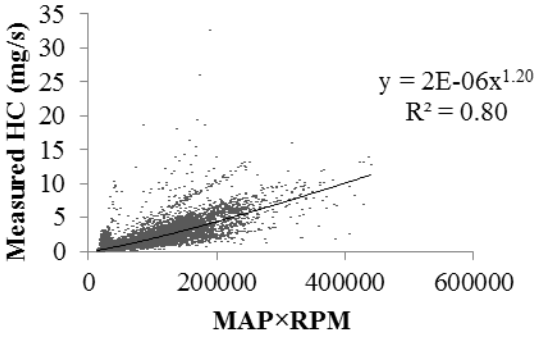

(c) Measured HC Emission Rates versus the Product of MAP and RPM

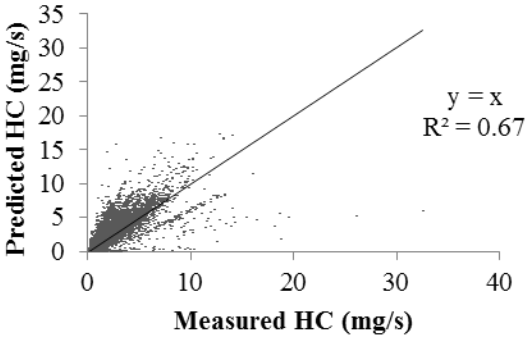

(d) Predicted versus Measured HC Emission Rates

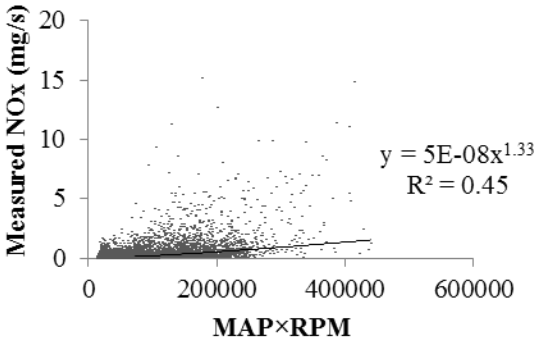

(e) Measured NO_x Emission Rates versus the Product of MAP and RPM

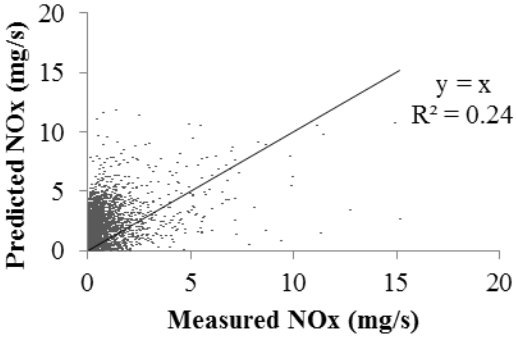

(f) Predicted versus Measured NO_x Emission Rates

Figure A-32 Relationship between emission rates and the product of Manifold Absolute Pressure (MAP) and engine Revolutions Per Minute (RPM) and comparison between predicted and measured emission rates for a 2010 Ford F150 measured during 110 miles of driving in the Raleigh, NC area.

A9 1998 Chevrolet S10

For the 1998 Chevrolet S10, more than 11,300 seconds of valid data were collected, which account for more than 95 percent of raw data from the field measurements.

A9.1 Internally versus Externally Observable Variables

The relationship between $P_{M\times R}$ versus VSP is illustrated in Figure A-33. Average $P_{M\times R}$ values are plotted versus VSP ranging from -30 to 30 kW/ton with a 1 kW/ton interval. This range accounts for over 99% of measured vehicle activity. At negative VSP, there is no load on the engine and, thus, $P_{M\times R}$ is approximately constant. For increasing positive VSP, $P_{M\times R}$ typically increases monotonically.

A regression analysis was conducted for $P_{M\times R}$ versus VSP for positive VSP values, as shown in Figure A-33(b):

$$P_{M\times R} = 43200 \times VSP^{0.35}, \text{ for VSP>0, } R^2 = 0.97 \quad \text{(A9-1)}$$

$P_{M\times R}$ is 33,100 kPa-rev/min for negative VSP, and is corrected to no less than 33,100 kPa-rev/min for positive VSP. The p-values for the estimated scaling parameter of 43,200 and power parameter of 0.35 are both less than 0.001, indicating statistical significance. $P_{M\times R}$ is highly correlated with VSP. Thus, $P_{M\times R}$ is a good surrogate for engine power demand for this vehicle.

A9.2 Fuel Use and Emission Rates versus Externally Observable Variables

The VSP-based approach for predicting fuel use and emission rates is illustrated in Figures A-34(a) through A-34(d). For each VSP bin, there is substantial variability in fuel use and emission rates, as described in the box and whiskers based on the 2.5-percentile, 25-percentile, 75-percentile, and 97.5-percentile of one second values within each VSP bin. The R^2 for fuel use and emissions of CO, HC, and NO_x are 0.68, 0.03, 0.10, and 0.20, respectively. Thus, VSP is shown to be a good basis for estimating fuel use, and is able to explain some of the variability in 1 Hz emission rates. Furthermore, VSP is accurate in quantifying the mean trend in these rates.

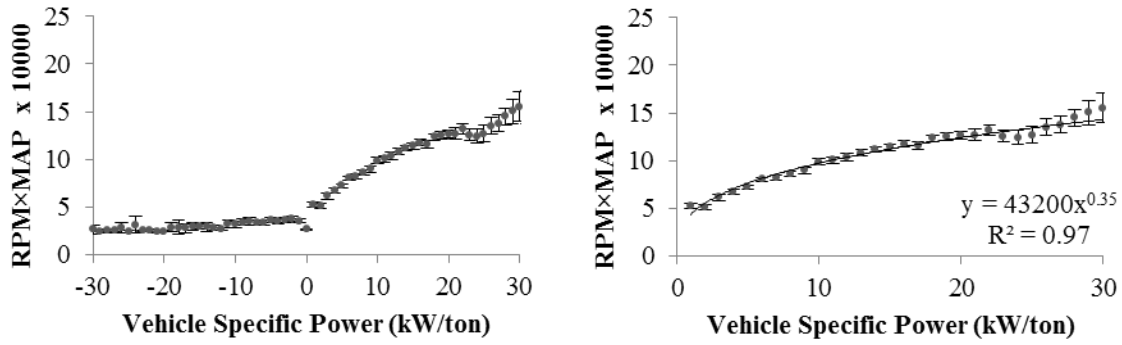

(a) Product of MAP and RPM versus Vehicle Specific Power

(b) Product of MAP and RPM versus Positive Vehicle Specific Power

Figure A-33 Measured product of Manifold Absolute Pressure (MAP) and engine Revolutions per Minute (RPM) versus Vehicle Specific Power (VSP) for a 1998 Chevrolet S10. Error bars indicate 95 percent confidence intervals.

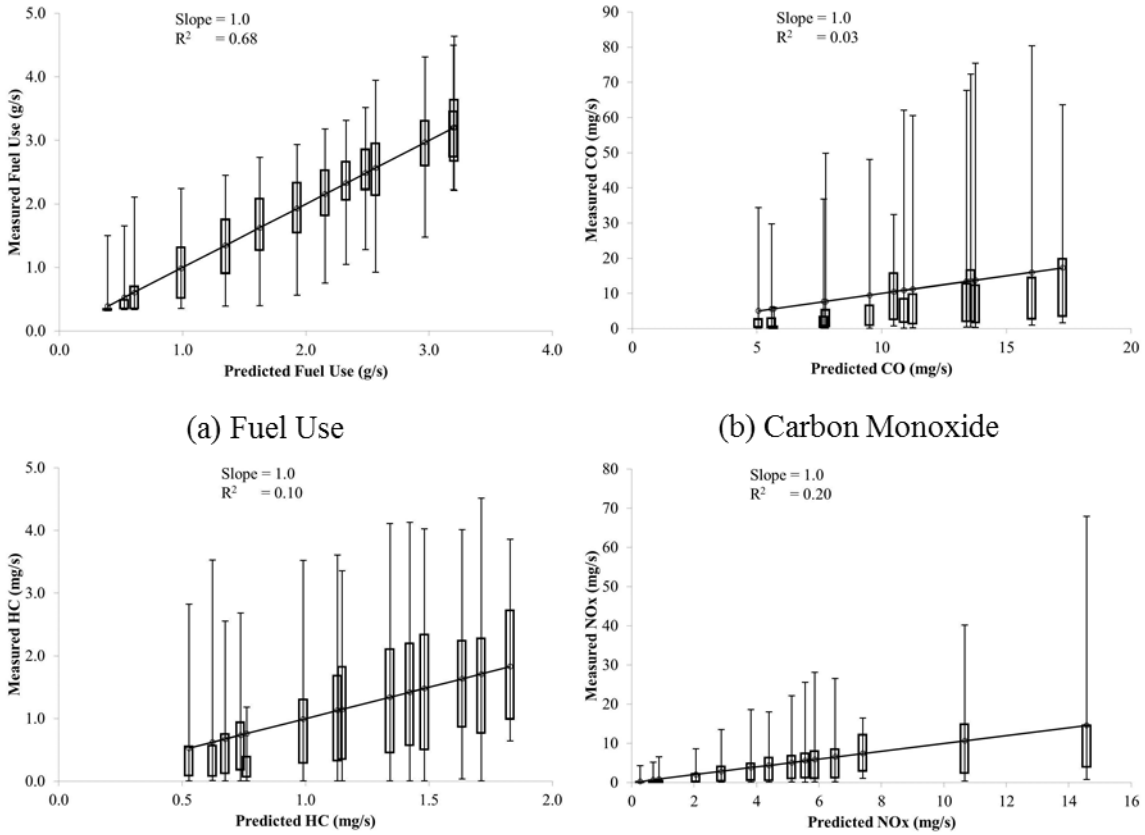

(a) Fuel Use

(b) Carbon Monoxide

(c) Hydrocarbon

(d) Nitrogen Oxides

Figure A-34 Comparison between measured and predicted fuel use and emission rates based on the Vehicle Specific Power-based model for a 1998 Chevrolet S10.

A9.3 Fuel Use versus Internally Observable Variables

Fuel use rates are proportional to each of MAP and RPM, as illustrated in Figures A-35(a) and A-35(b), respectively. The coefficients of determination for fuel use as a power function of MAP and RPM are 0.78 and 0.80, respectively. The p-values for the scaling and power parameters for both power regressions were less than 0.001, indicating statistical significance. Therefore, each of MAP and RPM can be an explanatory variable for fuel use, explaining a substantial amount of the variation in fuel use.

However, although fuel use rate is influenced by each of RPM and MAP, the variability in fuel use rate is better explained by $P_{M\times R}$, as shown in Figure A-35(c). The predicted fuel use with bias corrections in terms of $P_{M\times R}$ in the form of Equation (5) is:

$$m_{Fuel,pred}^{(5)} = 3.6\times10^{-6}\times(P_{M\times R})^{1.15}\times1.01-0.004\,,\ R^2 = 0.98 \qquad \text{(A9-2)}$$

The numerical values of "1.01" and "0.004" are the correction factors. Equation (A9-2) is used for predicting fuel use rates based on $P_{M\times R}$ for this vehicle.

A parity plot comparison between the Equation (A9-2) predicted versus measured fuel use rates is shown in Figure A-35(d), based on Equation (6). The data points follow a linear trend. The slope is 1 and the intercept is 0. The standard deviation of the residuals is 0.12 mg/s, which is small compared to mean fuel use rates of 1.2 mg/s. The R^2 for the linear fit is 0.98. The R^2 value of 0.98 is a significant improvement compared to the R^2 value of 0.68 based on the VSP-based approach. Therefore, the IOV-based model performs better than the EOV-based modal. There are some artifacts of the scatter plot that imply that the residual error may have non-constant variance with respect to the magnitude of fuel use rate. For very high fuel use rate the sample size is very small. However, from a practical perspective, this model is highly effective in predicting fuel use rate without any average bias.

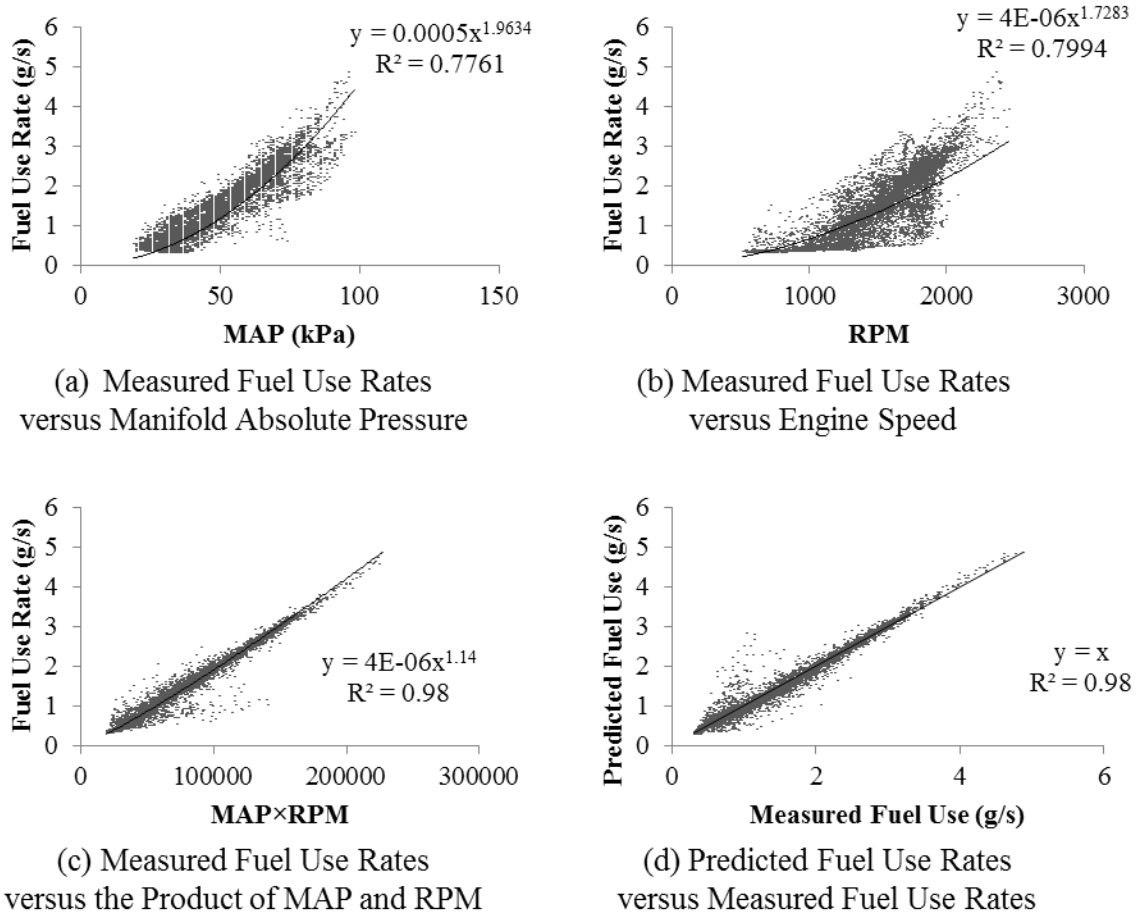

(a) Measured Fuel Use Rates versus Manifold Absolute Pressure

(b) Measured Fuel Use Rates versus Engine Speed

(c) Measured Fuel Use Rates versus the Product of MAP and RPM

(d) Predicted Fuel Use Rates versus Measured Fuel Use Rates

Figure A-35 Measured fuel use rates versus (a) Manifold Absolute Pressure (MAP) (b) engine Revolutions Per Minute (RPM), (c) the product of MAP and RPM, and (d) the predicted versus measured fuel use rates for a 1998 Chevrolet S10 measured during 110 miles of driving in the Raleigh, NC area.

A9.4 Emission Rates versus Internally Observable Variables

The relationships between emission rates of CO, HC, and NO_x versus and $P_{M\times R}$ are shown in Figures A-36(a), A-36(c), and A-36(e), respectively. For CO, most of the data points follow a power trend. A small portion of data has much higher CO emission rates compared to the fitted model. the IOV model based on $P_{M\times R}$ for CO emission rates is developed similarly to the model for fuel use rates. The model in the form of Equation (5) is:

$$m_{CO,pred}^{(5)} = 2.7\times10^{-7}\times(P_{M\times R})^{1.44}\times51-126\,,\ R^2 = 0.33 \qquad \text{(A9-3)}$$

The numerical values of "51" and "126" are the bias correction factors. Both the fitted scaling parameter of 2.7×10^{-7} and the power parameter of 1.44 have p-values of less than 0.001, indicating statistically significance.

A comparison of Equation (A9-3) predicted versus measured CO emission rates is shown in Figure A-36(b). The data fit a line with slope of 1 and the intercept of 0. The R^2 value of 0.04 is slightly higher compared to the R^2 value of 0.03 for the VSP-based model shown in Figure A-34(b). Both the IOV- and EOV-based models are not well predicting the CO emission rates.

Figure A-36(c) illustrates the relationship between measured HC emission rates versus $P_{M\times R}$. There appear to be some clusters in this scatter plot. The majority of HC emission rates ranging from 0 to approximately 5 mg/s follow a power trend versus $P_{M\times R}$. There also appear other clusters each containing a small portion of data. This vehicle has 4-gear automatic transmission. These clusters might be associated with gear selection. Although stratification of these data might be possible based on additional IOVs, these clusters cannot be discriminated based on $P_{M\times R}$ alone. For all data, the fitted model is:

$$m_{HC,pred}^{(5)} = 3.6\times10^{-6}\times(P_{M\times R})^{1.07}\times 6.0 - 2.2,\ R^2 = 0.30 \qquad \text{(A9-4)}$$

The numerical values of "6.0" and "2.2" are the bias correction factors. Both the fitted scaling parameter of 3.6×10^{-6} and the power parameter of 1.07 have p-values of less than 0.001, indicating statistical significance.

A comparison of Equation (A9-4) predicted versus measured HC emission rates is shown in Figure A-36(d). The R^2 is 0.23 and is a significant improvement compared to the R^2 of 0.10 based on the VSP-based model, as illustrated in Figure A-34(c). Therefore, the IOV-based model describes the HC emission rates well, and is better than the EOV-based model.

The relationship between measured NO_x emission rates versus $P_{M\times R}$ is illustrated in Figure A-36(e). The data appear to follow a power trend. The fitted model is:

$$m_{NOx,pred}^{(5)} = 4.1\times10^{-12}\times(P_{M\times R})^{2.34}\times 6.0 - 5.7,\ R^2 = 0.54 \qquad \text{(A9-5)}$$

The numerical values of "6.0" and "5.7" are the bias correction factors. Both the fitted scaling parameter of 4.1×10^{-12} and the power parameter of 2.34 have p-values of less than 0.001, indicating statistical significance.

A comparison of Equation (A9-5) predicted and measured NO_x emission rates is shown in Figure A-36(f). The R^2 is 0.26, which is slightly higher than the R^2 of 0.20 of the VSP-based model illustrated in Figure A-34(d). Therefore, the IOV-based model is better than the EOV-based model in predicting NO_x emission rates.

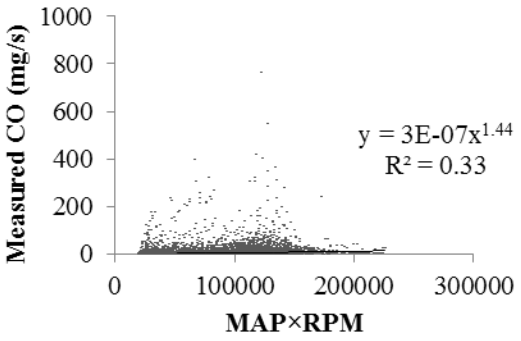

(a) Measured CO Emission Rates versus the Product of MAP and RPM

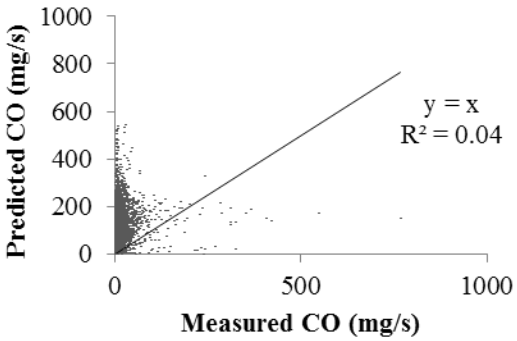

(b) Predicted versus Measured CO Emission Rates

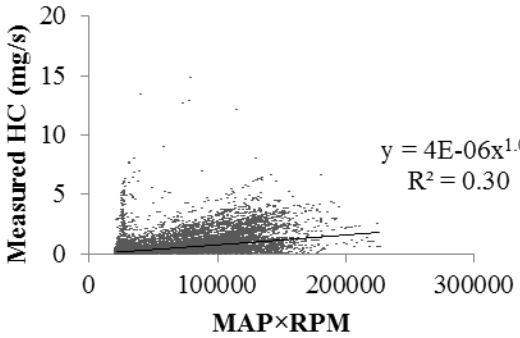

(c) Measured HC Emission Rates versus the Product of MAP and RPM

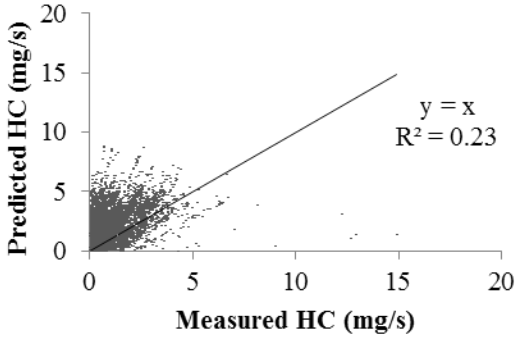

(d) Predicted versus Measured HC Emission Rates

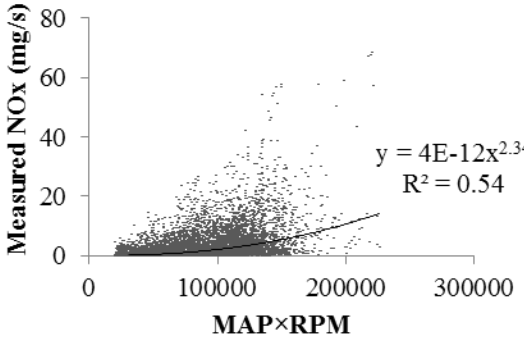

(e) Measured NO_x Emission Rates versus the Product of MAP and RPM

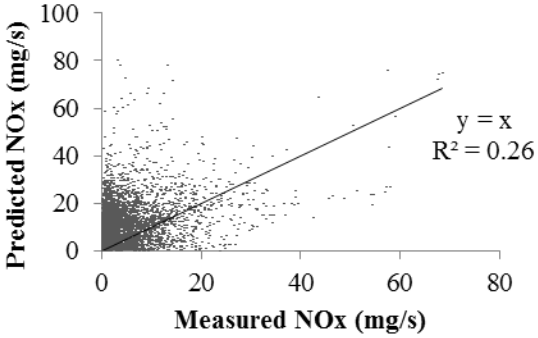

(f) Predicted versus Measured NO_x Emission Rates

Figure A-36 Relationship between emission rates and the product of Manifold Absolute Pressure (MAP) and engine Revolutions Per Minute (RPM) and comparison between predicted and measured emission rates for a 1998 Chevrolet S10 measured during 110 miles of driving in the Raleigh, NC area.

Part III: Implementation of Vehicle-Specific Fuel Use and Emissions Models Based on Internally Observable Activity Data into Traffic Microsimulation

Introduction

SwashSim, a microscopic traffic simulation program, has been in development over the last few years, led by Dr. Washburn. SwashSim is based on a modern programming language (C# in .NET Framework) and uses an object-oriented architecture. The object-oriented architecture allows the simulation tool to define and model objects (e.g., vehicles, vehicle components, roadway segments, drivers, etc.) much like they exist in reality. For defining the performance capabilities of vehicles, SwashSim includes classes (i.e., object definitions) that model the power/drivetrain capabilities of vehicles and determines acceleration capabilities. This ability is key to be able to produce the inputs necessary for the IOV fuel and emissions estimation models.

Vehicle Dynamics Modeling in SwashSim

This section provides an overview of the vehicle dynamics modeling approach that was developed and incorporated into SwashSim. This material can also be found in chapter 3 of "Principles of Highway Engineering and Traffic Analysis" (Mannering and Washburn, 2012). The approach at its most basic level determines maximum acceleration through the fundamental equation relating tractive force to resistance forces as per

$$F = m \times a + R_a + R_{rl} + R_g \tag{3-1}$$

The tractive force, *F*, referred to here as available tractive effort, is taken as the lesser of maximum tractive effort and engine-generated tractive effort. Maximum tractive effort is a function of several of the vehicle's physical characteristics (such as wheelbase, center of gravity, and weight) and the roadway coefficient of road adhesion. Maximum tractive effort represents the amount of longitudinal force that can be accommodated by the tire-pavement interface. Engine-generated tractive effort is a function of engine torque, transmission and differential gearing, and drive wheel radius.

The major resistance forces are aerodynamic, rolling, and grade. The equation for determining aerodynamic resistance is

$$R_a = \frac{\rho}{2} \times C_D \times A_f \times V \tag{3-2}$$

where

R_a = aerodynamic resistance in lb,
ρ = air density in slugs/ft^3,
C_D = coefficient of drag (unitless),
A_f = frontal area of the vehicle (projected area of the vehicle in the direction of travel) in ft^2, and

V = speed of the vehicle in ft/s.

The coefficient of rolling resistance for road vehicles operating on paved surfaces is approximated as

$$f_{rl} = 0.01 \times (1 + \frac{V}{147}) \quad (3\text{-}3)$$

where

f_{rl} = coefficient of rolling resistance (unitless), and
V = vehicle speed in ft/s.

The rolling resistance, in lb., is simply the coefficient of rolling resistance multiplied by $W \cos \theta_g$, the vehicle weight acting normal to the roadway surface. For most highway applications θ_g is very small, so it can be assumed that cos θ_g = 1, giving the equation for rolling resistance (R_{rl}) as presented in Equation $R_{rl} = f_{rl} \times$ W (3-4.

$$R_{rl} = f_{rl} \times \mathrm{W} \quad (3\text{-}4)$$

Grade resistance is simply the gravitational force (the component parallel to the roadway) acting on the vehicle. The expression for grade resistance (R_{rl}) is

$$R_g = W \times \sin \theta_g \quad (3\text{-}5)$$

As in the development of the rolling resistance formula, highway grades are usually very small, so $\sin \theta_g \cong \tan \theta_g$. Thus, grade resistance is calculated as

$$R_g \cong W \times \tan \theta_g = W \times G \quad (3\text{-}6)$$

where

G = grade, defined as the vertical rise per some specified horizontal distance in ft/ft.

Grades are generally specified as percentages for ease of understanding. Thus a roadway that rises 5 ft vertically per 100 ft horizontally (G = 0.05 and θ_g = 2.86°) is said to have a 5% grade.

The relationship between vehicle speed and engine speed is

$$V = \frac{2 \times \pi \times n_e \times (1 - i)}{\varepsilon_0} \quad (3\text{-}7)$$

where

V = vehicle speed in ft/s,
n_e = engine speed in crankshaft revolutions per second,
i = slippage of the drive axle, and
ε_0 = overall gear reduction ratio

The overall gear reduction ratio is a function of the differential gear ratio and the transmission gear ratio, which is a function of the selected transmission gear for the running speed. This equation can be rearranged to solve for engine speed given the current vehicle speed (if vehicle speed is zero, engine speed is a function of throttle input).

With the calculated engine speed, the torque being produced by the engine can be determined from the torque-engine speed relationship. Power is the rate of engine work, expressed in horsepower (hp), and is related to the engine's torque by

$$hp_e = \frac{2 \times \pi \times M_e \times n_e}{550} \quad (3\text{-}8)$$

where

hp_e = engine-generated horsepower (1 horsepower equals 550 ft-lb/s),
n_e = engine speed in crankshaft revolutions per second, and
M_e = engine torque in ft-lb.

The engine-generated tractive effort reaching the drive wheels is

$$F_e = \frac{M_e \times \varepsilon_0 \times n_d}{r} \quad (3\text{-}9)$$

where

F_e = engine-generated tractive effort reaching the drive wheels in lb,
M_e = engine torque in ft-lb.
ε_0 = overall gear reduction ratio,
n_d = mechanical efficiency of the drivetrain, and
r = radius of the drive wheels in ft.

It should be noted that since torque and horsepower are directly related, if only a power-engine speed relationship is available, this can be converted to a torque-engine speed relationship by using Equation 3-8.

For determining vehicle maximum acceleration, Equation $F = m \times a + R_a + R_{rl} + R_g$ (3-1 is rearranged and an additional term, γ_m, to account for the inertia of the vehicle's rotating parts that must be overcome during acceleration, is included as follows.

$$a = \frac{F - \sum R}{\gamma_m \times m} \quad (3\text{-}10)$$

γ_m, referred to as the mass factor, is approximated as presented in Equation $\gamma_m = 1.04 + 0.0025 \times \varepsilon_0^2$ (3-11.

$$\gamma_m = 1.04 + 0.0025 \times \varepsilon_0^2 \quad (3\text{-}11)$$

Initial Testing of SwashSim Vehicle Dynamics Modeling

Test Vehicle

Initial testing of the implementation of the vehicle dynamics modeling approach in SwashSim was done with a 2003 Honda Civic LX, a light duty passenger vehicle (pictured in Figure 3-1).

Figure 3-1. 2003 Honda Civic LX

Table 3-1 lists additional vehicle information that is needed for setting up the vehicle in SwashSim.

Table 3-1. 2003 Honda Civic LX Vehicle Characteristics Data

Dimensions	
Height (ft)	4.59
Width (ft)	5.56
Length (ft)	14.56
Weight (lb)	2,474
Wheel Radius (ft)	1.03

Engine	
4 cylinder, 1.7 L	
Maximum Torque (lb-ft)	105
Maximum Power (hp)	115
Transmission (automatic)	
Gear Ratios	
Gear 1	2.722
Gear 2	1.516
Gear 3	0.975
Gear 4	0.674
Differential Gear Ratio	4.07

Additionally, the torque/power versus engine speed relationship needs to be specified in SwashSim. This relationship for the 2003 Honda Civic is shown in Figure 3-2. Note that the lower (blue) curves correspond to the data collection vehicle used in this study.

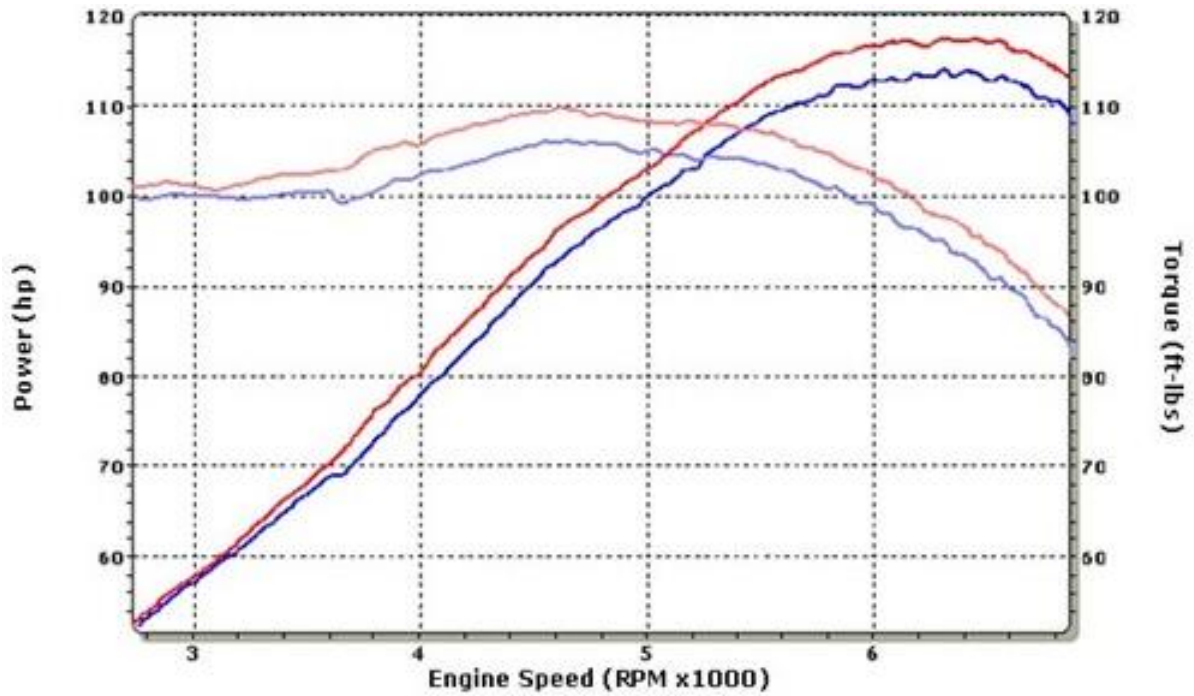

Figure 3-2. Torque/Power – Engine Speed Curves for 2003 Honda Civic LX (E-Trailer, 2014)

Test Equipment

An OBD scantool (i.e., OBDLink SX Scan© Tool (Figure 3-3) with OBDWiz© diagnostics software (Figure 3-4)) was used to record OBD parameters at approximately 1 Hz frequency, including RPM, engine load, intake manifold absolute pressure, vehicle speed and time stamp.

Figure 3-3. (a) OBDLink SX© Scan Tool cable and (b) cable attached to the OBD-II port of test vehicle

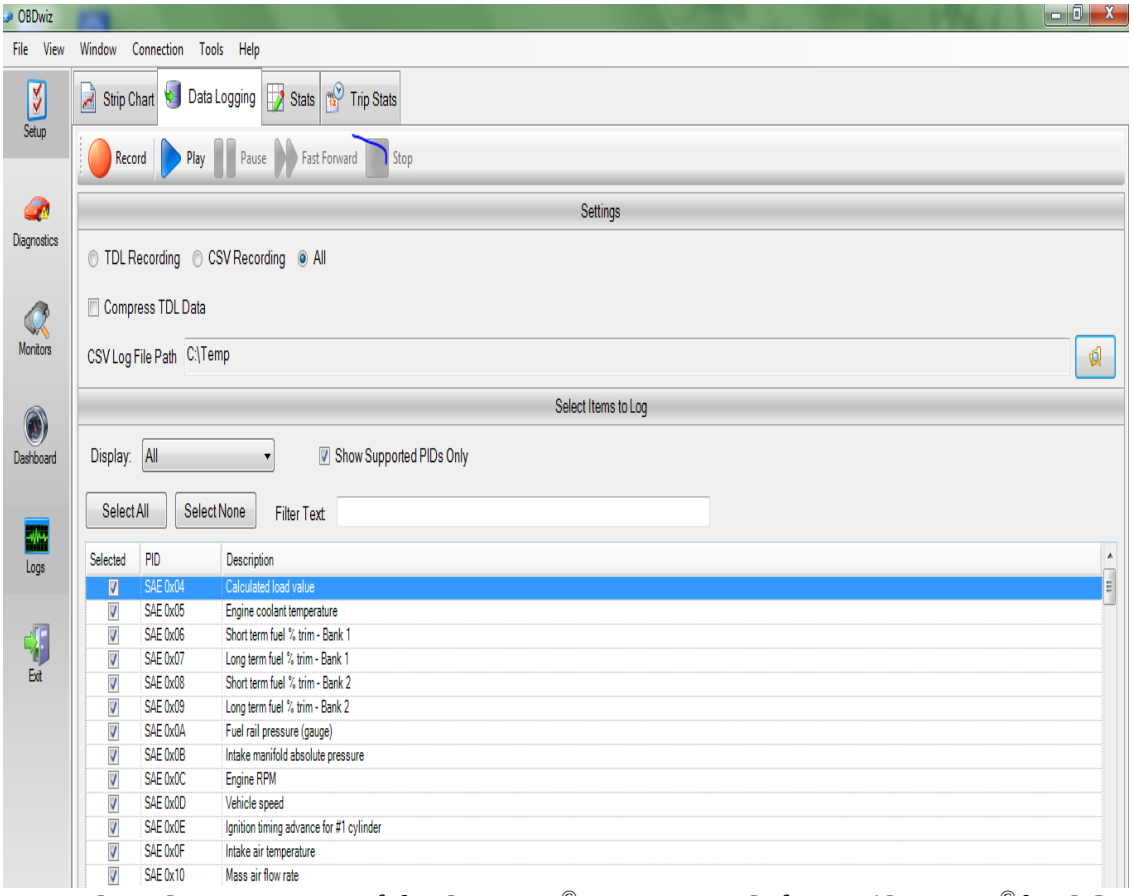

Figure 3-4. Screen capture of the OBDWiz© Diagnostics Software (OBDWiz© by OCTech, LLC, http://www.obdsoftware.net/OBDwiz.aspx)

Data Collection

OBD data were collected from a section of freeway and a section of arterial. The freeway section was a six-mile-long section of Interstate 75 (I-75) between the cross streets of SW Archer Road and NW 39th (depicted in Figure 3-5) The posted speed limit for this section is 70 mi/h.

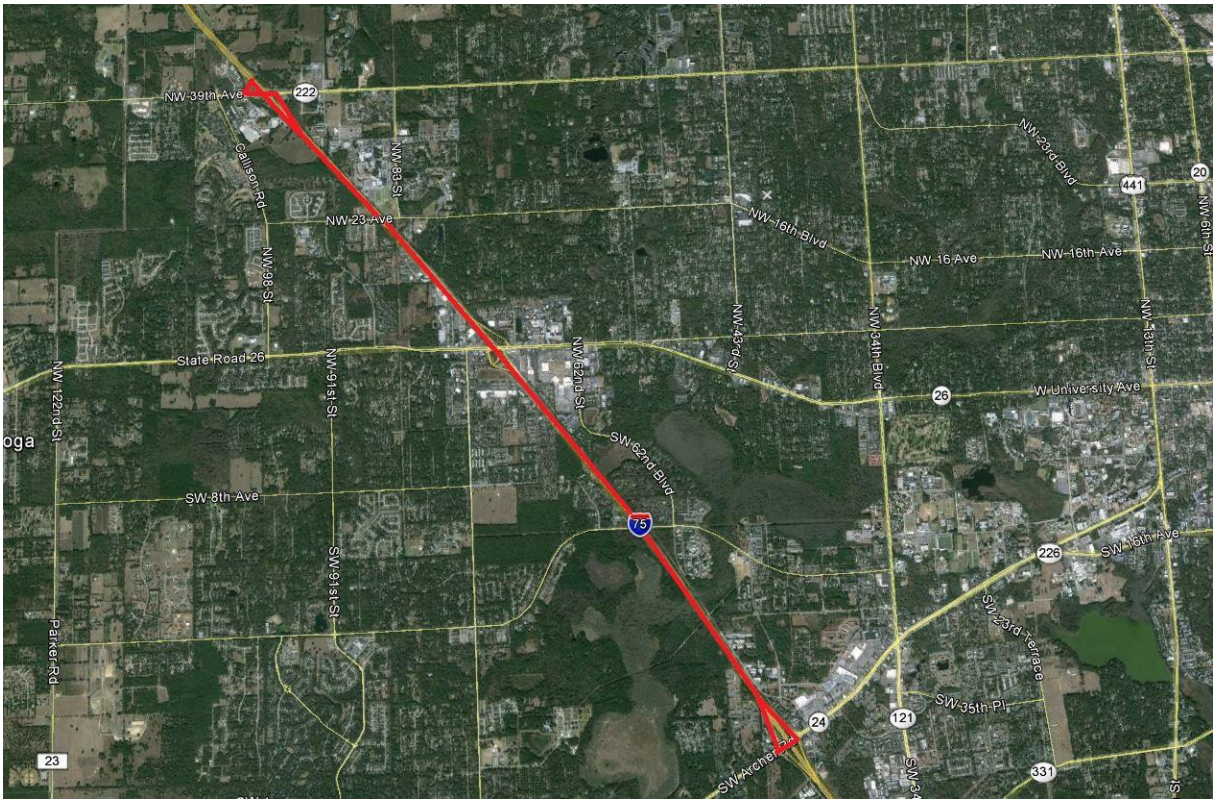

Figure 3-5. Aerial Photo of Freeway Section for OBD Data Collection

The arterial section is a little over a mile in length. It is along a section of Newberry Road (SR-26) between the cross streets of NW 98th Street and NW 122nd Street (depicted in Figure 3-6). The posted speed limit is 45 mi/h.

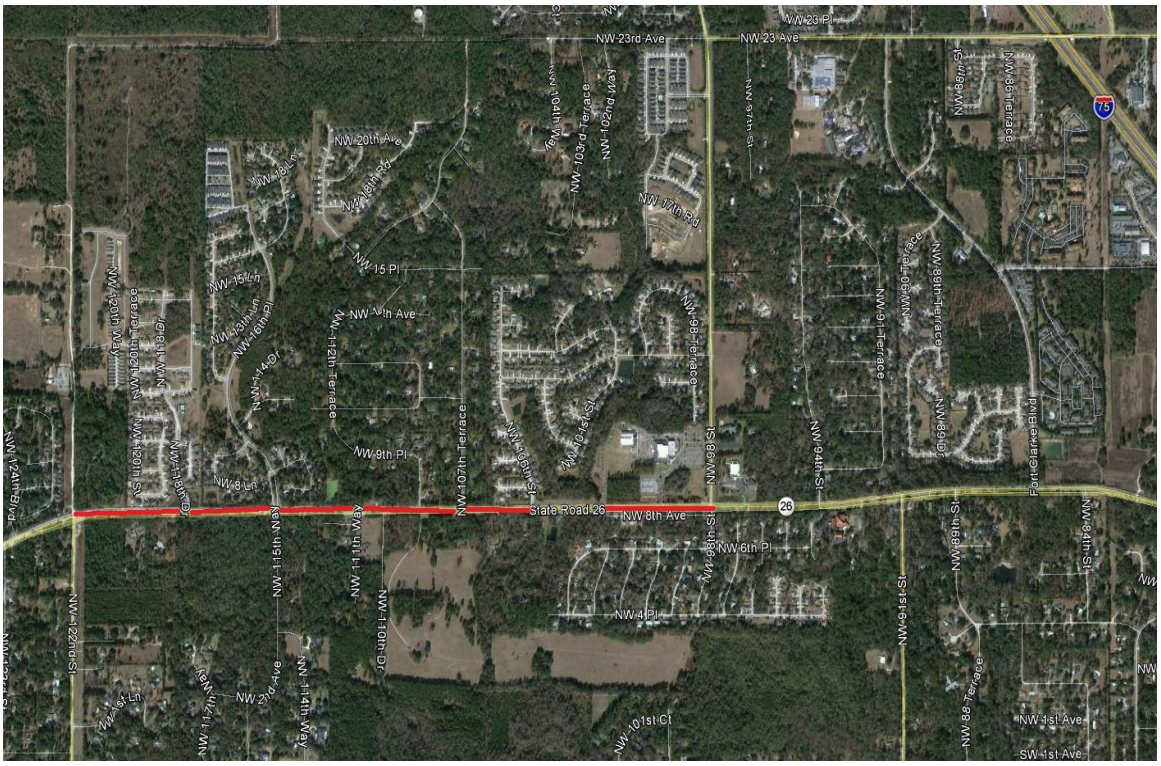

Figure 3-6. Aerial Photo of Arterial Section for OBD Data Collection

Both test sections had an approximately 0.5% grade in the travel direction. During the data collection effort, a total of 3,355 seconds of valid OBD data were collected in the field for three different types of driving behavior, ranging from non-aggressive, moderate, and aggressive. This stratification was done in order to observe and account for these driver type differences that affect the internal engine variables of interest.

Field Data Results and Analysis

Figure 3-7 is a plot of the product of MAP x RPM versus VSP.

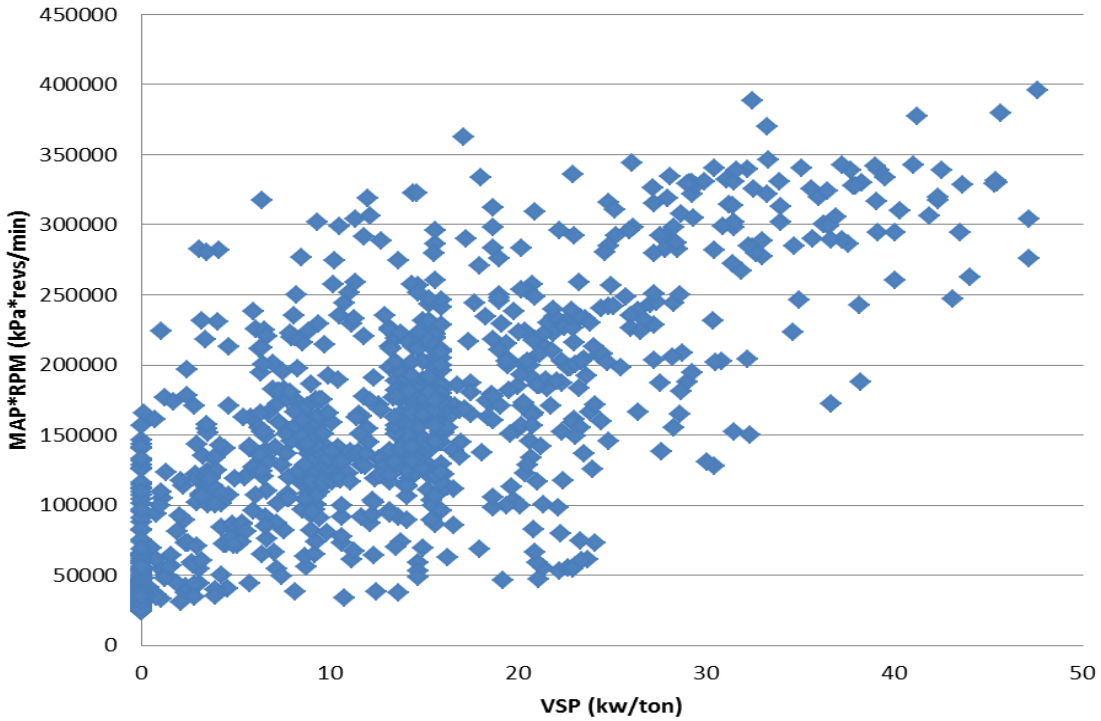

Figure 3-7. MAP x RPM versus VSP

Figure 3-8 is a plot of the product of MAP and RPM versus calculated engine load.

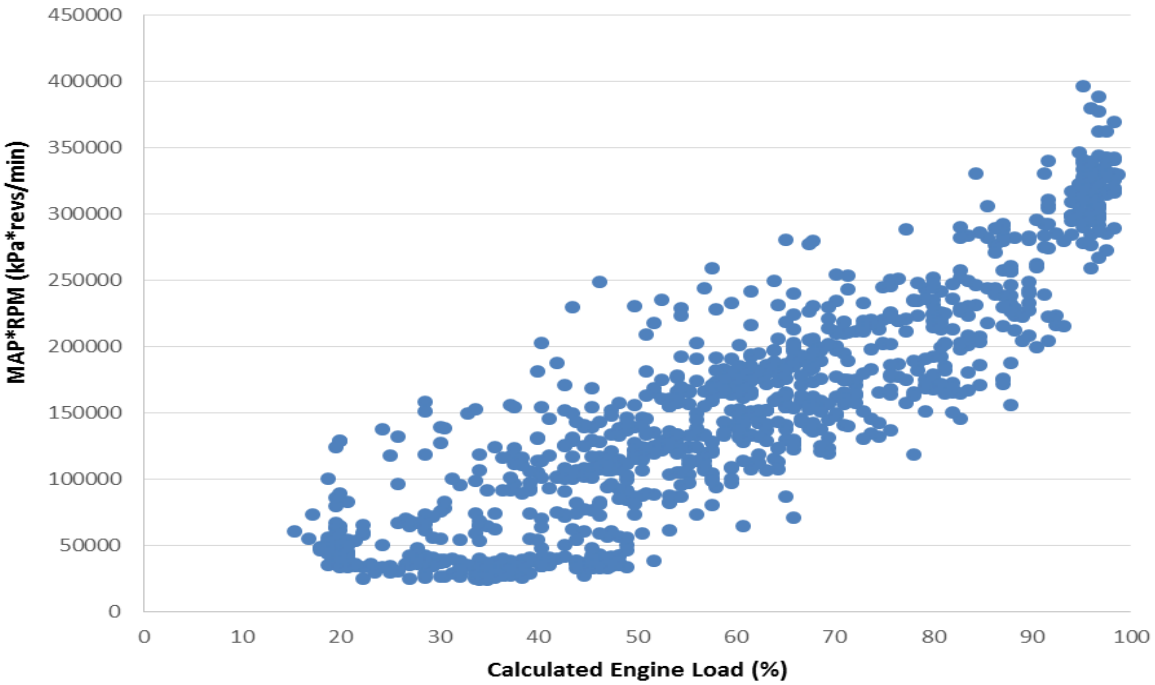

Figure 3-8. MAP x RPM versus Calculated Engine Load

Consistent with Frey et al. (2010), the field data support a power model fit to the MAP x RPM versus VSP relationship and a linear model fit to the MAP x RPM versus calculated engine load.

A regression analysis of the data in Figure 3-7 yields the following model with an R^2 value of 0.72.

$$MAP \times RPM \ = \ 107458 \ \times VSP^{0.1553} \tag{3-12}$$

With VSP calculated as

$$VSP = 0.278 \times V \left[0.305 \times a + 9.81 \times \left(\sin\left(a \times \tan\frac{r}{100}\right)\right) + 0.132\right] + 0.0000065 \ \times V^3 \tag{3-13}$$

where

VSP = Vehicle Specific Power (kw/ton)
V = Vehicle Speed (km/h)
a = Vehicle Acceleration (km/h/s)
r = Roadway Grade (%)

With RPM being generated in SwashSim through the vehicle dynamics equations, MAP is simply calculated in SwashSim as

$$MAP \ = (107458 \ \times VSP^{0.1553})/RPM \tag{3-14}$$

A regression analysis of the data in Figure 3-8 yields the following model with an R^2 value of 0.76.

$$MAP \times RPM \ = \ 3556.4 \times Calculated\ Engine\ Load \ - \ 66189 \tag{3-15}$$

The calculated engine load value is then obtained by rearranging the above equation, as follows.

$$Calculated\ Engine\ Load = (MAP \times RPM + 66189)/3556.4 \tag{3-16}$$

Verification of SwashSim Implementation

Simulation runs for a multilane highway of 1.5 miles in length were performed for varying desired speeds of 30 to 70 mi/h, to cover the range of speeds for both arterial and freeway conditions. As Figure 3-9 and Figure 3-10 confirm, the SwashSim outputs match with the models developed from the field data.

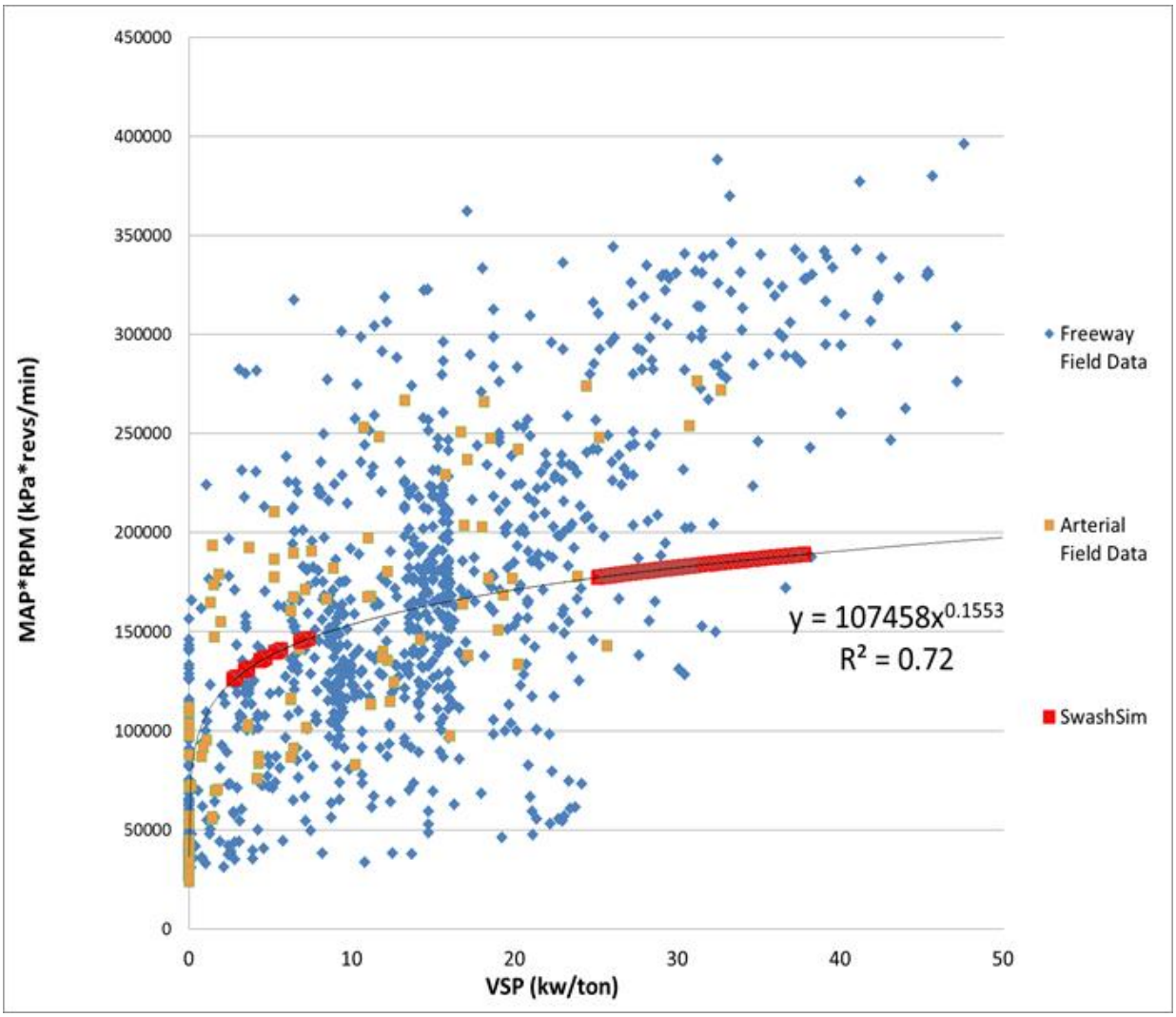

Figure 3-9. Comparison of Field and SwashSim MAP x RPM versus VSP Data

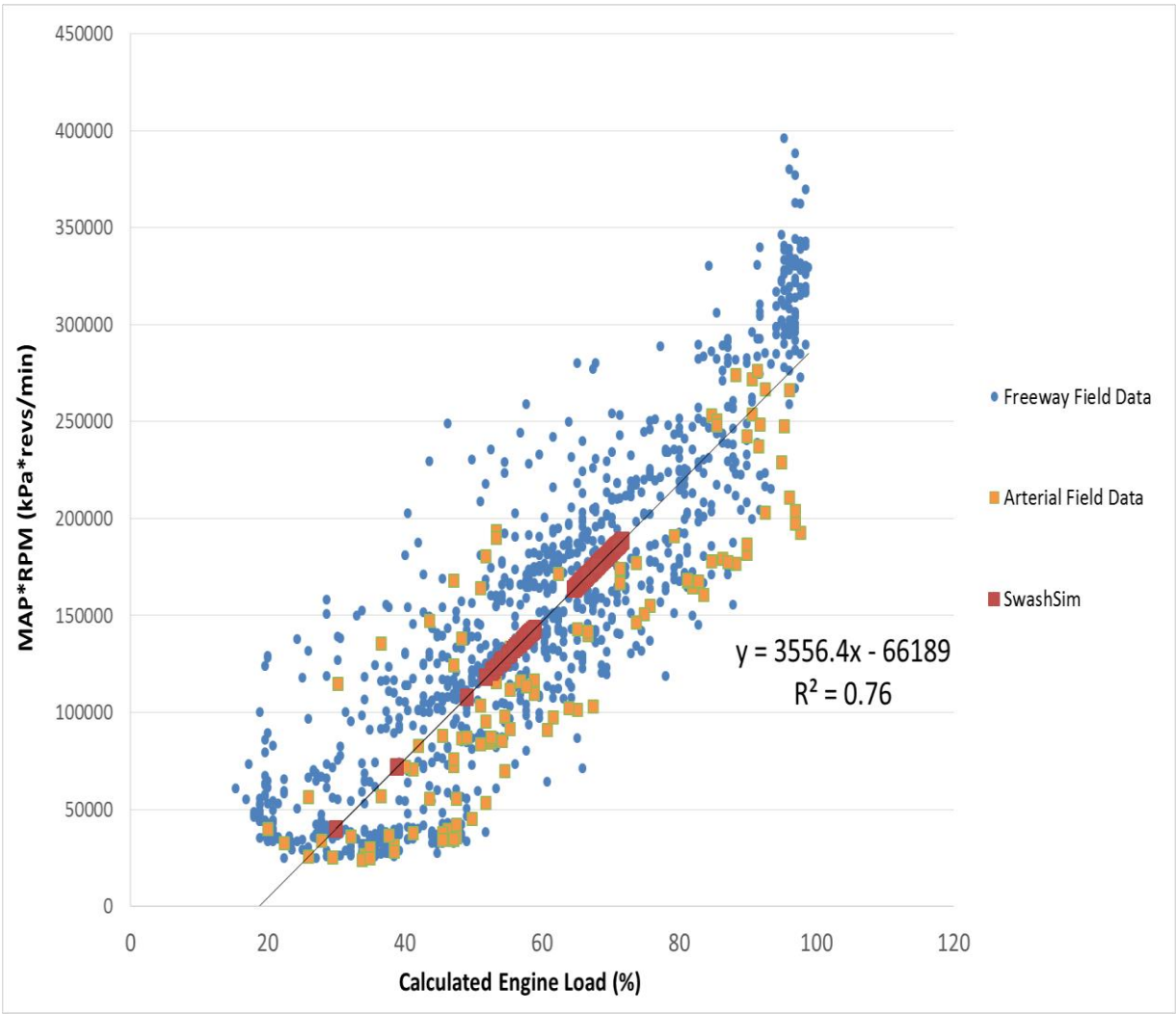

Figure 3-10. Comparison of Field and SwashSim MAP x RPM versus Calculated Engine Load Data

Another verification between the OBD field data and simulation results was performed to observe the relationship between engine RPM and vehicle speed, both of which are directly related to selected transmission gear. Figure 3-11 shows these results.

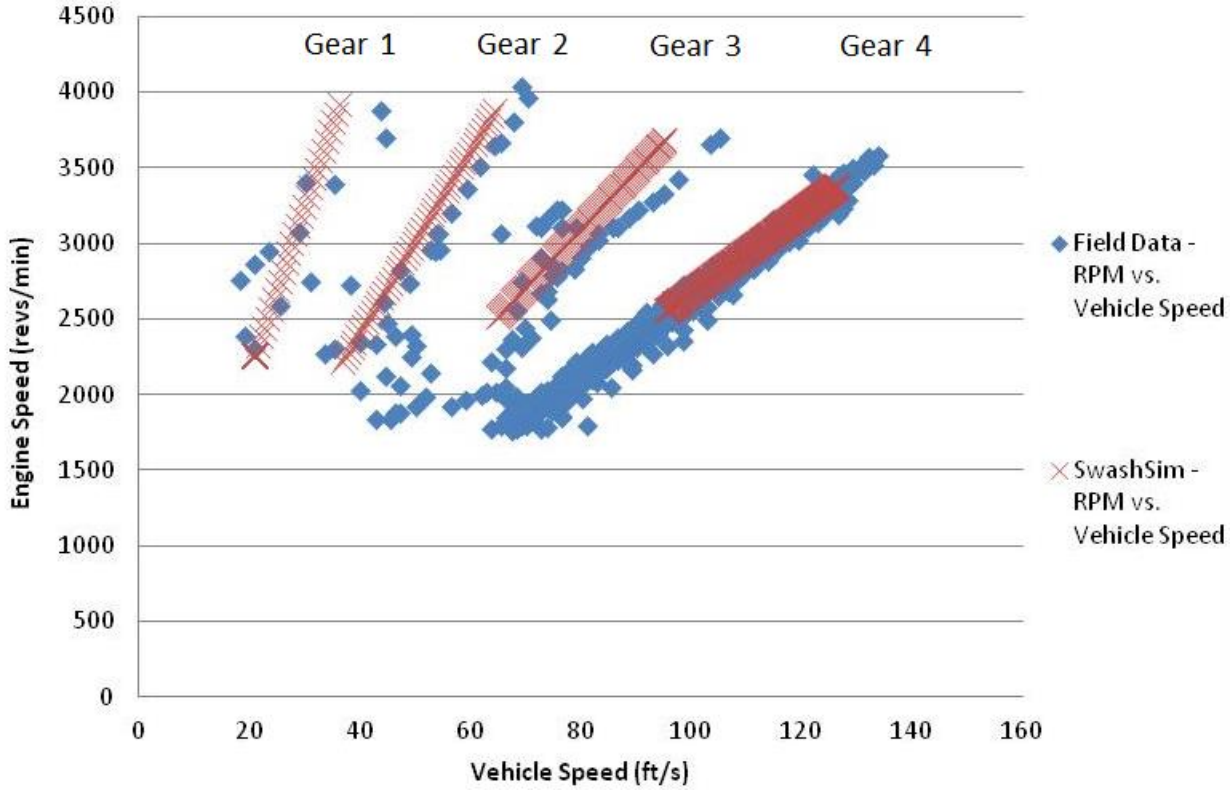

Figure 3-11. Comparison of Field and SwashSim Engine Speed versus Vehicle Speed Relationship

It can be observed from Figure 3-11 that SwashSim does a very good job of replicating the 4-speed transmission of the OBD data collection vehicle.

Implementation of Test Vehicles into SwashSim

Simulation Setup

The following figures show the various input screens used in SwashSim to specify the necessary inputs to facilitate the IOV-based EU&E approach.

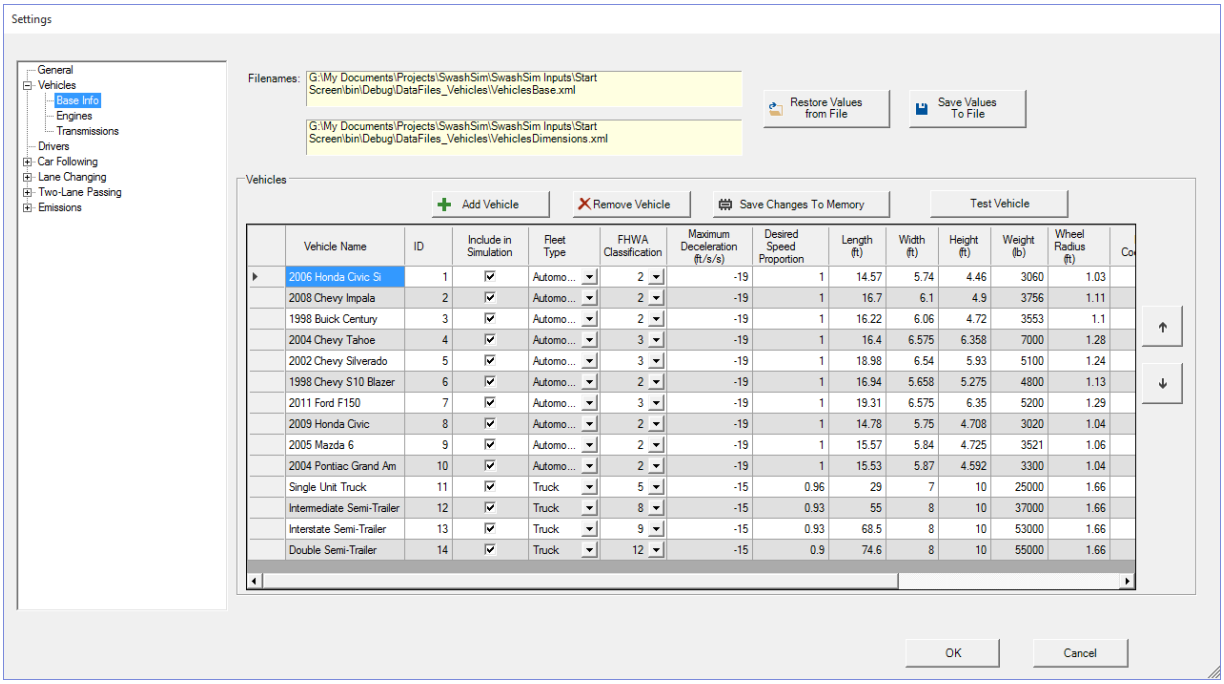

Figure 3-12. SwashSim basic descriptive information and vehicle dimensions input screen.

The input screen shown above handles the specification of vehicle dimensions and classification information. Additionally, the ID's of the associated engine and transmission are specified on this screen.

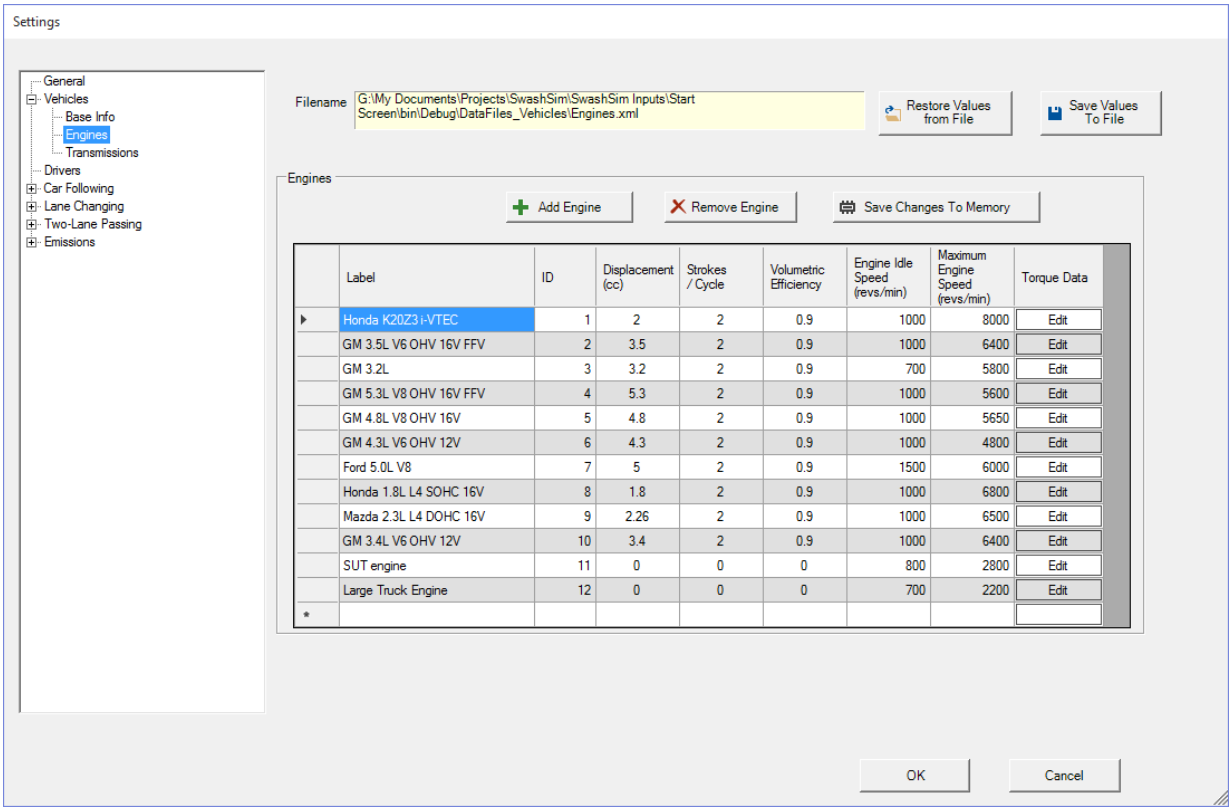

Figure 3-13. SwashSim basic engine information input screen.

The input screen shown above handles the specification of engine information. This screen links to the input screen shown below, through which the torque-engine speed relationship is specified.

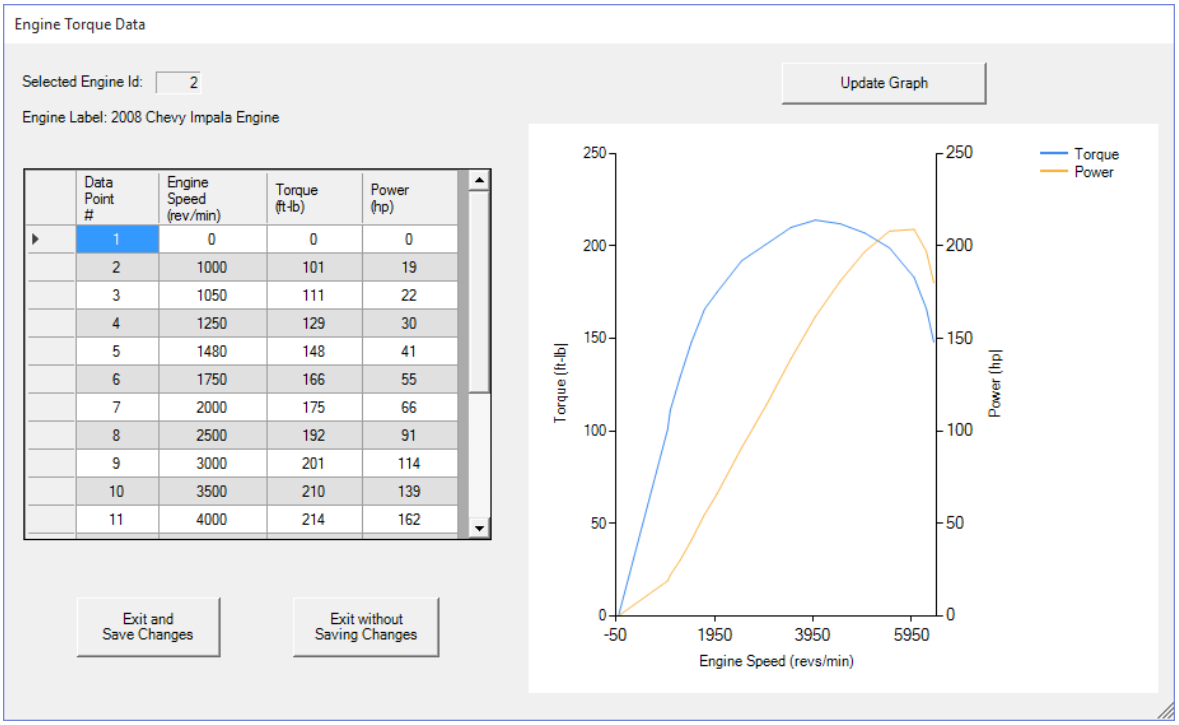

Figure 3-14. SwashSim engine torque/power versus engine speed relationship input screen.

The input screen shown below handles the specification of transmission information.

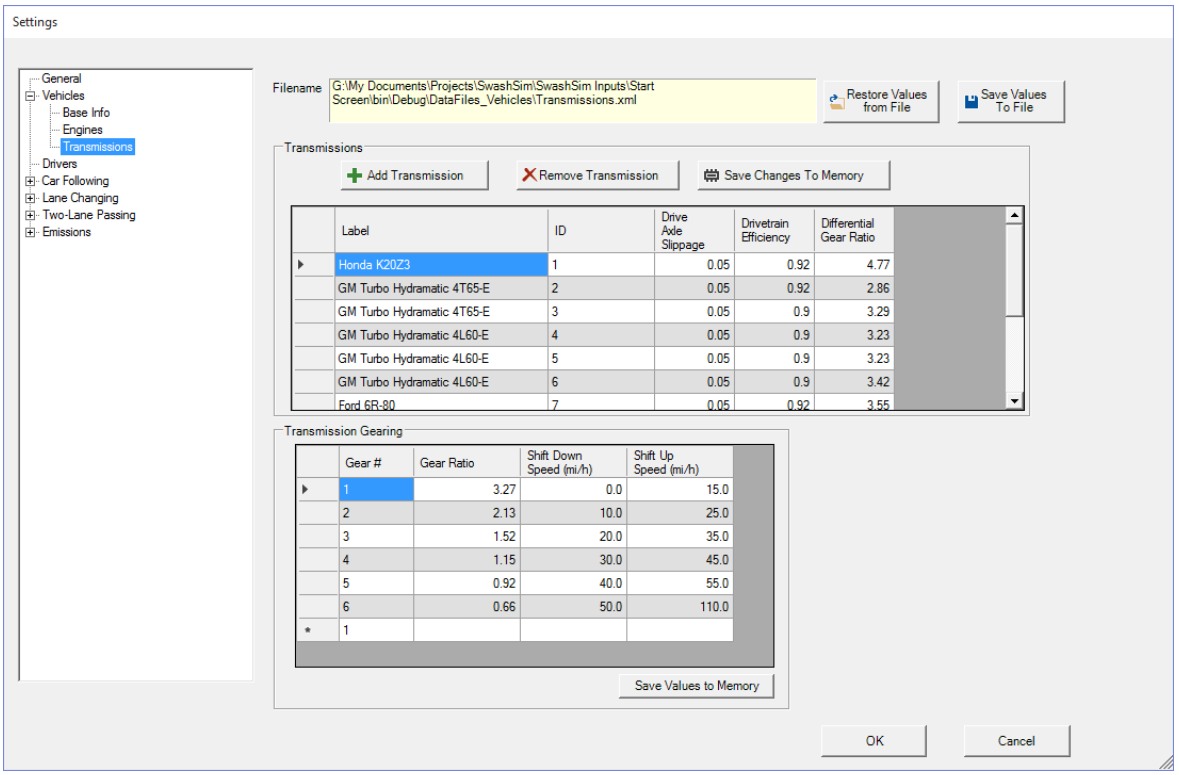

Figure 3-15. SwashSim transmission information input screen.

The input screen shown below handles the specification of the parameter values for the IOV-based EU&E models discussed in Part 2 of this report.

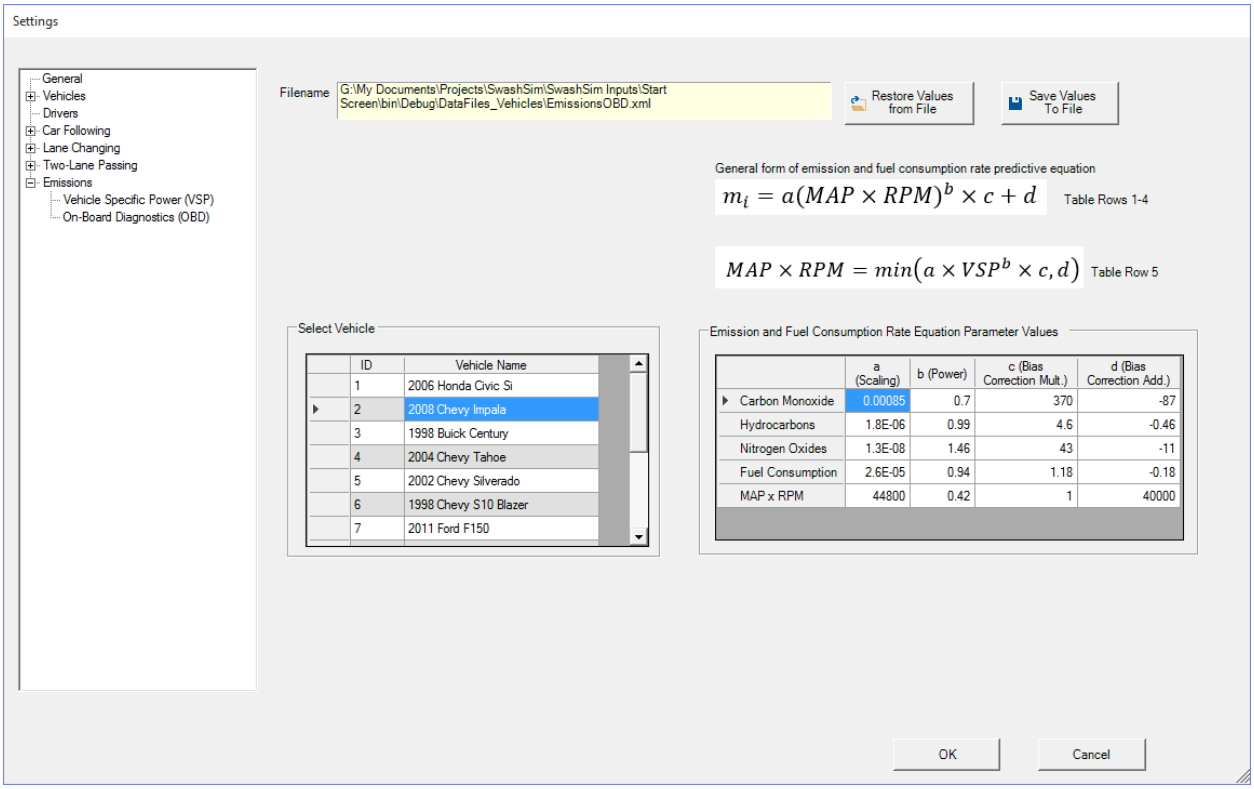

Figure 3-16. SwashSim EU&E model parameters input screen.

Test Results

The following figures are based on fuel use and emissions output from a sample SwashSim simulation run. The results are consistent with the implemented IOV-based EU&E estimation equations from Part 2 of this report.

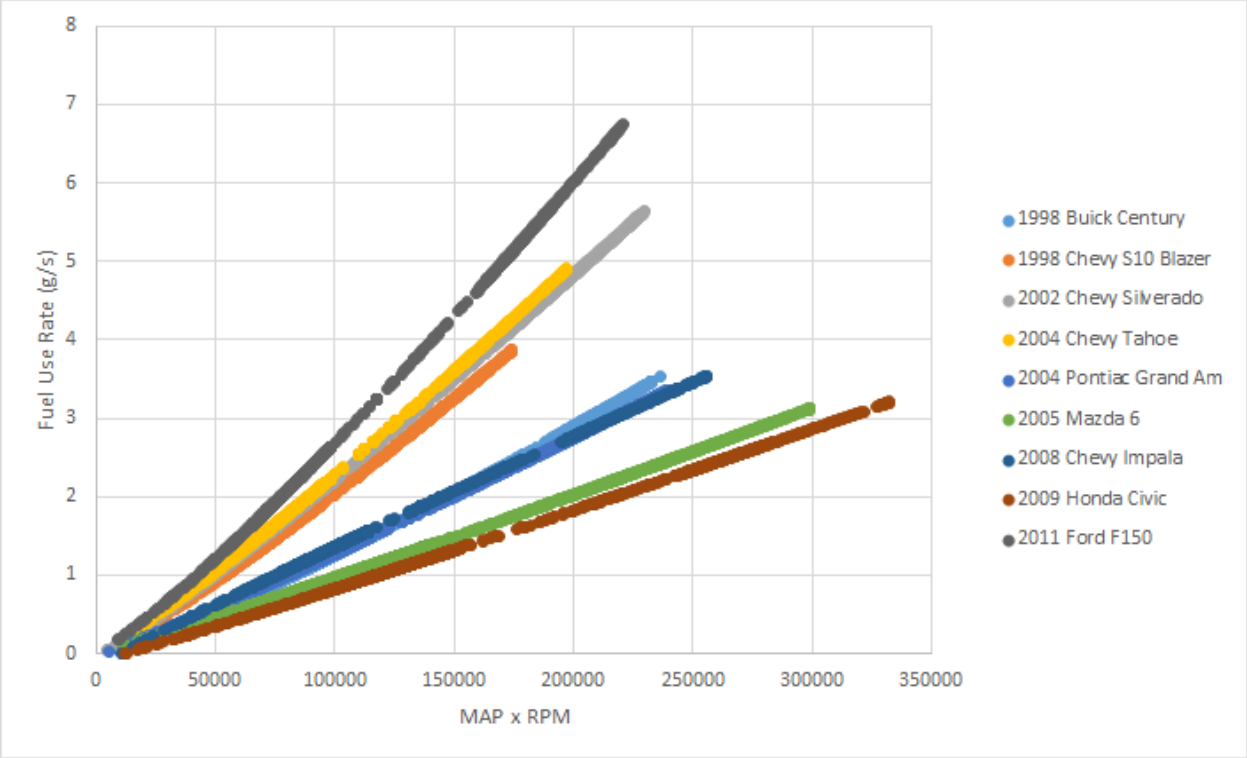

Figure 3-17. SwashSim sample results for fuel use rate versus MAP x RPM.

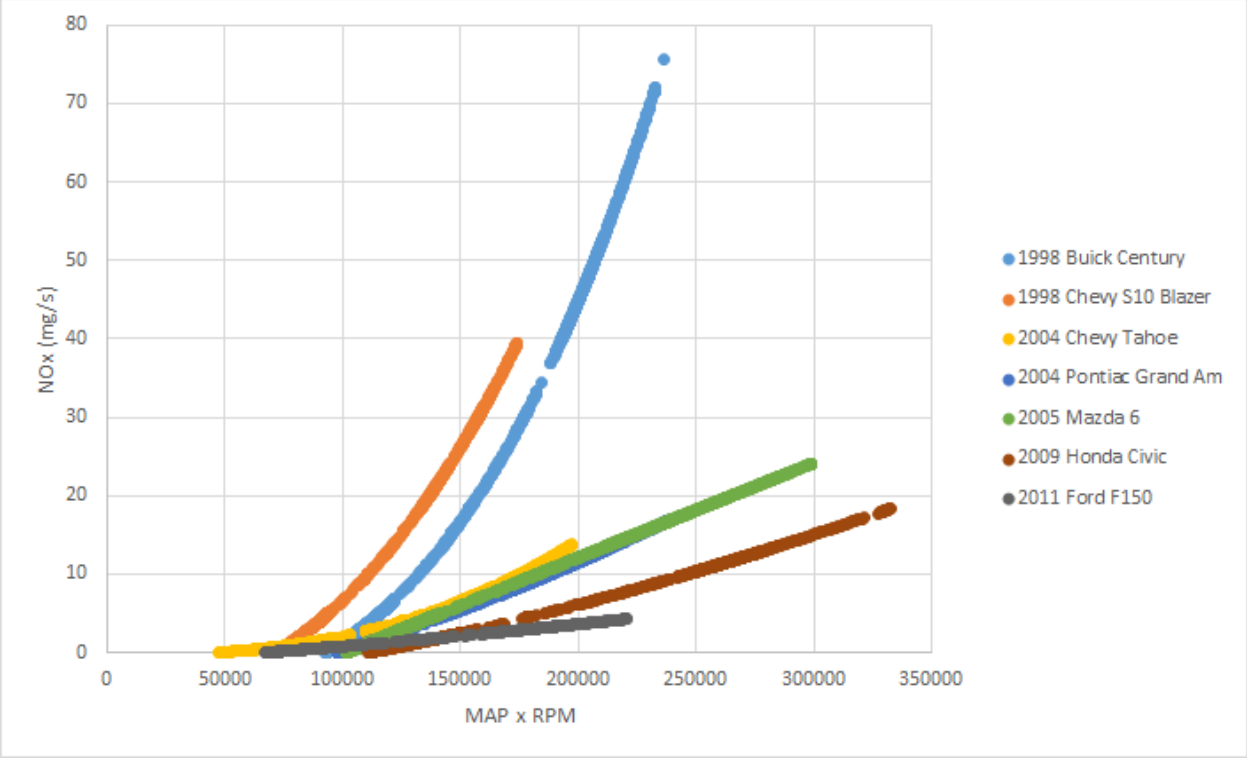

Figure 3-18. SwashSim sample results for NOx emissions versus MAP x RPM.

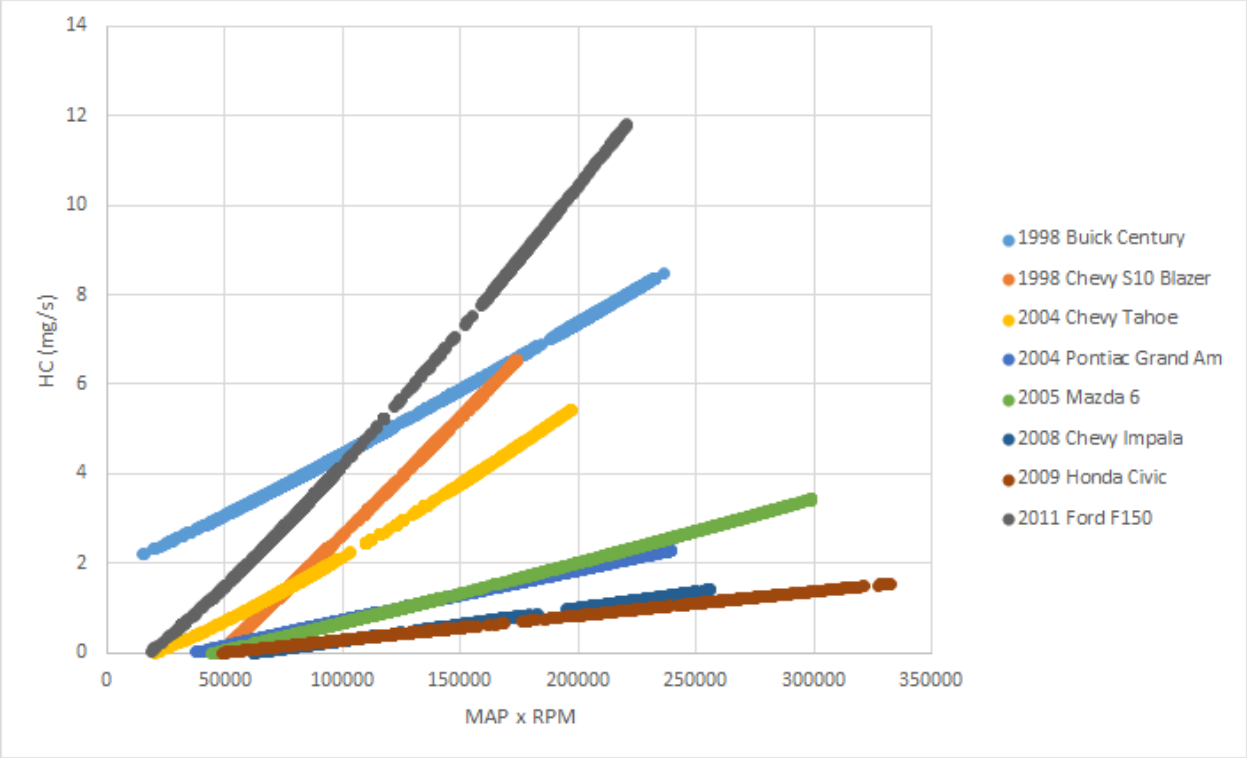

Figure 3-19. SwashSim sample results for HC emissions versus MAP x RPM.

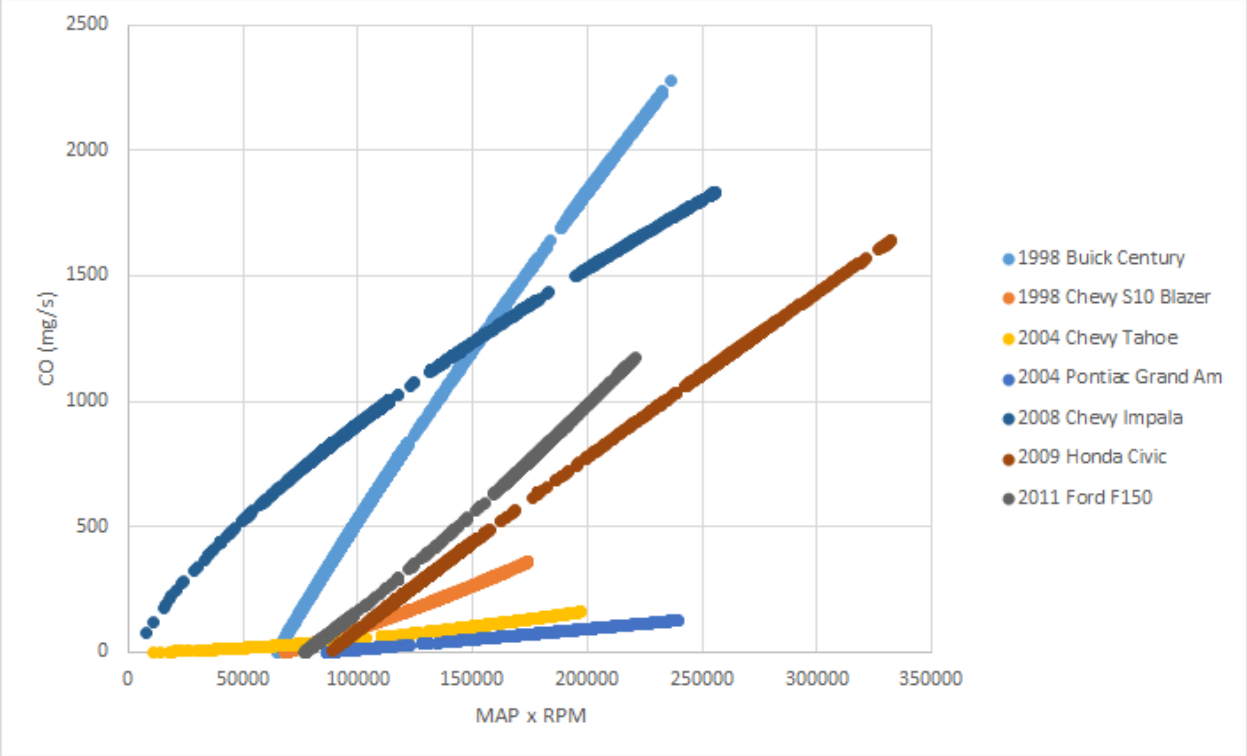

Figure 3-20. SwashSim sample results for CO emissions versus MAP x RPM.

References

Dzhelekarski, P., & Alexiev, D. (2005). *Reading and interpreting diagnostic data from vehicle OBDII system*. ELECTRONICS, *5*, 12-22.

Frey, H. C., Zhang, K., & Rouphail, N. M. (2008). *Fuel use and emissions comparisons for alternative routes, time of day, road grade, and vehicles based on in-use measurements*. Environmental Science & Technology, *42*(7), 2483-2489.

Frey, H. C., Zhang, K., & Rouphail, N. M. (2010). *Vehicle-specific emissions modeling based upon on-road measurements*. Environmental Science & Technology, *44*(9), 3594-3600.

Godavarty, S., Broyles, S., & Parten, M. (2000). Interfacing to the on-board diagnostic system. In *Vehicular Technology Conference, 2000. IEEE-VTS Fall VTC 2000. 52nd* (Vol. 4). IEEE.

International Organization for Standardization (1994). Road vehicles-Diagnostic systems: CARB requirements for interchange of digital information. ISO 9141-1.

International Organization for Standardization (1995). *Road vehicles-Diagnostic systems-Keyword protocol 2000-Part 2*. Draft International Standard, ISO/DIS 14230-3. 1-97.

Kalin, I. (2013, February 5). *Apps for Vehicles Challenge Finalists Announced*. Retrieved February 12, 2013 from http://energy.gov/articles/apps-vehicles-challenge-finalists-announced.

Mannering, F.L., and Washburn, S.S. (2012). *Principles of Highway Engineering and Traffic Analysis* (5th ed). Hoboken, NJ: John Wiley and Sons, Inc.

Society of Automotive Engineers (1997). *OBD II Scan Tool - On-Board-Diagnostics and multiplex Technical Reports: SAE J1978*. Society of Automotive Engineers.

Society of Automotive Engineers (1997). *Diagnostics for Light and Medium Duty Vehicles Standard Manual: SAE J2178/3*. Society of Automotive Engineers.

Society of Automotive Engineers (1997). *Diagnostics for Light and Medium Duty Vehicles Standard Manual: SAE J2178/4*. Society of Automotive Engineers.

Society of Automotive Engineers (1997). *E/E diagnostic test modes - Diagnostics for Light and Medium Duty Vehicles Standard Manual: SAE J1979*. Society of Automotive Engineers.

Society of Automotive Engineers (1997). *OBD II scan tool - Diagnostics for Light and Medium Duty Vehicles Standard Manual: SAE J1978*. Society of Automotive Engineers.

Society of Automotive Engineers (1997). *Enhanced E/E Diagnostic Test Modes - Diagnostics for Light and Medium Duty Vehicles Standard Manual: SAE J2190*. Society of Automotive Engineers.

Talbot, D. (2013, February 1). *Programming Cars: Using the GM In-Dash SDK*, December 2013. Retrieved December 18, 2013 from http://www.codeguru.com/csharp/programming-cars-using-the-gm-in-dash-sdk.htm.